5-2014

A Comparison and Evaluation of Different Dynamic Characterization Approaches for Bridges

Juan Javier Torres Torres Goitia
University of Arkansas, Fayetteville

A Comparison and Evaluation of Different Dynamic Characterization Approaches for Bridges

A Comparison and Evaluation of Different Dynamic Characterization Approaches for Bridges

A thesis submitted in partial fulfillment
of the requirements for the degree of
Master of Science in Civil Engineering

By

Juan Javier Torres Goitia Velasco
University of Arkansas
Bachelor of Science in Civil Engineering, 2010

May 2014
University of Arkansas

This thesis is approved for recommendation to the Graduate Council

_____
Dr. Kirk Grimmelsman
Thesis Director

_____
Dr. Micah Hale
Committee Member

_____
Dr. Ernie Heymsfield
Committee Member

Abstract

The objective of this thesis was to compare different dynamic characterization approaches for full scale bridge structures to devise a rapid and reliable Structural Health Monitoring (SHM) program in the aftermath of a natural or manmade hazard. Present methods for structural condition evaluation of bridge structures rely heavily on on-site visual inspections of each structure by specially trained engineers and technicians. It has been proved in the literature that this current method is subjective, time consuming and manpower intensive, all of which are not suited for the critical conditions following a hazard event. This study focused on comparing three different full scale dynamic test methods on two in-service fundamentally different bridge structures to provide recommendations on achieving a reliable characterization of the structures, while keeping testing efforts at a minimum. The three dynamic field test included Operational Modal Analysis, or ambient vibration testing, and controlled input vibration testing using an instrumented impact hammer and an electro-dynamic mass shaker. The two bridge specimens tested were a Parker pony truss structure and a concrete deck on steel girders structure. The effectiveness and limitations of each dynamic testing and characterization strategies and data acquisition architectures, data processing techniques, and their optimal integration was systematically evaluated for each bridge structure. Specifically, modal flexibility was the main comparison tool within the dynamic testing, given that this parameter provides a global representation of the structure's response under dynamic loads such as traffic and ambient noise. It was concluded that Impact Vibration testing was the preferred dynamic characterization method for rapid and reliable for post hazard condition evaluation of both structures.

Acknowledgements

I would like to express my gratitude to my parents, Carmen and Javier, for their support and unconditional trust through this process. Without their constant encouragement this thesis would not have been possible.

I am grateful for the constant encouragement and support from my advisor, Dr. Kirk Grimmelsman. I will always be thankful for the mentorship he provided. Also, I would like to thank Eric Fernstrom for the many hours of support and guidance provided while interpreting this research's results.

I would also like to thank my committee members: Dr. Micah Hale and Dr. Ernie Heymsfield for showing interest in my research and for offering their words of advice.

Table of Contents

1 Introduction 1

1.1 Background 1
1.2 State of Bridge Population 3
1.3 Types of Hazards Causing Bridges Failures 4
1.4 Current Bridge Evaluation Methods 8

1.4.1 Visual Inspection 9
1.4.2 Nondestructive Load Testing 10
1.4.3 Current Post-Hazard Condition Evaluation Methods 13

1.5 Motivation 15

1.5.1 Limitations of Visual Inspection for Evaluating Bridges 15

1.6 Objectives and Scope 17

1.6.1 Introduction 17

1.6.1.1 Comparison of Modal Parameters extracted from the Proposed Test Methods .. 19
1.6.1.2 Optimum SHM Strategy 19

1.6.2 Scope of Work 21

1.7 Organization of Thesis 21

2 Background and Literature Review 23

2.1 Introduction 23
2.2 Issues with Visual Inspection Methods for Bridge Evaluation 24

2.2.1 Visual Inspection 24
2.2.2 Post-Hazard Evaluation of Bridges 27

2.3 Full-Scale Testing 30

2.3.1 Static Load Testing 31
2.3.2 Full-Scale Dynamic Testing 34

2.3.2.1 Operational Modal Analysis 35
2.3.2.2 Experimental Modal Analysis 39

2.4 Modal Flexibility 47
2.5 Summary and Discussion 52

3 Experimental Program 54

3.1 Introduction 54
3.2 Test Specimens 54

3.2.1 Baptist Ford Bridge 54
3.2.2 Hartbarger Bridge 57

3.3 Test Design and Execution 60

3.3.1 Experimental Equipment. 61
3.3.2 Ambient Vibration Testing 69
3.3.3 Impact Hammer Testing 69
3.3.4 Shaker Testing 70

3.3.4.1 Design of the Shaker Excitation Signals 72

3.4 Data Analysis Methods 85

3.4.1 Ambient Vibration Data Analysis 85
3.4.2 Forced Vibration Data Analysis 87
3.4.3 Modal Flexibility 94

4 Results 96

4.1 Introduction 96
4.2 Natural Frequencies and Damping Ratios 96

4.2.1 Hartbarger Bridge 96
4.2.2 Baptist Ford Bridge 110

4.3 Mode Shapes 119

4.3.1 Hartbarger Bridge 119
4.3.2 Baptist Ford Bridge 126

4.4 Modal Flexibility Matrix 131

4.4.1 Hartbarger Bridge 131
4.4.2 Baptist Ford Bridge 134

4.5 Summary 143

5 Conclusions and Future Work 146

5.1 Conclusions 146
5.2 Future Work 153

6 Bibliography 155

List of Figures

Figure 1.1: State of U.S. Bridge Infrastructure (Bureau of Transportation Statistics, 2011). 4

Figure 1.2 Type and Number of Bridge Failures 1989 - 2000 (Wardhana & Hadipriono 2003). .. 7

Figure 1.3 Sumary of the Organization of AASHTO's Manual. 11

Figure 3. 1 Side View of the Truss (Torres Goitia, AR, 2012)..... 56

Figure 3.2 Bridge Elevation (Fernstrom et al., 2012). 56

Figure 3. 3 End View of the Bridge (looking west) (Torres Goitia, AR, 2012). 57

Figure 3.4 View of the Hartbarger Girder Bridge (looking east) (Torres Goitia, AR, 2012). 58

Figure 3. 5 Plan and Cross-Section Views of Typical Bridge Span (Fernstrom et al.2012). 59

Figure 3. 6 Photograph of the Underside of a Typical Span (Torres Goitia, AR, 2012). 60

Figure 3.7 PCB Model 393B05 Accelerometer (www.pcb.com). 64

Figure 3.8 PDC Model 393C Accelerometer (www.pcb.com). 64

Figure 3.9 Instrumentation Layout for the Baptist Ford Bridge. 65

Figure 3. 10 Instrumentation Layout for the Hartbarger Bridge. 66

Figure 3.11 Sensor Installation Details (Torres Goitia, AR, 2012). 66

Figure 3.12 Large Sledge Impact Hammer (with different rubber tips) (www.pcb.com). 67

Figure 3.13 Electro-dynamic Shaker with Reaction Masses (Torres Goitia, AR, 2012)..... 68

Figure 3.14 Waveform Generator and Shaker Amplifier 69

(Torres Goitia, AR, 2012). 69

Figure 3.15 PXI Mainframe, APS Shaker Amplifier and APS Shaker (left to right) (Torres

Goitia, AR, 2012)..... 72

Figure 3. 16 Time Domain Representation of the Burst Random Excitation Signal. 73

Figure 3. 17 Frequency Domain Representation of the Burst Random Excitation Signal. 74
Figure 3.18 Time Domain Representation of the linear sine sweep signal (100 sec, 1-55 Hz).... 76
Figure 3.19 Frequency Domain Representation (FFT) of the Sine Sweep Signal (Single sided absolute value amplitude spectrum of Y(t), 1Hz – 55 Hz). 77
Figure 3. 20 Time Domain Representation of the Tukey Windowed Sine Sweep (100 sec, 1-55 Hz)..... 78
Figure 3.21 Frequency Domain Representation (FFT) of the Single Sided Amplitude Spectrum of the Tukey Windowed Sine Sweep signal (1 Hz – 55 Hz). 79
Figure 3.22 Time Domain of Tukey Windowed Targeted Sine Sweep Signal. 80
Figure 3.23 Frequency Domain Representation (FFT) of the Single Sided Amplitude Spectrum of the Tukey Windowed Targeted Sine Sweep signal (1 Hz – 55 Hz). 81
Figure 3.24 Accelerometer Layout for Preliminary Testing of the Baptist Ford Bridge. 83
Figure 3.25 Frequency Domain Response Single Sided Amplitude Spectrum of Y(f) of Sensor A3 for Each Excitation Signal. 84
Figure 3. 26 Data Processing Flow Chart. 88
Figure 4.1 CMIF plot, Impact Test. 97
Figure 4.2 Pseudo impulse response function plot from ambient vibration data (Hartbarger Bridge). 99
Figure 4.3 Pseudo frequency response function plot from ambient vibration data (Hartbarger Bridge). 100
Figure 4.4 eFRF plot for mode 1, impact test, (Hartbarger Bridge). 103
Figure 4.5 eFRFs for all modes from ambient vibration test (Hartbarger Bridge). 104
Figure 4. 6 Synthesized eFRF for same output/input location (Hartbarger Bridge). 105

Figure 4. 7 Synthesized eFRF for different output/input locations (Hartbarger Bridge)..... 106

Figure 4.8 Actual shaker field test execution, Hartbarger Bridge. 107

Figure 4.9 CMIF plot, Impact testing. 112

Figure 4.10 pIRF plot, Ambient Data Test. 113

Figure 4.11 pFRF plot, Ambient Data Test. 114

Figure 4.12 eFRF plot, Mode 3, Impact Test Data. 115

Figure 4.13 eFRF plot, Ambient Test Data..... 116

Figure 4.14 Synthesized eFRF same output/input locations, Baptist Ford Bridge. 117

Figure 4.15 Synthesized eFRF different output/input locations, Baptist Ford Bridge. 118

Figure 4.16 Global Bending Mode Shapes, Hartbarger Bridge. 122

Figure 4.17 Localized Bending Mode Shapes, Hartbarger Bridge. 123

Figure 4.18 Global Torsion Mode Shapes, Hartbarger Bridge. 124

Figure 4.19 Bride Deck's Bending Modes, Hartbarger Bridge. 125

Figure 4.20 Global bending mode shapes (Baptist Ford Bridge). 128

Figure 4.21 Global torsional mode shapes (Baptist Ford Bridge). 129

Figure 4.22 Local bridge deck modes (Baptist Ford Bridge). 130

Figure 4. 23 Modal flexibility matrix convergence (Mean Displacements Under Uniform Load Vector) (Hartbarger Bridge). 133

Figure 4.24 Displacement profile obtained by loading modal flexibility matrix from impact testing results with uniform load (1 lb/DOF) (Hartbarger Bridge). 134

Figure 4. 25. Convergence of Modal Flexibility for impact test (Mean Displacements Under Uniform Load Vector) (Baptist Ford Bridge). 136

Figure 4.26 Displacement profile obtained by loading modal flexibility matrix from impact testing results with uniform load (1 lb/DOF) (Baptist Ford Bridge). 137
Figure 4.27 Convergence test for modal flexibility using shaker testing data with burst random input (Mean displacements under uniform Load Vector) (Baptist Ford Bridge). 139
Figure 4.28 Displacement profile obtained by loading modal flexibility matrix from burst random signal shaker testing results with uniform load (1 lb/DOF) (Baptist Ford Bridge). 140
Figure 4.29 Convergence test for modal flexibility using shaker testing data with swept sine input (Mean displacements under uniform Load Vector) (Baptist Ford Bridge). 142
Figure 4.30 Displacement profile obtained by loading modal flexibility matrix from swept sine shaker testing with uniform load (Baptist Ford Bridge). 143

List of Tables

Table 3.1 Shaker Excitation Signals Evaluated in Preliminary Field Test. 84

Table 4.1 Summary of Natural Frequencies & Damping Estimates for Hartbarger Bridge. 109

Table 4.2 Summary of Natural Frequencies & Damping Estimates for Baptist Ford Bridge. ... 119

Table 4.3 MAC values (%) between mode shapes identified from impact testing and ambient vibration testing. 126

Table 4.4 MAC values (%) for different vibration test methods in relation to impact testing results. 131

Table 4.5 Modal A Values for Impact Test (Hartbarger Bridge). 133

Table 4.6 Modal A values from impact testing (Baptist Ford Bridge). 135

Table 4.7 Modal A values from shaker testing with burst random input (Baptist Ford). 138

Table 4.8 Modal A values from shaker testing with swept sine input (Baptist Ford Bridge). ... 141

1 Introduction

1.1 Background

The condition of a nation's transportation infrastructure directly affects the well-being of communities. In such a dynamic global economy, distant markets are brought together by transportation infrastructures. Lean transportation is essential for any successful economy, providing the means for supplying goods and transporting people in a timely manner wherever markets demand them. Communities rely on the prompt availability of products to keep business thriving and only a healthy transportation infrastructure can deliver on such needs. Providing effective infrastructure management will prove beneficial to society as a whole. The fact that transportation infrastructure assets are becoming aged beyond their expected life-span raises serious concerns about the condition of the nation's transportation infrastructure system.

In addition to wear caused by traffic and deterioration, natural or man-made hazards can limit the serviceability of transportation infrastructure systems. The damages caused by such hazards limit the utility of roads and bridges in the aftermath of the event, and also prevent quick emergency response and recovery operations to the affected region. Bridges are most vulnerable under these conditions and are usually considered critical paths on the infrastructure network. The serviceability failure of a single bridge will usually cause greater harm to a community than that of a single road. Bridges overcome both natural and man-made obstructions that roads can't, thus their performance is crucial for a rapid emergency response. In cases where a section of road must be closed, the detour will usually be marginal; however, if a bridge is closed the resulting detour can easily approach tens of miles or more.

In the case of a hazard event, the utility of a bridge structure will be impacted whether or not the structure has sustained damages during the event. The bridges located in the vicinity of a

hazard must be inspected and evaluated for serviceability and safety before they can be cleared for emergency or normal operations. The re-routing of traffic and emergency operations can cause an overload on alternative bridges that have not been directly affected by the incident, but are under-designed for these increased traffic conditions. If a bridge is directly damaged, the severity of the damage and the global impact on the structure can take days to be thoroughly evaluated by visual inspections and the decision to post the bridge, limit the traffic volume or consider it safe relies on the accuracy of such inspections. The use of bridges without first reliably assessing their serviceability and safety should be restricted in all cases due to a possible catastrophic failure of the structure. The bridge should be proven safe to sustain design service loads, but also possibly increased live loads due to emergency operations. On the other hand, unnecessary limitations on a bridge's carrying capacity can also prove injurious to the quick access of emergency equipment and personnel to the affected region.

Bridges are a crucial element for the nation's overall economic and societal well-being. Communities directly depend on a sound bridge network to connect their markets and population to the rest of the country and the world. A comprehensive bridge management program is a crucial step to attaining a safe and reliable bridge network system. The need for evaluating the safety and serviceability of bridges is even more critical in the aftermath of hazard events. Emergency response and recovery operations will usually waste precious time finding detours after a bridge has failed or is closed to traffic due to safety concerns. Thus, in order to safely accommodate resources and fully take advantage of a bridge network's carrying capacity, a reliable post-hazard condition evaluation program is a crucial need.

1.2 State of Bridge Population

The Federal-Aid Highway Act of 1956, signed by president Dwight D. Eisenhower, led to the construction of the current Interstate Highway System. The catalyst for this campaign was national security; however, the benefit for the economy and society as a whole was immense. A growing percentage of infrastructures in this nationwide system are reaching the end of their design life-cycles, and in many cases, improper or a complete lack of maintenance and increasing service demands have further shortened their life-cycles.

The nation's aging bridge infrastructure network represents a significant challenge for providing safe and efficient services for an ever increasing population. According to the American Association of State Highway and Transportation Officials (AASHTO), as of 2010, the average bridge in the United States is 43 years old. The Federal Highway Administration (FHWA) estimates that one in four of the nation's more than 600,000 bridges are deficient with an associated cost of $65 billion to address current bridge deficiencies and other needed improvements (FHWA 2010). These challenges have been at the forefront of transportation authorities' attention in attempting to prioritize maintenance and repair procedures with decreasing available funds. Maintenance and health monitoring of the nation's bridge infrastructure is vital to maintain its purpose and to efficiently allocate limited resources when needed. Figure 1.1 summarizes the condition of the entire bridge inventory of the U.S. according to the Department of Transportation's (DOT) Research and Innovative Technology Administration (RITA). This data raises concerns about the years to come; not only will the bridges get older, but also population growth will increase the burden on these structures. Proper maintenance and monitoring programs are essential to this vast bridge network system in order to prevent it from further degrading.

	2000	2001	2002	2003	2004	2005	2006	2007	2008	2009	2010
TOTAL all bridges	**589,674**	**589,685**	**590,887**	**591,940**	**593,813**	**(R) 590,553**	**597,340**	**599,766**	**601,396**	**603,259**	**604,460**
Urban	133,384	133,401	135,339	135,415	137,598	(R) 137,598	146,041	151,171	153,407	156,305	157,571
Rural	456,290	456,284	455,548	456,525	456,215	452,955	451,299	448,595	447,989	446,954	446,889
Structurally deficient bridges, total	**86,678**	**83,595**	**81,261**	**79,775**	**77,752**	**75,923**	**73,784**	**72,520**	**71,461**	**71,177**	**69,220**
Urban	13,079	12,705	12,503	12,316	12,175	12,600	12,585	12,951	12,896	12,828	12,443
Rural	73,599	70,890	68,758	67,459	65,577	63,323	61,199	59,569	58,565	58,349	56,777
Functionally obsolete bridges, total	**81,510**	**81,439**	**81,537**	**80,990**	**80,567**	**80,412**	**80,317**	**79,804**	**79,933**	**78,477**	**77,412**
Urban	29,398	29,383	29,675	29,886	30,298	31,391	32,292	33,139	33,691	33,743	33,714
Rural	52,112	52,056	51,862	51,104	50,269	49,021	48,025	46,665	46,242	44,734	43,698

Figure 1.1: State of U.S. Bridge Infrastructure (Bureau of Transportation Statistics, 2011).

The data in Figure 1.1 characterizes the normal operating condition of bridges and does not reference any type of hazard events causing failures or deficiencies, which raises another concern related to emergency operations circulating over these bridges. Not only should government agencies evaluate the normal operating conditions of the nation's bridge inventory but also assess the infrastructure's readiness for emergency response operations to safely take place under critical circumstances. There are many natural and manmade hazards that can threaten the structural integrity of a bridge and a comprehensive bridge maintenance program calls for a thorough consideration of these hazards in the overall condition rating of bridges.

1.3 Types of Hazards Causing Bridges Failures

When analyzing bridge failures, it is important to define failure as it relates to the structural utility and integrity of a bridge. Bridge failures are defined as the incapacity of a bridge structure to perform under the design and construction requirements. Due to the implicit structural redundancy of the many elements that make up a bridge structure, failure does not necessarily

imply total collapse. Bridge failures can be further classified in two categories, collapse and distress. Collapse, total or partial, occurs when all or a substantial part of the bridge has fallen. In a total collapse, most of the primary structural members have fallen and no travel lane is passable. In a partial collapse, some primary structural members have fallen and the conditions threaten the safety of those traveling on or under the bridge. Distress is the unserviceability of a structure or its components that may or may not result in a collapse (Wardhana & Hadipriono 2003). Distressed structures are usually more elusive since deterioration occurs over a prolonged period of time, many distress signs are usually hidden from view, and due to structural redundancy, might pass unnoticed to bridge inspectors. Having an understanding of what bridge failures entail, a description of the most frequent hazards causing bridge failure follows.

The most frequent causes of bridge failures are floods and collisions. Other principal causes for bridge failures include overloading, design, detailing, construction, material defects and maintenance. Failures caused by design and/or detailing can be categorized under the same failure class and include a combination of structural load analysis errors and omissions in the design stage and discontinuity or loss of design criteria in the detailing stage. Construction failure occurs when the contractors deviate from details and specifications or when poor workmanship goes unnoticed by the field supervisor. Defective or substandard materials originated by the manufacturer can also cause bridge failure. All of these four failure types briefly described above, are considered internal enabling causes as they are encompassed inside the structure and their deterioration enables failure. Natural hazards, such as floods, earthquakes, fire, ice, and landslides and human hazards such as collisions, vandalism or terrorist attacks are considered external triggering causes of failure since their occurrence takes place on the bridge and trigger its failure. Examples in this class of failure include scour occurrence after a flooding

event, the flood causes scour which triggers foundation settlement or collapse. Failure caused by poor maintenance is classified as a procedural cause which stems from a poor bridge management system unable to provide a safe and effective bridge maintenance program. This cause is usually hidden from public and most of the times remain unpublished by the entity responsible for the bridge. Rarely does one sole failure class cause the failure of a bridge structure; it is their eventual combination that fails a bridge.

Most state governments have virtually no detailed record or databases on bridge failures, so a detailed recollection of the forensics of bridge failures is scarce. It wasn't until 1990, following the 1987 Thruway Bridge collapse, that the New York Department of Transportation (NYDOT), started collecting information and creating a database on bridge failures in the United States. Also, Wardhana & Hadipriono (2003) published a study on the failure of 503 bridges of various types over a period of 12 years, from 1989 to the year 2000. Out of these cases, 456 cases of bridge failure were found from the NYDOT database and only 13% were found from the civil engineering news media (Wardhana & Hadipriono 2003). This publication also revealed that from those documented bridge failures, the dominant types of structures that fail are steel beam/girder and steel truss bridges, combined constituting 50% of the total bridge failures being documented. Figure 1.2 summarizes these results.

Bridge type	Material	Number of failures	Percentage
Arch	—	17	3.38
Bailey	Steel	1	0.20
Bascule	—	2	0.40
Beam/girder	Concrete	29	5.77
—	Steel	145	28.83
—	Timber	13	2.58
Box	Concrete	2	0.40
—	Timber	5	0.99
Box girder	Concrete	9	1.79
—	Steel	3	0.60
Cable	Steel	1	0.20
Corrugated pipe	Steel	4	0.80
Covered	Timber	6	1.19
Culvert	Steel	17	3.38
—	Other	2	0.40
Slab	Concrete	25	4.97
—	Steel	1	0.20
Span	Steel	7	1.39
—	Timber	8	1.59
Stringer	Steel	12	2.39
—	Timber	12	2.39
Truss	Steel	107	21.27
—	Timber	9	1.79
Tied arch	Concrete	1	0.20
Floating	—	2	0.40
Pedestrian	—	2	0.40
Miscellaneous	—	61	12.13
Total	—	503	100.00

Figure 1.2 Type and Number of Bridge Failures 1989 - 2000 (Wardhana & Hadipriono 2003).

The information related to bridge failures triggered by hazard events is also very limited. The NYDOT has taken the first step in developing a more accurate and detailed bridge failure database, however much more work is needed. Due to the infrequency of bridge failures relative to a bridge's life cycle, the effort to document them should require small resources from the bridge owner, private or public.

An observation that can be made from the above discussion is that the data available documenting the failure mechanisms for bridges due to any number of causes, including natural or manmade hazards, is still very limited and is based largely on observations gleaned from failed structures. The analysis of such failures will likely become even more clouded in future years as the bridge inventory continues to age and deteriorate. The interactions between the various and constantly developing damage and deterioration effects with external triggering events are currently very uncertain, and are not likely to become less so in the near future. There is clearly a need for evaluating bridge structures from a global perspective that incorporates the various mechanisms and conditions of damage and deterioration present in the structure at the time it is evaluated in a more transparent manner. As will be shown in the next section, current bridge evaluation methods generally focus on identifying and locating defects, deterioration and damage in a structure in a very local sense. Their effects on the global serviceability and safety of the structure must then be somehow extrapolated from such data. This is clearly not an approach that lends itself to very rapid or reliable evaluations of existing bridge structures.

1.4 Current Bridge Evaluation Methods

Highway bridges are routinely evaluated to assess their condition and to determine their load rating. The objective of these evaluations is to ensure the safety of the structures for normal

service. The following sections discuss the current accepted methods for structural health evaluation of bridge structures.

1.4.1 Visual Inspection

Current bridge inspection and evaluation routines rely largely on labor intensive subjective measures to visually quantify the condition of the various elements that make up an entire bridge system. In the 1990's, the U.S. Department of Transportation FHWA's Recording and Coding Guide for the Structure Inventory and Appraisal of the Nation's Bridges, referred to as the Guide from here on, was used by FHWA officials and state transportation authorities to create a database of the nation's bridge network sufficiency ratings on a per bridge basis. The FHWA set the standards for the implementation of the Guide through the National Bridge Inspection Standards (NBIS), which specified requirements for inspections, frequency of inspections, qualifications of personnel, inspection reports and preparation and maintenance of state's bridge inventories. The Guide was comprised of individual "Items" that provided information about the bridge and its condition in a code-like fashion, assigning a numerical code to each Item. With these coded Items a Structure Inventory and Appraisal Sheet was created including the relevant data portraying the bridge. This information can be summarized in eleven categories: Identification, Structure Type and Material, Age and Service, Geometric Data, Navigation Data, Classification, Condition, Load Rating and Posting, Appraisal, Proposed Improvements and Inspections. After each of the "Items" in the eleven different categories were coded, the Guide provided a "Sufficiency Rating Formula" which evaluated the available data, in numerical code form, by calculating four separate factors to obtain a numeric value which was indicative of the bridge sufficiency to remain in service. The results of this method assigned a percentage to the bridge in which 100 percent represented an entirely sufficient bridge and a zero percent would

represent an entirely insufficient bridge. This database, while representing an improvement in the utilization of bridge inspection and evaluation results for operational and maintenance management decisions for bridges, is still not an ideal source of data for post-hazard evaluations of existing bridge structures. It does serve as a historical record of conditions and performance of a particular bridge that might serve as a component of a more rational bridge evaluation methodology. The obvious limitation of this data is that most of it is based on qualitative data acquired during visual inspection that may or may not be combined with an idealized and generally conservative structural analysis of the bridge.

1.4.2 Nondestructive Load Testing

In 2008 AASHTO published the first edition of The Manual for Bridge Evaluation (AASHTO 2008). The Manual is presently in its second edition, and has incorporated a number of interim revisions. (AASHTO 2011). According to AASHTO (2008), "The Manual has been developed to assist Bridge Owners by establishing inspection procedures and evaluation practices that meet the NBIS" (ASSHTO 2008). The Manual includes eight sections, each representing a distinct phase in the overall bridge inspection and evaluation program. Figure 1.3 shows a condensed summary of the organization of The Manual along with a brief description of the contents of each section.

Figure 1.3 Sumary of the Organization of AASHTO's Manual.

Section 8 of the Manual describes nondestructive load testing methods for bridges. The manual defines load testing as "the observation and measurement of the response of a bridge subjected to controlled and predetermined loadings without causing changes in the elastic response of the structure." (AASHTO, 2011). Although load tests can be used for verifying the

performance and behavior of the bridge at the local (component) or global (system) levels, the emphasis in the Manual is on the use of load testing as a means for load rating of bridges. In other words, load testing is presented as an alternative approach to analytical load rating procedures for bridges.

The Manual notes that there are two basic types of load tests available for evaluating bridges: (1) diagnostic load testing and (2) proof load testing. Both types of load tests involve placing heavy predetermined loads on the structure, usually in the form of loaded dump trucks, and measuring various responses of the bridge such as member strains and displacements. Diagnostic load testing is applicable to bridges for which sufficient documentation exists to develop an analytical model of the structure, and can be used to evaluate factors such as the actual load distribution to the various elements, the physical behavior of the bridge, and how the bridge responds to controlled loads. Diagnostic load testing is also used to validate analytical models of a bridge or to calibrate them to better reflect the measured in-situ behavior. Proof load testing is applicable to bridges where documentation is not sufficient to create an analytical model of the structure, and is used to establish the safe load carrying capacity of a bridge for linear-elastic behavior.

The Manual also includes a discussion of dynamic testing and further classifies such testing into three types: (1) Weigh-In Motion Testing, (2) Dynamic Response Tests, and (3) Vibration Tests. The first two methods are performed in conjunction with the normal operating traffic on the structure, or using known truck loads crossing the bridge at normal operating speeds. These tests are primarily used to support fatigue evaluations of the bridge through characterization of the actual live loads and their corresponding stress ranges, or for determining a more reliable measures of the dynamic load allowance (impact factor) for use in load rating. Vibration tests are

used to establish the dynamic characteristics of the bridge (natural frequencies, mode shapes, and damping ratios). The Manual notes that vibration tests can sometimes be used to evaluate defects and deterioration since they will in turn affect the dynamic characteristics of the bridge.

Because the emphasis of the Manual is condition evaluation and load rating of bridges in support of regular operational and maintenance management decisions for bridges, there is no discussion of the use of such nondestructive testing for post-hazard condition evaluation of bridges. Diagnostic and proof-load testing are obviously not ideal approaches for rapid post-hazard evaluation of bridges given the logistical considerations in executing these tests and the limitation of these approaches to bridges with linear-elastic behavior, and the dangers inherent in subjecting bridges with uncertain conditions and safety margins to heavy loads. Dynamic tests (vibration tests) may be more suitable for this purpose in that the logistics associated with these tests are more suitable for rapid implementations, linear-elastic behavior of the structure can be evaluated by dynamic testing without the need to place heavy loads on the bridge, and dynamic testing can be used to characterize the global behavior of the structure (including the effects of any defects, deterioration and damage) through its measured dynamic properties. The Manual gives no guidance with respect to dynamic testing for post-hazard evaluations of bridges.

1.4.3 Current Post-Hazard Condition Evaluation Methods

The available literature on methods for post-hazard condition evaluation of bridges is relatively limited. Federal agencies lack generalized guidelines on the optimal evaluation procedures for bridges following manmade or natural hazards. The trend leans toward event-specific guidelines covering just one type of hazard, and most of the existing literature only includes repair cost evaluations. Most approaches for post-hazard condition evaluation also limit their application to earthquakes and do not provide a real time condition evaluation of the

structure to assess the structure's ability to safely carry emergency response operations. Their focus is primarily related to forensic evaluations of damaged structures.

In order to fully benefit from rapid condition evaluation alternatives, knowledge on the physics of the parameters being measured is essential. The types of structural damages and their significance in a bridge system are far from being well-understood and defined from a global performance perspective. Only when a structural state can be understood and defined, is it possible to rationally address what to measure and how to directly interpret or relate the measurements to the condition of given structures. Thus, the importance of appropriate modeling of both damaged and undamaged structures for field testing validation is immense.

Another challenge worth noting for post-hazard evaluation alternatives is data management. Since the frequency of hazard events is marginal in the life span of a bridge, it would be uneconomical to continuously monitor the bridge under normal operating conditions exclusively for post-hazard evaluations. However, as mentioned above, a benchmark adequate condition needs to be established first for further comparison with damaged conditions. Thus, a data management program needs to be planed ahead of time in order to fully take advantage of the benefits of sensing without collecting unnecessary voluminous amounts of data. A solution of this problem might be periodic monitoring of the structure to detect any deviations so as to have a recent condition evaluation in the wake of a hazard event.

Clearly, more work needs to be done to standardize post-hazard condition evaluation standards. Given the above challenges and the ad hoc nature of current post-hazard condition evaluation techniques, the motivation for comparing and evaluating different structural characterization approaches of bridges through dynamic testing, the overarching topic of this research thesis, will now be introduced.

1.5 Motivation

1.5.1 Limitations of Visual Inspection for Evaluating Bridges

The relation between visible signs of damage and the corresponding condition and soundness of the structure is often very difficult to establish. There might be a dramatic difference in the meaning of a certain visual damage for a steel, pre-stressed, or a normally reinforced concrete bridge, and often, the effect might be observed but the decision making has to be carried out based on heuristics and experience (Catbas and Aktan 2002). Current bridge inspection programs are performed with significant subjectivity introduced by the inspectors. The Manual provides qualification requirements for the personnel in charge of the organizational unit given the responsibilities for bridge inspection, reporting and inventory and for the individual in charge of a bridge inspection team. However, the persons carrying out the inspection need only, as a minimum, to be a Level I safety inspector under the requirements of the National Certification in Engineering Technologies (NICET). This Level I qualification requires minimal relevant experience or entry-level training in bridge safety inspection (NICET 2004). Even though Level I inspectors are closely verified by their supervisors, Level III or IV inspectors, this practice still introduced subjectivity when rating a bridge and makes the bridge inspection process inefficient due to the required scrutiny by the supervisors in order to guaranty representative and consistent inspections, ratings and reports.

Even though The Manual addressed many of the Guide's shortcomings and provides the guidelines for a much more comprehensive bridge inspection program, some challenges remain unaddressed for a reliable, consistent and rapid structural health monitoring program suited for post-hazard conditions. The condition of each element is still rated qualitatively. Their condition is defined in engineering terms and based on a scale of one to five, one representing perfect

condition and five advanced deterioration, and it is left to the judgment of the inspector to assign a numerical value to these element condition descriptions. Thus, the level of expertise of the inspection personnel is a key factor for obtaining representative condition ratings. Because of this, the variability of the condition ratings between inspectors is high; an element might visually seem in good or adequate condition for an inexperienced inspector but poor or damaged for a more experienced one, or vice versa. Man power, time and cost are also associated flaws of current visual inspections supported by the NBIS.

Also, no guidance is provided as for what types of inspections are adequate for post-hazard conditions, in which partial failure of the structure might have occurred but is hidden for visual inspection. As already mentioned, structural elements of a bridge system do not perform independently, but interact with other elements to form one structural system. Thus, visual inspections will not fully characterize the severity, of the damages caused in the aftermath of a hazard event.

Given the needs of the nation's approximately 600,000 bridges and current financial limitations, an adequate standardized bridge inspection system is paramount. Besides routine inspections, the need of a post-hazard inspection system that allows rescue operations, engineers, and highway officials to act safely and quickly is crucial. In such adverse conditions, the unnecessary posting of a bridge can limit the accessibility of emergency operations to affected areas, which outweighs the benefits of current excessively conservative load carrying capacity evaluations. Furthermore, current visual inspections are neither rapid nor remote, requiring hours, if not days, to evaluate the condition of the bridge and personnel needs to be in site to perform the inspection. In post-hazard conditions time is of the essence and access to the bridge cannot be assured. Catbas and Aktan (2002) suggest that if a spectrum of appropriate

experiments and indices are integrated within a structural characterization framework, and the structure is monitored for a sufficiently long time, it is possible to accomplish successful condition and damage assessment. Civil engineers have become cognizant of the limitations in their current practice for condition assessment based on visual inspection solely and more reliable and versatile methods will enhance current inspection practices.

1.6 Objectives and Scope

1.6.1 Introduction

This research thesis evaluates and compares different dynamic bridge condition evaluation techniques in a Structural Health Monitoring (SHM) framework. Most of the emphasis will be focused on evaluating alternatives suited for quick and reliable post-hazard condition evaluations. Three specific dynamic testing methods will be evaluated and compared: (1) ambient vibration testing, (2) impact hammer testing, and (3) shaker vibration testing. All of these tests will be performed in two fundamentally different full–scale and in-service bridges near Fayetteville, AR. The structural and operational characteristics of both structures will be introduced in more detail in Chapter 3. Each type of test's suitability for quick and reliable post hazard evaluation will be evaluated and recommendations will be made based on each test's attributes and limitations. The research described herein is funded by the Department of Homeland Security (DHS) through the MBTC DHS 1104 project entitled Structural Health Monitoring and Assessment of Critical Intermodal Transportation Infrastructure Assets. The overall objective of that project is to investigate and evaluate the use of SHM methods to overcome the challenges introduced earlier in this chapter.

This particular research thesis is a follow up of Herman's (2011) research thesis, "Laboratory Evaluation of Dynamic Characterization Methods for Rapid Condition Assessment of Bridges".

In his research, Herrman performed laboratory investigations of dynamic characterization tests using two small-scale physical model structures. The major objective of the research was to recommend an optimum bridge health monitoring strategy using dynamic testing suited for rapid and reliable post-hazard structural condition evaluation. In order to reach this objective, three additional objectives were created. First, the effectiveness of different types of dynamic testing, different instrumentation schemes and different data acquisition methods were evaluated. The optimum sensor quantity required for representative measurements was subsequently studied. The last objective was to obtain a load rating from the flexibility matrix extracted from the dynamic testing. These objectives were evaluated in conjunction with the laboratory model structures for undamaged and several controlled damage scenarios to assess the variability of the results.

This proposed research thesis will build on Herrman's research thesis and will further extend the study outside laboratory conditions. Because this research thesis will be performed for in-service bridge structures, the study will not include evaluation of induced damage and will only characterize the parameters under as-is conditions having knowledge that the bridges are performing safely. These measured parameters will be taken as the benchmark condition state of the bridges. To reach this research's overarching objective, two specific objectives are established for this study:

- Comparison of modal parameters extracted through the proposed test methods
- Optimum SHM Strategy

Each of these objectives will be explained in more detail below.

1.6.1.1 Comparison of Modal Parameters extracted from the Proposed Test Methods

The three different dynamic testing methods that are compared and evaluated in this research include ambient vibration testing, impact hammer testing and shaker testing. Chapter 2 describes the principal characteristics of each of these test methods and provides a review of the literature related to their application for evaluating bridges. For each test, two full scale structures will be instrumented with accelerometers and data will be collected and processed. From the processed data the modal parameters of each structure will be extracted and compared against the other test methods. These parameters include natural frequencies, mode shapes, damping and modal flexibility (for impact and shaker tests only). Modal parameters are unique to every structure and can be regarded as a structural signature which deviations reflect alterations affecting the entire structure. It is intended to compare the parameters extracted through each test and reveal any discrepancies between test methods. A high degree of reproducibility of the modal parameters is expected for each test method performed on the structures. However, based on the fundamental differences of controlled tests, i.e. impact and shaker, and uncontrolled test, ambient vibration, the modal parameters estimated will inevitably contain some variance. The characteristics of both types of tests, controlled and uncontrolled, and their influence in modal parameter extraction / estimation will be further developed in the following chapters.

1.6.1.2 Optimum SHM Strategy

Having processed all the data and evaluated the different diferent modal parameters obtained from the field tests, recommendations will be made to reveal the suitability of each testing condition for each of the structures being tested. Because the selected bridges are known to have vast different structural characteristics, it is believed that the extraction of representative modal

parameters for both bridges will directly depend on the test method being implemented. Also, the tests will be compared and rated in terms of:

- Overall testing time:
    - This includes set up and pick up time as well as the duration of the actual test.

- Ease of performing the Test:
    - The technical and logistical issues associated with each test.

- Required data processing effort:
    - Each test requires different algorithms for the processing stage, each posing different challenges.

- Reliability and precision of the results.
    - Any significant limitations on the quality or accuracy of each method's results will be highlighted and recommendations will be made accordingly.

After a thorough comparison has been made on the mentioned categories and each test's adequacy is rated according to each structure, an overall evaluation of the suitability of each test will be made on a SHM framework. An optimum SHM strategy capable of reliable and rapid structural condition evaluation will then be suggested supported by the results obtained from the field tests.

1.6.2 Scope of Work

The scope of this study encompasses full-scale, in-service bridges under operative environmental conditions and applies to structures having similar structural characteristics as those of the two selected bridges; a three span pony truss bridge and a ten span steel stringer bridge. Only one span on each bridge will be tested. The selection of two such different structural systems was made to reveal any unique characteristics of the bridges by using the same testing methods on both structures. The longest span being tested measures 100 ft., thus the results of this study are representative of short to medium span length bridges. As mentioned above, the current operative condition of the bridges will be evaluated and no induced damage scenarios will be included. The measured parameters will be assumed to be representative of satisfactory service conditions. Studies such as temperature effects and soil-foundation interaction are beyond the scope of this research thesis. This research thesis overall scope will address the challenges for a rapid and reliable post-hazard condition evaluation of operative structures similar than the ones being tested through the use of the mentioned dynamic tests.

1.7 Organization of Thesis

The following chapters of this thesis will be organized as follows. Chapter 2, “Background and Literature Review”, includes a tailored literature review providing an overview to the relevant topics of this research. The flaws of current visual inspection routines supported by the NBIS, already introduced in this chapter, will be backed up with available references. The available alternatives for post hazard condition evaluation with the most potential will be introduced, and the focus will be limited to full scale testing, as localized condition evaluation falls outside of the scope of this research. The chapter will conclude with an overview of the available full scale dynamic testing literature resources. The characteristics and deliverables of

the two categories of dynamic testing, ambient vibration and controlled vibration testing, will be studied and their fundamental differences will be outlined making reference to accepted literature resources among the modal testing community. Chapter 3, "Experimental Program", will provide an outline of the tasks and stages of the proposed field test along with a description of both test specimens. The design and execution of field tests will also be explained in this chapter. The achievement of final results for each test type will be depicted using flow charts, including all stages from data collection to modal parameters extraction, along with explanations for each of these stages in the data processing phase. Chapter 4, "Results", will present the findings obtained from the field tests for each of the two structures. These results include: natural frequencies, mode shapes, damping ratios, modal scaling and modal flexibility. Any observed discrepancies between test methods performed on a same bridge will be analyzed and any highlighted characteristics between the two structures will be evinced. The final chapter of this thesis, "Conclusion and Future Work" will assess the achievement of the proposed deliverables and objectives and will suggest an optimum post hazard condition evaluation for structures similar to the ones tested. Any future work that the researcher deems necessary due to limitations on the experimental findings will also be suggested in this chapter

2 Background and Literature Review

2.1 Introduction

This chapter presents, through review and analysis of the literature, the relevant issues associated with the research described in this thesis. Chapter 1 introduced conventional approaches for evaluating bridges, both for routine inspection and for post-hazard evaluations. The limitations associated with current routine inspection practices will be highlighted in this chapter using available literature. Conventional alternatives for the evaluation of bridges that are suitable for post-hazard condition evaluation applications are reviewed, and the associated limitations and challenges of these alternatives are discussed. Many of these approaches focus mainly on localized damage scenarios and rely on subjective visual inspections. Full-scale testing and evaluation methods are also reviewed. The available full-scale testing methods can be categorized into static load testing and dynamic testing methods. Dynamic testing methods have important experimental, logistical and practical advantages over static load testing for many

bridge evaluation objectives, and the two main dynamic testing approaches are described through relevant studies. The two main dynamic testing approaches that have been employed on bridges are experimental modal analysis (EMA), which is also referred to as forced-vibration testing, and operational modal analysis (OMA), which is also widely referred to as ambient vibration testing. A separate section on the development and implementation of modal flexibility for damage detection in full-scale dynamic testing is presented towards the end of this chapter.

2.2 Issues with Visual Inspection Methods for Bridge Evaluation

The visual inspection methods used for evaluating bridges were introduced in Chapter 1. The lack of guidelines for more robust evaluation methods above and beyond visual inspections for post-hazard evaluations of bridges, referred to as "Damage Inspections" in the Manual for Bridge Evaluation (MBE) (AASHTO, 2011), is notable. The following section describes specific limitations associated with visual inspections. The most promising conventional alternatives suitable for post-hazard condition evaluation are also discussed along with any limitations these techniques may have.

2.2.1 Visual Inspection

According to a 2010 report by the USDOT, the FHWA lacks the criteria and guidance necessary to determine states' compliance with bridge inspections standards (FHWA, 2010). Inconsistencies in FHWA's enforcement of bridge inspections standards under the National Bridge Inspection Program (NBIP) are attributed to a lack of standardized criteria defining how bridge engineers and federal agencies should assess states' overall compliance with the NBIP.

Phares et al. (2004) present the results of a comprehensive study that evaluated the accuracy and reliability of routine highway bridge visual inspections. The writers found that all structural condition documentation is collected with significant variability. Particularly, "95% of primary element condition rating for individual bridge components will vary within two rating points of the average and only 68% will vary within one point" (Phares et al., 2004). The authors also point out that the documentation based on the element ratings and handwritten field notes and photographs are often used to assign a "low" condition rating and many times attempt to fully describe the condition of the bridge. Another significant finding from this study was that the variability in field inspections is most prominent in the assignment of condition ratings and that the NBIS condition rating system definitions may not be sufficiently refined to allow reliable routine inspection results. Although the focus of this study was routine visual inspections, it is reasonable to assume most of these limitations along with others would be applicable to damage inspections of bridges.

An excessively conservative inspection routine can also unnecessarily limit the load capacity rating for a bridge. Lenett et al. (1999) performed a series of nondestructive field tests and visual evaluations of a decommissioned bridge comprised of steel girders supporting a reinforced concrete deck in Ohio. The load rating calculated for the bridge using visual inspection data and the then current Ohio DOT rating procedures indicated that the bridge could only support truckloads of 57,192 lbf. However, the objective data acquired from static load testing of the bridge, which was subjected to truckloads of 63,400 lbf, revealed maximum superstructure deflections and live-load stresses that were well within AASHTO limits. The experimentally derived load rating implied that the bridge could support loads much greater than those computed

using standard AASHTO load rating procedures. Restrictions to the load capacity rating based on overly conservative and subjective evaluations could prove problematic for facilitating the emergency response and recovery operations that follow hazard events.

In addition to the issues discussed above, other limitations associated with the visual inspection practices for bridges mainly relate to the visual inspection stage. Visual inspections are neither rapid nor remote. Also, the relation between such visible signs of damage and the corresponding condition and soundness of the structure is often very difficult to establish. There might be a dramatic difference in the meaning of a certain visual damage for a steel, prestressed, or a reinforced concrete bridge, and often, the effect might be observed but the decision making has to be carried out based on heuristics and experience (Catbas and Aktan, 2002). This leads to another issue: the qualifications of inspection personnel. The persons carrying out the inspection only need to be a Level I safety inspector under the requirements of the National Certification in Engineering Technologies (NICET). This Level I qualification requires minimal relevant experience or entry-level training in bridge safety inspection (NICET, 2004). Even though Level I inspectors are closely guided by their supervisors, Level III or IV inspectors, this practice still introduces subjectivity when evaluating and rating a bridge and makes the process inefficient due to the required scrutiny by the supervisors in order to ensure representative and consistent inspections, ratings and reports.

Catbas and Aktan (2002) also suggest that if a spectrum of appropriate experiments and indices are integrated within a structural identification framework, and the structure is monitored for a sufficiently long time, it is possible to accomplish successful condition and damage

assessment. Civil engineers are also becoming increasingly cognizant of the limitations in their current practice for assessing the condition and safety of bridges based on visual inspection.

2.2.2 Post-Hazard Evaluation of Bridges

Literature on condition and safety assessment procedures for damaged structures in the aftermath of hazard events is limited. Federal agencies lack general guidelines on the adequate procedures following a manmade or natural hazard. The trend leans toward event specific guidelines covering just one type of hazard and most of the literature only discusses repair cost evaluations. Some methods are being developed that are potentially applicable for post hazard condition evaluation, however, their application to this specific purpose remains unstated.

Makie et al. (2009) evaluated how damage and decision models link the structural response to decisions on repair actions and costs on current bridges owned and maintained by the California Department of Transportation (Caltrans). The authors note that probabilistic evaluation of the performance of these bridges under rare, but strong, ground motions is essential for successful evaluation of the entire regional transportation network performance during and after an earthquake. The authors evaluated the performance of bridges at the demand, damage, and loss levels using the Pacific Earthquake Engineering Research (PEER) center's probabilistic Performance-Based Earthquake Engineering (PBEE) framework. This publication highlights that the efficacy of next-generation bridges needs to be evaluated at the performance level, in quantities such as repair time, down time, and traffic carrying capacity, not in terms of traditional engineering quantities so widely used in current visual inspections. This approach is limited in its application to earthquakes, and does not provide a real-time condition evaluation of the structure to assess the structure’s ability to safely carry emergency response operations.

Glaser and Tolman (2008) introduce an alternative in which proactive interventions can be made in real time when structural performance indicators start to deviate. These performance indicators are monitored with transducers placed in the structure. However, the authors highlight that only if the physics of the measured parameters are well understood can appropriate transducers with the necessary features be developed. Benefiting from the versatility of micro-electromechanical systems (MEMS) technology, the authors redefine the term "sensor", previously viewed as synonymous with the term transducer, to describe a MEMS unit comprising the traditional transduction elements along with substantial signal processing, computational ability and wireless communication. These individual units can further be combined into smaller-than-full-scale comprehensive sensing platforms called Motes, which can be further combined into a large, organic, network capable of dense and detailed sensing. Mote networks are well suited for any sudden or temporary monitoring situation. Therefore, their potential use in emergency situations under adverse and post-hazard event conditions is promising. However, for large operational civil structures, the noise levels are usually large whereas the signals from localized damage are small, resulting in a small S/N ratio. This problem can be solved by using spatially dense sensing networks of wireless Motes since the resulting finer resolution supplies additional information whereas the noise remains constant.

A major challenge in evaluating the state of damaged civil engineering structures lies in creating robust condition models. For most typical civil engineering structures under normal operating or even hazard conditions, there are no reliable models for predicting induced damages. The types of structural damages and their significance in a bridge system are far from being well-defined and understood from a global performance perspective. It is possible to

rationally address what to measure and how to directly interpret or relate the measured signals to the condition of given structures only when a structural state can be defined and understood (Glaser and Tolman, 2008). The goal of structural state identification through models is to infer characteristics of structural systems, which cannot be measured directly, through the correlation of mathematical models and experimental response data. In case the performance parameters of a structure under optimal operating conditions are not known, FE models are used to extract them and then a comparison is made between them and field tests results. Thus, the importance of appropriate modeling of both damaged and undamaged structures for field tests assurance is immense.

Another challenge worth noting for post-hazard evaluation alternatives is data management. Since the frequency of hazard events is marginal in the life span of a bridge, it would be uneconomical to continuously monitor the bridge under normal operating conditions. A benchmark condition needs to be established first to facilitate future comparisons and evaluations with a damaged condition. Thus, a data management program needs to be planned ahead of time in order to take full advantage of the benefits of sensing without collecting unnecessarily voluminous amounts of data. A solution of this problem might be periodic monitoring of the structure to detect any deviations so as to have a recent performance evaluation in-hand when a hazard event occurs.

Much research has also been performed on remote sensing techniques. For example, researchers from the Michigan Technological University evaluated commercially available remote sensing technologies for assessing highway bridge condition. The technologies evaluated included ground penetrating radar (GPR), spectral analysis, 3D photogrammetry, electro-optical

(EO) satellite and airborne imagery, optical interferometry, LiDAR, thermal infrared, acoustics, digital image correlation (DIC), backscatter and speckle radar, InSAR and high resolution "Street View- style" digital photography (Ahlborn et al., 2010). Most of these techniques only provide a visual assessment of the surface condition of the deck, CoRe elements and subsurface elements. Only EO satellite and airborne imagery, optical interferometry, and LiDAR visually monitor the global condition of the bridge. However, these techniques fall short on quantitatively evaluating the actual performance or safety of a bridge, since they rely mostly on pictures of the structure and point out localized damages only.

Clearly, more work needs to be done to standardize post-hazard condition evaluation methods. Knowing the challenges and the capabilities of available sensing technologies will prove vital for comprehensive bridge management systems to be able to respond under such adverse conditions and provide a safe and efficient bridge network. Given the above challenges and the *ad hoc* nature of current post-hazard condition evaluation techniques, the motivation for comparing and evaluating different full-scale structural characterization approaches for bridges is evident.

2.3 Full-Scale Testing

The benefits of performing full-scale testing on bridge structures include a more robust characterization of the global structure, damaged or not, and the quantitative versus qualitative descriptions of condition and performance that are available from the test results. Also, if a baseline description of the global response of a bridge can be obtained when it is in good condition, subsequent full-scale tests could provide a globalized assessment of the structure with considerably less effort and time than visual inspection based assessments would require. The

following sections will discuss two available full-scale testing methods for bridges: static load testing and dynamic testing. For the latter, two subcategories will be further explained; Experimental modal analysis (EMA) or forced-vibration testing, and operational modal analysis (OMA) or ambient vibration testing. A common practice in full-scale testing applications is to validate the experimental results using analytical or finite element (FE) models. Numerous publications exist on the many approaches for developing representative FE models of civil structures. However, the development of a FE validation model is beyond the scope of this research thesis and thus no emphasis will be made on reviewing literature in this area.

2.3.1 Static Load Testing

Section 6 of the MBE (AASHTO, 2011) describes standard procedures for determining the load capacity of existing bridges. The Manual offers methodologies for establishing the load rating using the Load and Resistance Factor Rating method, which is consistent with the current design approach used for new bridge structures, and methodologies using Allowable Stress Rating and Load Factor Rating approaches. It has been shown that these load rating methods are conservative in most cases. FE models can also be developed to find the reactions on different CoRe elements in the bridge and then the bridge's load capacity can be extrapolated using the resulting data; however, FE models are based on a number of simplifying assumptions and idealizations. Alternatively, static load testing using known truck loads can be performed to quantitatively characterize a bridge at its global level, validate FE models and calibrate load rating results. The structural stiffness parameters of a bridge can also be identified through static load testing. Although there are many papers available in the literature related to static load

testing, only a few key papers relevant to the scope of this study and to the types of bridge specimens selected are reviewed in this section.

Bowen (2003) conducted a quasi-static load test study on the Llano Bridge in Llano, TX, to compare field measurements with standard load rating methods and finite element model results. The bridge evaluated was a Pratt truss with a polygonal top chord. The trucks used for the testing approximated AASHTO HS20 loading. Strain gage data were taken and converted into member stresses. The longitudinal members of the floor system were instrumented with strain gages to obtain the actual load distribution. The field test data showed that the load-related moments in the floor beams and stringers were significantly lower than predicted by the standard AASHTO load rating. The field test data also showed load stresses smaller than predicted by the FE model of the bridge floor system.

Sanayei et al. (2012) performed static load NDT of the Vernon Ave. Bridge in Barre Massachusetts for a baseline FE model validation and an AASHTO load rating calibration. The bridge was a continuous three-span concrete slab on steel stringer bridge, a triaxle dump truck served as the load test truck. The study showed that load rating factors obtained using NDT data were higher than conventional load rating factors attributable to the FE model and the AASHTO provisions.

It can be concluded that field test data characterizes the structural behavior of bridges in a more accurate way than FE models or AASHTO load ratings do. However, this testing method is inadequate for damaged structures under critical post-hazard conditions. First, there is an inherent risk in placing large static loads on bridges with uncertain damage conditions or load capacities for the purpose of evaluating the load capacity. In such cases, the testing must be

carefully designed and executed, and the corresponding structural responses must be monitored closely. There is also the potential that the static load test might lead to additional structural damage being inflicted to the bridge which may not be evident initially, but may lead to a rapid deterioration and sudden collapse after the test is concluded. This requires bridges that have been the subject of a proof load test to be monitored periodically. This concern presents an even greater risk for already damaged structures. Static load testing is clearly not an approach that can be implemented rapidly and without significant care for bridges that may have been damaged as a result of a hazard event. Furthermore, the instrumentation employed for static load testing typically includes strain gages and sometimes displacement gages. Both sensor types can be time consuming and expensive to install on a bridge, and the use of displacement gages can require construction of an external reference frame.

Baraka et al. (2005) monitored bridge deformations during static load testing of the Maadia Bridge along the Northern International Coastal Road in Egypt. The authors stated the technical difficulties they encountered while measuring the structure's displacement. The deformation of the bridge was measured by using mechanical dial gauges (deflectometers) fixed between the bridge beams and a metal or wooden frame stationed in the ground. The authors note that in cases where the bridge crossed over a body of water or raised its span tens of meters above the ground, the installation of the deflectometers was extremely difficult and expensive. Also, any settlement in the ground below the frame may affect the mechanical dial gauge reading and any deformation in the frame due to observer weight may affect the dial gauge reading. Under these conditions, other means of deflection measurements should be sought.

There are other problems associated with static load testing. If strain gages are used to measure structure responses, the potential for errors due to temperature effects, nonlinearities, and electronic noise need to be dealt with and controlled. Finally, there are also logistical requirements associated with static load tests, such as: time and access equipment to install the sensors on the structures, traffic disruptions, and personnel to position the test loads on the structure, which eliminates any chance for remote testing. Static load testing does addresses many of the flaws encountered in localized visual inspections and the limitations of some local NDT techniques. However, this technique is not appropriate for rapid and remote condition assessment of damaged structures under critical post-hazard conditions.

2.3.2 Full-Scale Dynamic Testing

The following sections describe the fundamentals of full-scale dynamic testing for bridges. Two distinct categories of dynamic testing are addressed, namely operational modal analysis (OMA) and experimental modal analysis (EMA). In both test approaches, the usual objective is to identify the modal parameters of the structure. The modal parameters include the natural frequencies, mode shapes and damping ratios. These are global characteristics of the structure and are directly related to the mass and stiffness properties of the structure. Theoretically, changes to the structure due to damage can be detected by identifying changes in the modal parameters. It is also possible to obtain an approximation of the stiffness matrix for a bridge experimentally using the identified modal parameters. This approximate measure is possible for certain types of dynamic testing and is referred to as modal flexibility. The identified modal flexibility matrix is advantageous in that it quantitatively describes the in-situ performance of a

structure in a manner that automatically incorporates the effects of any deterioration or damage that may be present in the various structural components on the global behavior of the structure.

The basics of each of the test approach will be described in the following sections including: the fundamental assumptions, source of dynamic excitation, execution of the test, data processing methods, and the typical results obtained. The advantages and limitations of each type of test are also described. Each of these test approaches is also described in the context of relevant studies.

2.3.2.1 Operational Modal Analysis

Operational modal analysis is one of the most commonly used testing techniques for characterizing the dynamic properties of an in-situ bridge structure. This dynamic testing approach is also widely referred to as ambient vibration testing (AVT). In OMA testing, only the vibration responses of the bridge are measured while the structure is dynamically excited by ambient natural sources such as wind and micro tremors, and by operating traffic loads. The dynamic excitation is not controlled or measured, but is assumed to be stationary and uncorrelated Gaussian white noise. The dynamic excitation is also assumed to be spatially well-distributed on the structure. The bridge's vibration responses are measured with accelerometers deployed on a stationary or roving instrumentation scheme. In the latter scheme, a limited number of reference accelerometers are left at the same locations for each roving setup and are subsequently used to stitch together the measurements recorded from the different setups.

Once ambient vibration data is collected, there are numerous ways to process the data for identifying the modal parameters of a structure. The following discusses some of these

approaches from the literature that are from studies that are similar in nature to the research performed for this thesis.

Rainer and Pernica (1979) determined resonant frequencies of a three span, flat slab post-tensioned bridge in Ottawa Canada subjected to ambient vibration from peaks in the Fourier spectra. Damping values were estimated form the Half-Power Bandwidth (HPBW) method. However, Abdel-Ghaffar and Housner (1978) discussed the difficulties encountered when estimating damping values by applying the HPBW method on ambient vibration measurements due to closely spaced spectral peaks and spectral overlap that caused widening of the peaks resulting in damping overestimation.

Piombo et al. (1993) reported modal parameter estimation using the Auto-Regressive Moving Average Vector (ARMAV) method. This technique can be applied when the excitation is not exactly known, but only mean and standard deviation are known. The method was tested using vibration data obtained from a one-span concrete bridge excited by its operational traffic. Good agreement was found between modal parameters estimated by the ARMAV method and those from typical modal analysis procedures, such as the frequency domain Peak Picking (PP) technique.

Amussen et al. (1998) used the random decrement (RD) technique to identify the dynamic properties of the Vestvej Bridge in Denmark subject to ambient vibration. First, auto and cross correlation functions were estimated using the RD technique. This technique was first verified on a laboratory structure as described in Ibrahim et al. (1996). To enhance this method's speed, the authors developed a vector triggering system for the RD technique which was shown to be five times faster than conventional RD techniques. The polyreference time-domain curve fitting

algorithm and the Ibrahim time domain curve fitting methods were then applied random decrement signatures to estimate the modal properties of the bridge.

Ren et al. (2004) performed experimental and analytical analysis of the Tennessee River Bridge, a steel arch structure, by ambient vibration testing. The modal parameters were identified using several modal identification techniques including: PP from the Power Spectral Densities (PSD), ARMAV, the natural excitation technique (NExT) (James et al., 1993) and Stochastic Subspace Identification (SSI). The authors note that the SSI is an "incredibly difficult procedure to explain in detail in a short way, in particular, for civil engineers who are not familiar with control engineering where the SSI stems from" (Ren et al., 2004). However, the authors conclude that the SSI method provides much better mode shapes than the PP method because the SSI can construct a stabilization diagram in an effective way aiding in the selection of true modes instead of those related to operational deflection shapes.

Finally, Brincker et al. (2001) introduced a new frequency domain technique called Frequency Domain Decomposition (FDD) for the modal identification from ambient responses. This technique is closely related to the classic approach where the modal parameters are estimated by implementing a PP routine to the spectral densities in the frequency domain. However, by introducing a decomposition of the spectral density function matrix, the response can be separated into a set of single degree of freedom systems, each corresponding to an individual mode. By using this decomposition technique, closely spaced modes in the frequency domain can be identified with high accuracy even in the case of strong noise contamination of the signals.

One major advantage of OMA is its ease of implementation. Since only output measurements are required, only a small crew is required for instrumenting the structure, the test data can be collected continuously and/or remotely, and the testing does not interfere with traffic. Also, the test utilizes freely available dynamic excitation from the environment and operating traffic, so large and expensive dynamic excitation devices do not need to be placed on the structure. Another key advantage is the wide range of frequencies that are exited using this approach. It is especially effective for identifying very low frequencies which are frequently difficult to excite with mechanical excitation devices. The ambient excitation of the structure is assumed to consist of an almost infinite number of harmonics with different periods of vibration, thus providing a large range of excitation. Every harmonic component whose period corresponds to a natural period of the structure is amplified in the measured responses due to resonance. The modal parameters that can be extracted from this test include natural frequencies, damping ratios and operational mode shapes.

OMA also has some significant limitations. One particular limitation is related to the actual nature of the dynamic excitation. Although the dynamic excitation is unmeasured and uncontrolled, it is assumed to be uncorrelated and stationary white noise. This assumption is accurate in many cases; however, the random operating traffic is typically the most dominant source of dynamic excitation for an in-service bridge. The traffic related excitation is most definitely band-limited and is not likely to have the comparable excitation levels for the full frequency band of interest for many structures. This may require a longer testing duration to average out uncertainties, such as those due to the random mass and position of traffic on the structure. This could be especially significant for short to medium span bridge structures. This

type of testing is also limited by the fact that since the excitation is unmeasured, mass unit normalized mode shape vectors cannot be obtained. Pre- and post-multiplying the mass matrix by mass unit normalized mode shape vectors results in the identity matrix. Such scaling of the modal vectors is required for estimating the modal flexibility matrix for a structure, and this is generally accomplished through forced-vibration measurements in which both the inputs and outputs are measured.

Bernal (2004) published a paper on modal scaling from known mass perturbations. A consequence of the lack of deterministic information on the input in ambient vibration testing is the fact that the scaling constants that connect the eigensolution to the physical system matrices are not determined during the identification. The information needed to make up for the loss of deterministic input, the author says, can be obtained either from a priori knowledge on the system or from the realization of complementary tests. While this represents a workaround to the lack of known input, it is not likely to be a very practical approach for structures with uncertain structural condition. Furthermore, it removes many of the logistical and experimental advantages associated with the ambient vibration testing method.

2.3.2.2 Experimental Modal Analysis

Experimental Modal Analysis (EMA) is a type of full-scale dynamic test in which the dynamic excitation forces acting on the structure are controlled and measurable. It is typically performed by exciting the structure with linear or eccentric mass shakers, or using instrumented impact or drop hammers and measuring the corresponding response of the structure. In this type of test, both the measured dynamic excitation and the vibration responses of the structure are typically used to formulate frequency response functions (FRF) along with the other signature

dynamic characteristics of the structure. Under EMA tests, the magnitude of the input excitation typically dwarfs environmental noise excitations, thus allowing the extraction of more consistent and reproducible modal parameters.

Linear mass electrodynamic shakers can produce a wide variety of excitation signal functions. These excitation signals usually consist of random, burst random, pseudorandom, periodic random, chirp, and swept-sine signals. These functions usually act throughout much of the time window providing a good signal to noise ratio. Random signals are advantageous in averaging out nonlinear responses; however, they distort the FRF near resonance if Hanning window is applied in the data processing stage. Burst random signals do not require a window to stop signal leakage, however, this input requires many averages and is not as good as random for averaging out nonlinear responses. Pseudorandom signals offer the best signal to noise ratio and fewer samples are needed, though this deterministic signal does not average out nonlinear responses. Both periodic random and chirp signals do not require a window to stop leakage, however periodic random averages out nonlinear responses while the deterministic signal of a chirp signal does not. Chirp signals offer good signal to noise ratio and fewer/faster samples are needed, in contrast with the periodic random signal where many averages are required and settling time is required before collecting each different pseudorandom time block. For swept-sine excitations, the signal sweeps through a pre-determined frequency band. The amplitude and period of the signal can be adjusted when creating the signal or through waveform generators with an amplifier capable of this options. As will be shown in Chapter 3, some windowing techniques can be applied to the swept-sine signal to obtain a better frequency domain representation of the signal.

Most bridge structures are, at least, slightly nonlinear and one advantage of shaker testing over impact hammers is that shakers provide lower amplitude input forces, thus minimizing the excitation of system nonlinearities. Data processing efforts for response data containing high degrees of nonlinearity are considerably greater than those minimizing the nonlinear responses. If the shaker input is a random forcing function, this function provides the best linear approximation, in a least squares sense, of the FRF for the specified input conditions by averaging out nonlinear responses (Mayes & Gomez 2006).

When conducting an impact hammer test, the impulsive excitation stimulates a broad range of frequencies in the structure thus exciting a broad range of structural mode shapes. The frequency band and amplitude of the impulse excitation can be modified to some extent by placing rubber tips with different hardness values on the hammer. These tips range from soft, providing an input force over a longer time window thus exiting lower frequencies, to stiff, which provide an input over a much shorter time window thus exciting higher frequencies. Using too small of a frequency range will limit the modes captured, while using too large of a range may excite nonlinearities of the system present at higher modes, as well as not put as much energy into each of the individual modes (Herrman 2011). The mass can also be adjusted on most instrumented hammers providing for some additional control of the excitation force provided. The force with which the impact is applied to the structure should also be taken into consideration in order not to over range the sensors' capacity or cause nonlinearities in the structure, or not impart enough force to adequately excite the structure.

In a number of test cases, FRF measurement data with only one reference DOF will contain sufficient information to extract modal parameters. The assumption is that the selected reference

DOF contains information about all the modes, which is to say that the reference DOF is not in a nodal position for any mode. In practice, this means that all the modes are not buried in other modes or noise in the FRFs. In order to identify a proper reference DOF, some pre-testing often has to be performed. For a hammer test (roving), this means that only one response DOF is needed, i.e., only one accelerometer position (point and direction). For a shaker test (fixed), it means that only one excitation DOF is required, i.e., only one shaker position (point and direction). If all reference (output) locations are also input locations, a full FRF matrix is obtained.

MIMO testing consists of a multi-reference test. More shakers are used to simultaneously excite the structure at more DOFs, resulting in measurements of more columns of the FRF matrix. The main advantage of MIMO is that the input force energy is distributed over more locations on the structure. This provides a more uniform vibration response over the structure, especially in cases of large and complex structures and structures with heavy damping. In order to get sufficient vibration energy into these types of structures, there is a tendency to 'overdrive' the excitation DOF when only a single shaker is used. This can result in non-linear behavior and deteriorates the estimation of the FRFs. Excitation in more locations often also provides a better representation of the excitation forces that the structure experiences during real-life operation.

As is the case for OMA, there are numerous data processing techniques for EMA data analysis. The main difference between OMA and EMA stems from the measurability of the excitation input. Many data processing techniques can take advantage of knowing the excitation input to better characterize the data into the structure's signature modal parameters. The following further explores the details relevant to EMA. An emphasis will be made on time

domain and frequency domain methods, on comparing damping estimation methods, and also on the implementation of modal scaling. Due to the similar implications of each excitation type, no attempt is made to discuss shaker or impact testing excitations separately. Instead example studies from both types are presented.

Douglas (1976) performed controlled vibration test on a six span continuous composite girder bridge in Western Nevada for modal parameter estimation. The natural frequencies and mode shapes were obtained using a PP routine. Damping was estimated using the Moving Window Spectral Decay method.

Pardoen et al (1981) performed controlled vibration tests of the steel frame Toe-Toe bridge in New Zealand and used the power spectra to identify resonant frequencies and modal amplitudes, while FRF's were used to determine modal phasing information.

Muria- Vila et al (1991) experimentally determined modal parameters of the 3-span cable-stayed Tampico Bridge in Mexico from both, a controlled vibration test and an ambient vibration test. The authors noted that damping values between both test types were considerably different. Thus, special interest was placed on damping estimation methods. Logarithmic decrement method, HPBW method and Kawasumi & Shima (K&S) methods (Kawasumi and Shima, 1965) were compared. The K&S method reasonably agreed with the value calculated by the logarithmic decrement ratio. However, the K&S method generally overestimated the damping values, while the HPBW method generally underestimated the damping value for the low sampling frequency resolution used.

Cantieni and Pietrzko (1993) performed shaker testing of the Wimmis footbridge in Switzerland. A servo-hydraulic vibrator was used to excite the bridge and the bridge was

instrumented for a total of 70 degrees of freedom. Frequencies and damping values were estimated for this SIMO test using the Least Squares Complex Exponential (LSCE) technique which analyses impulse response functions. Mode shapes were estimated using a Linear Least Squares technique in the frequency domain.

Farrar et al. (1994) applied the LSCE method to cross correlation functions, calculated from the inverse Fourier transform of the cross power spectra between various accelerometer readings and one reference accelerometer to identify resonant frequencies and modal damping values for the ambient vibration test of the I-40 Bridge over the Rio Grande in New Mexico. In the same study, forced vibration tests were carried out and under this condition the dynamic properties were determined using a global rational-fraction polynomial technique.

Catbas et al. (1998) performed an experimental damage detection modal analysis test, using an automated drop hammer, to the three-span steel stringer Seymour Bridge in Cincinnati Ohio. Modal parameters were identified using the Complex Mode Indicator Function (CMIF). This data analysis procedure was successful in uncoupling closely-spaced modes. Most ambient system identification algorithms assume that the unmeasured input is stationary random and ergodic, damping is small and proportional, and modes are well separated. These assumptions lead to several problems including less accurate estimates of modal parameters, improperly scaled mode shapes that cannot be used to predict system response, and inability to resolve modal parameters associated with closely spaced modes.

Farrar et al. (2000) identified the variability of modal parameters of the Alamosa Canyon Bridge, a seven span concrete deck-on-steel-girder structure. Temporal variability, excitation sources, and data acquisition and reduction methods were considered as factors affecting the

recorded modal parameters of the bridge. The first step in the analysis of the data was the approximation of number of modes to be fitted using the Multivariate Mode Indicator Function (MIF) and the CMIF. The authors then applied an Eigensystem Realization Algorithm (ERA) which is based on the formation of a Hankel matrix containing the measured discrete-time impulse response data, computed using the inverse FFT of the measured FRF's. Discrimination procedures were applied to select the physically meaningful modes. The authors used three indicators tailored for compatibility with ERA: Extended Modal Amplitude Coherence (EMAC), Modal Phase Collinearity (MPC), and Consistent Mode Indicator (CMI), which is obtained by the product of EMAC and MPC

Zhang (1994) reported on a controlled vibration test of a three-span continuous steel stringer bridge in Cincinnati, OH. Both impact hammer and shaker tests were performed. Modal parameters obtained from the shaker test showed much closer correlation with those from the FE model than those from the impact test. The authors developed a Coordinate Modal Scaling Factor (COMSF) index to identify errors in an impact test by checking a scaling factor from a specific measuring point. If the value of the Coordinate Modal Assurance Criterion (COMAC) is larger than one at a particular measurement point, a difference in magnitude exists at the measurement point. On the other hand, a COMAC value less than one indicates a phase difference.

Allemang (2003) discussed the scaled modal assurance criterion (SMAC) which is essentially a weighted modal assurance criterion (WMAC) where the weighting matrix is chosen to balance the scaling of translational and rotational degrees-of-freedom included in the modal vectors. This development is needed whenever different data types (with different engineering

units) are included in the same modal vector to normalize the magnitude differences in the vectors. This is required since the modal assurance criterion minimizes the squared error and is dominated by the larger values.

One of the main advantages of EMA tests over OMA tests is that the excitation forces can be customized for any type of structure. If the natural frequencies of a structure are known from previous tests or from models, the signal function used in shaker testing can be created so that it excites the structure at its modal frequencies, instead of blindly sweeping through a larger frequency band, thus, allowing more time for the signal function to act in the frequencies of interest. Also, if the mode shapes of the structure are known, EMA tests can be performed avoiding nodal points, or zero points, for the input locations. Impact hammer tests can benefit from this by reducing the number of impact locations located at nodal points of the structure. The deterministic nature of input sources provides an enhanced S/N ratio, overcoming the issues encountered in many OMA tests. The overall characterization of a structure's dynamic parameters can be better achieved through the use of controlled vibration tests.

Some limitations of this type of test are the cost and specialized equipment required to perform the test. In all, the cost of equipment can easily reach five digit figures and their proper maintenance and care also add up considerably to the overall cost. The personnel required for this type of test typically exceed that of OMA testing and proper knowledge on the operation of testing equipment is required. There are also technical issues and limitations related to the performance of the test itself. Most shaker tests of large scale structures utilize proof masses, and there is the potential for shaker-structure interaction at the natural frequencies of the structure. Undetected overloading of sensors or signal conditioning equipment is one of the most

significant causes of bad data from both impact and shaker modal tests. Good practice is to set the bandwidth of the data acquisition system and analog filters to a very high frequency to be sure that no signal conditioning equipment or sensors are being overloaded. Once such verification is made, the bandwidth can be narrowed down to the frequencies of interest.

Damping estimates can contain errors from FRF distortion due to leakage, which is a distortion in the Discrete Fourier Transforms (DFT) calculation due to energy relevant to one frequency leaking to neighboring frequency lines. This problem can be attributed to a shaker signal function that is non-periodic in the time window. Signals such as Chirp and burst random can overcome this by beginning and ending each time window at zero. Leakage distortion will overestimate damping. Another source of damping overestimation can be attributed to the windowing applied, such as Hanning window, which can cause distortion of the FRF at the natural frequency. This situation arises when part of the response in the windowed data belongs to a force applied earlier in time that has been reduced by the Hanning window. Taking longer blocks of data for each excitation mitigates this error by including the response of a force that has not been drastically windowed. Finally, another concern needing attention is the driving point location. Driving points at or near a node of a particular mode will produce a very small signal from the mode of interest near the associated resonant frequency. All modal parameters estimates for that mode will be affected by this weak signal, cascading progressively worse for frequency, damping, mode shape and modal mass.

2.4 Modal Flexibility

Flexibility is a significant source of information for structural condition assessment because it reveals the internal force distribution due to external loading and support conditions including

structure–foundation–soil interaction and continuity conditions. Flexibility can be used to facilitate detection of local damage and the ability to compute flexibility coefficients directly from modal testing provides a powerful tool for damage detection practices. Flexibility is typically obtained from static load testing, but the fact that modal flexibility can be derived from modal parameters makes the use of modal flexibility for structural characterization purposes quite economical considering the logistic and technical requirements associated with static load testing.

FRF and static flexibility matrices are very much related. In Catbas et al. (2006), the authors develop the relationship between FRF and modal flexibility matrices, which is presented next. The general mathematical formulation for the equation of motion of a multi-degree of freedom system using Newton's second law is given as:

$$[M]\{\ddot{x}\} + [C]\{\dot{X}\} + [K]\{X\} = \{F\} \qquad (2.1)$$

The Laplace transform of this equation, assuming all initial conditions are zero, yields

$$[s^2[M] + s[C] + [K]]\{X(s)\} = \{F(s)\} \qquad (2.2)$$

Letting

$$[B(s)] = [s^2[M] + s[C] + [K] \qquad (2.3)$$

then the previous equation can be written as

$$[B(s)]\{X(s)\} = \{F(s)\} \qquad (2.4)$$

Where, [B (s)] is referred to as the system impedance matrix. The transfer matrix can then be formulated as

$$[B(s)]^{-1} = [H(s)] \qquad (2.5)$$

Then the following equality can be defined:

$$[H(s)]\{F(s)\} = \{X(s)\} \qquad (2.6)$$

The FRF is the transfer function evaluated along the frequency axis:

$$[H(s)]_{s=j\omega} = [H(\omega)] \qquad (2.7)$$

Frequency response functions can be defined in terms of the system characteristics (mass, stiffness, and damping) as follows:

$$[-\omega^2 [M] + j\,\omega [C] + [K]]^{-1} = [H(\omega)] \qquad (2.8)$$

In full-scale field test measurements, mass, stiffness, and damping characteristics are not known initially. By implementing a modal parameter estimation algorithm (Allemang and Brown 1998), a frequency response function between point *p* and *q* can be written in partial fraction form as follows:

$$H_{pq}(\omega) = \sum_{r=1}^{m} \left[\frac{(A_{pq})_r}{j\omega - \lambda_r} + \frac{(A_{pq}^*)_r}{j\omega - \lambda_r^*} \right]$$

where $H_{pq}(\omega)$ = frequency response function at point p due to input at point q; A_{pqr} = residue for mode r; ω = frequency variable; and λ_r = r^{th} complex eigenvalue or system pole. The

authors also note that $H_{pq}(\omega)$ is the dynamic response, $X_p(\omega)$, at point p due to dynamic input, $F_q(\omega)$, at point q in the frequency band of m modes. This equation can be written in terms of the experimentally identified modal parameters as follows:

$$H_{pq}(\omega = 0) = \sum_{r=1}^{m} \left[\frac{\psi_{pr}\psi_{qr}}{M_{A_r}(j\omega - \lambda_r)} + \frac{\psi_{pr}^{*}\psi_{qr}^{*}}{M_{A_r}^{*}(j\omega - \lambda_r^{*})} \right]$$

where ψ_{pq} = mode shape coefficient between point p and q for the r^{th} mode and M_{A_r} = modal scaling for the r^{th} mode. Using this last relationship, the modal flexibility coefficients and the modal flexibility matrix can then be computed in terms of the identified modal parameters of the structure evaluated at $j\,\omega=0$ as

$$H_{pq}(\omega = 0) = \sum_{r=1}^{m} \left[\frac{\psi_{pr}\psi_{qr}}{M_{A_r}(-\lambda_r)} + \frac{\psi_{pr}^{*}\psi_{qr}^{*}}{M_{A_r}^{*}(-\lambda_r^{*})} \right]$$

Finally, the modal flexibility matrix can be written as follows:

$$[H] = \begin{bmatrix} H_{11}(\omega = 0) & H_{12}(\omega = 0) \cdots & H_{1N}(\omega = 0) \\ H_{21}(\omega = 0) & \cdots \quad \cdots & \vdots \\ \vdots & \vdots \quad \vdots & \vdots \\ H_{N1}(\omega = 0) & \cdots \quad \cdots & H_{NN}(\omega = 0) \end{bmatrix} \qquad (2.9)$$

The general formulation given previously is independent of the normal mode assumption or unit mass normalized vectors. However, this formula is only an approximation of a real flexibility matrix due to the truncated number of modes obtainable in field test measurements. The error between the modal flexibility obtained from limited modal vectors identified experimentally and the exact flexibility from static load tests is known as the flexibility

truncation error. A truncation error study using FE methods prior to the modal testing can determine the necessary frequency band to achieve minimum truncation. The authors suggest that by monitoring a sufficiently broad frequency band, temporal truncation can be minimized with an appropriate number of identified experimental modes. They also developed cutoff criteria for the number of modes, m, termed as load dependent modal convergence criteria to minimize the temporal truncation (Catbas et al. 1997).

Aktan et al (1998) studied truncation error with an analytical model of the Cross–County Bridge. The study shows that the uniform loading surface (ULS) of the bridge is not sensitive to the mode number used or the boundary conditions. Also, the authors conclude that modal flexibility and ULS would be exact if all of the DOFs in the system are measured. In the case where only a small subset DOFs are measured, which is always true in reality, the truncation effects of the modal flexibility and ULS are important in structural identification.

Catbas et al. (1997) presented a comparative study on the post-processing of experimental modal data from a full-scale steel stringer bridge for damage identification. Modal flexibility of the bridge was calculated for the measured degrees of freedom. Modal flexibility of the bridge showed good agreement with static instrumentation results under truck loading. It was shown that the modal flexibility would be a close approximation of the real flexibility for controlled input dynamic test measurements.

Catbas et al. (2004) developed and implemented a parameter estimation method using the CMIF algorithm to determine the modal properties with proper scaling to obtain modal flexibility. This method proved to be very successful among many others with the data acquired from an aged and deteriorated highway bridge. The authors have also shown how the

displacement coefficients can be reliably obtained from the modal flexibility using modal testing data. Also, the authors highlight that the reliability of the modal parameters improve with MIMO tests as compared to those from SIMO tests.

Catbas et al (2006) studied the use of modal flexibility for damage detection purposes. Deflection profiles for two different bridges, a steel stringer bridge and a posttensioned concrete box girder bridge were compared based on classical static load proof test to the ones obtained by using modal flexibility analysis under both controlled input tests and ambient vibration tests. The deflected shape of a girder under virtual uniformly distributed load termed "bridge girder condition indicator" (BGCI) obtained from a full and an incomplete modal flexibility shows that if the structure can be well excited within the truncated measurement grid and temporal modal truncation is minimized by adding adequate number of modes, it is then possible to obtain very reliable girder deflection profiles (BGCI) from the incomplete modal flexibility. Also, the authors determined that any deflection change less than 10% cannot be attributed to damage with high confidence for the three-span, highly deteriorated and redundant steel stringer bridge. Finally, as the modal scaling cannot be identified without the input, pseudoflexibility was derived to determine unscaled deflection profiles. Promising results which correlated with actual displacement measurements were obtained for the damaged condition of the posttensioned bridge

2.5 Summary and Discussion

The previous literature review studied available resources for the proposed research thesis. The flaws of current NBIP routine visual inspections were evinced through reports and studies from federal agencies and publications. The lack of standardized provisions for post-hazard

inspections was discussed along with current research studies attempting to fill this gap. Full scale testing was then explored to highlight the benefits it has over localized visual inspection routines. Two categories of full scale testing were discussed; static load testing and dynamic load testing. It was shown that static load testing, although adequate for global condition assessment of a bridge, was inadequate for rapid structural health monitoring of damaged structures under critical pos-hazard conditions. The implementation of full scale dynamic testing was then introduced and further subdivided into two categories; ambient vibration testing and controlled vibration testing. The different stages for performing both types of tests were explained and backed with publications and studies. Finally, the implementation of Modal Flexibility for damage detection purposes was studied. It was shown that flexibility is typically obtained from static load testing, but the fact that modal flexibility can be derived from modal space parameters makes the use of modal flexibility for structural characterization purposes quite economic considering the logistic and technical limitations associated with static load testing.

3 Experimental Program

3.1 Introduction

The experimental program designed and implemented for the research will be introduced in this chapter. The bridges evaluated by field testing are described in terms of their geometric and structural characteristics, and their operational details. The test design and execution for each structure is presented, including the types and locations of sensors, the excitation devices and excitation methods employed. The execution of the ambient vibration tests and the controlled vibration tests for each bridge is also discussed. A separate section is devoted to presenting a study of the shaker excitation signals that was performed to identify the optimal swept sine excitation approach for each bridge using a linear mass shaker. Finally, the data analysis methods implemented for each type of vibration test are presented.

3.2 Test Specimens

This section describes the two bridges that were evaluated as part of the experimental program in this research.

3.2.1 Baptist Ford Bridge

The first bridge evaluated for the research program was the Baptist Ford Bridge. This bridge has already been used as a test specimen for several previous vibration studies conducted by University of Arkansas researchers because it has relatively low traffic levels, and because it can be instrumented and tested without special access equipment and with minimal disruption of the normal operation of the bridge. The bridge and its structural components have been described in Fernstrom, Grimmelsman and Wank (2012), and the description is repeated here for reference.

The Baptist Ford Bridge is a Parker pony truss structure that entered service in 1930 and carries two lanes of vehicular traffic across the West Fork of the White River in Greenland, AR.

The bridge has three identical, simply-supported truss spans that are each 100 ft in length and consist of ten panels. The total width of the bridge, measured from center-to-center of the trusses, is 22.5 ft. The trusses have a camelback configuration and the vertical height of the truss at midspan is 14 ft. The deck is an 8 in thick reinforced concrete slab supported by I-shaped, rolled steel floor beams spanning between the lower panel points of the upstream and downstream trusses. The truss members consist of rolled and riveted build-up sections as follows: (1) top chords: two channels, a top cover plate, and lacing bars; (2) bottom chords: two channels with batten plates; (3) verticals: I-beams; and (4) diagonals: I-beams for stress reversal members and two angles with batten plates for tension-only members. The interior bearings of the truss spans are supported on concrete piers and the exterior bearings of the two end spans supported on concrete wall abutments. Construction plans and shop drawings were not available for the bridge and the foundation details are unknown. The geometric and section properties for the trusses were determined using field measurements of the member dimensions.

The side and elevation views of a typical truss span are shown in Figure 3.1 and Figure 3.2, respectively. Figure 3.3 shows a photograph taken from the end of the bridge looking west. This bridge is currently in service, but does not service significant traffic levels. It had an average daily traffic (ADT) of 25 vehicles as of 1992, and the ADT was estimated to be 35 vehicles in 2012. The bridge carries two-way traffic, although the lane widths are less than 12 feet. The bridge deck also lacks shoulders. The bridge is also posted on the National Register of Historic Places.

The Arkansas Highway and Transportation Department (AHTD) assigned inventory structure number for the bridge is 18802. A 2011 visual inspection report for the bridge indicated that the deck, the superstructure and substructure were rated satisfactory with each scoring 6 points out

of 9. The bridge was assigned a sufficiency rating of 81.2% according to current inspection procedures.

Figure 3. 1 Side View of the Truss (Torres Goitia, AR, 2012).

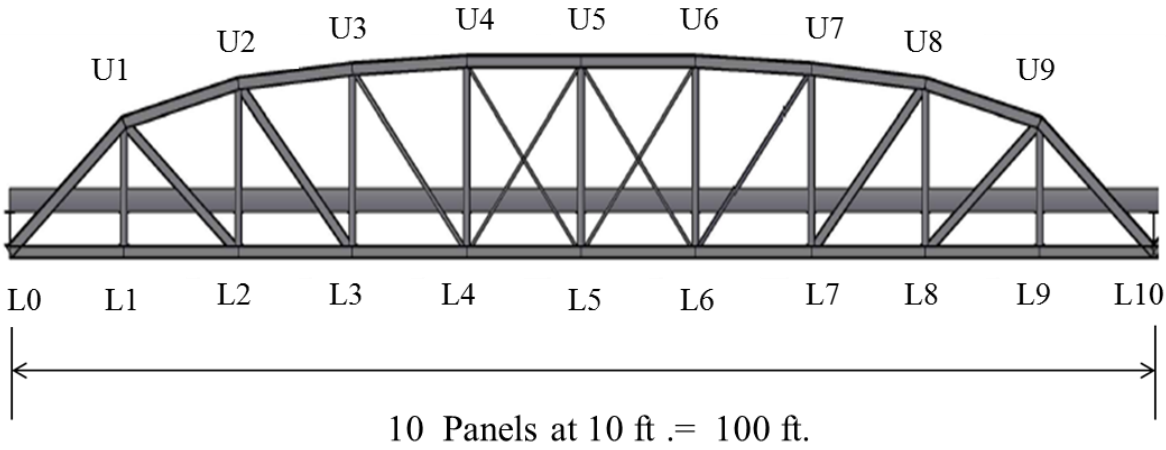

Figure 3.2 Bridge Elevation (Fernstrom et al., 2012).

Figure 3. 3 End View of the Bridge (looking west) (Torres Goitia, AR, 2012).

3.2.2 Hartbarger Bridge

The second bridge that was evaluated for this research project was a more modern concrete deck on steel beam bridge. The bridge was opened in 1987 and consists of ten simply-supported spans of composite concrete deck on rolled steel beams (Figure 3.4). Each span has a length of 50 ft and an overall width of 27.5 ft. The superstructure plans and detailing for each span are identical and consist of an 8 in. thick concrete deck supported on four W27x94 beam sections (Figure 3.5 and Figure 3.6). The beams are spaced laterally at 7.5 ft. The eight interior spans of the bridge are supported on concrete piers. The two end spans of the bridge are supported on concrete stub abutments and concrete piers. Each of the ten spans has fixed bearings on one end and expansion bearings on the other end. The fixed bearings are composed of a sole plate connected to the concrete substructure with anchor bolts. The expansion bearings are composed of steel sliding plates. All geometric and section properties were obtained through field measurements because construction plans and shop drawings could not be located for the bridge.

The foundation details for the intermediate piers and the abutments are unknown. The bridge is located on a floodplain of the White River in Fayetteville, Arkansas.

The Bridge is currently open to traffic. It had an ADT of 270 vehicles in 1987 and an ADT of 380 vehicles in 2007. The bridge carries two-way traffic on two 12 foot wide lanes. The AHTD assigned inventory structure number for the bridge is 4587. A recent inspection of the bridge performed in October 2010 rated the deck, superstructure and substructure as all being in very good condition. The bridge was assigned a sufficiency rating of 84.8 % after its 2010 inspection.

Figure 3.4 View of the Hartbarger Girder Bridge (looking east) (Torres Goitia, AR, 2012).

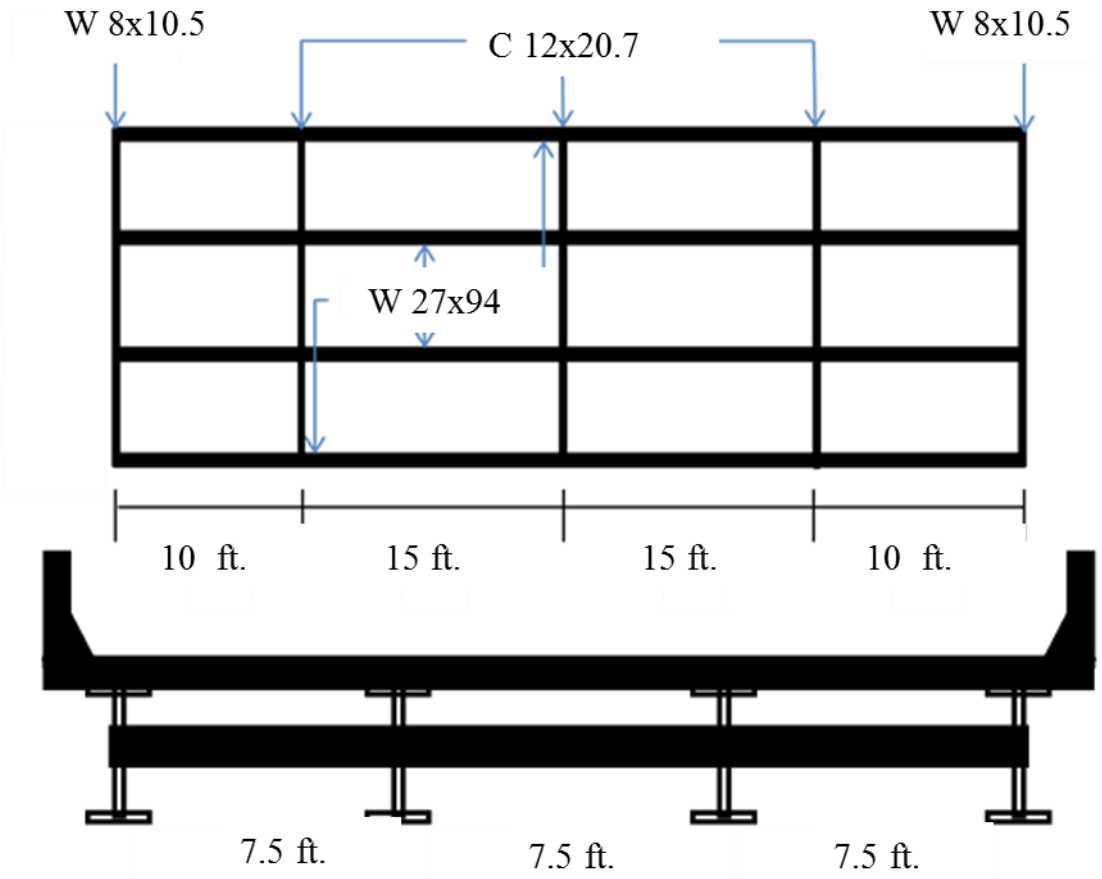

Figure 3. 5 Plan and Cross-Section Views of Typical Bridge Span (Fernstrom et al.2012).

Figure 3. 6 Photograph of the Underside of a Typical Span (Torres Goitia, AR, 2012).

3.3 Test Design and Execution

The following sections describe the design and execution of the field testing program for the two bridges that were evaluated. The sensors and data acquisition devices used are described along with the placement of the sensors for each bridge test. The basic characteristics of the excitation devices used for the controlled vibration testing are also described.

The instrumentation scheme employed for each bridge was slightly different due to their different structural configurations and geometries. The instrumentation scheme developed for a given bridge was the same for the ambient and controlled vibration tests. The controlled shaker vibration tests were performed on each bridge using a portable linear mass shaker and employed a swept-sine excitation signal developed specifically for these bridges. The development and details of this excitation signal are also described in the following section. The impact vibration

test was performed using a portable instrumented sledge hammer, which characteristics will be outlined below.

3.3.1 Experimental Equipment.

Two different types of accelerometers were used to record the vibrations of the two bridges during the ambient and controlled vibration testing programs. The first type of was a Model 393B05 accelerometer (Figure 3.7) from PCB Piezotronics, Inc. The second type was a Model 393C accelerometer (Figure 3.8) also from PCB Piezotronics, Inc. Both types of accelerometers are designed for seismic testing of structures and provide an output voltage proportional to structural vibrations (in units of g's), but have slightly different amplitude ranges, frequency ranges, and sensitivities. The Model 393B05 accelerometer has a peak amplitude range of 0.5 g, a frequency range of 0.7 to 450 Hz, and a nominal sensitivity of 10 Volts/g. The Model 393C accelerometer has a peak amplitude range of 2.5 g, a frequency range of 0.025 to 800 Hz, and a nominal sensitivity of 1 Volt/g. The frequency ranges of both accelerometers were more than adequate for a nominal frequency range of interest established for both bridges (1 Hz to 100 Hz). The nominal sensitivities of each accelerometer determined their locations on each of the bridges. The accelerometer with the lower sensitivity, but larger amplitude range (Model 393C) was generally placed at locations on each bridge where the vibration amplitudes were expected to be largest, e.g. near the middle of the span. The accelerometer with larger sensitivity but less amplitude range (Model 393B05) was generally placed on each bridge where the vibration amplitudes were expected to be smaller, e.g. closer to the supports.

The final instrumentation schemes developed for each bridge are shown in Figure 3.9 (Baptist Ford Bridge) and Figure 3.10 (Hartbarger Bridge). The instrumentation scheme for the Baptist Ford Bridge included a total of 27 accelerometers that were distributed along 3

longitudinal lines. Two of these lines represented the upstream and downstream truss lines, and the third line was the longitudinal centerline of the bridge. The accelerometers located on the two truss lines were installed on a railing support angle that was attached to the truss members at each panel point. These accelerometers were physically installed on the truss members using magnets (see Figure 3.11). The accelerometers that were located on the longitudinal centerline of the bridge were installed on heavy steel plates also using magnets as shown in Figure 3.11. Stiff clay was placed between the heavy steel plates and the concrete deck to permit the plates to be leveled and to ensure the plates remained stable throughout the testing.

The instrumentation for the Hartbarger Bridge consisted of 28 vertically oriented accelerometers that were attached to the bottom flanges of the steel beams using magnets. Each beam line had a total of 7 transverse sensor lines spaced at 6.25 ft increments from the supports. As mentioned previously, the more sensitive accelerometers were placed at transverse lines were the bridge vibration responses were expected to be smaller.

All vibration data were recorded using hardware from National Instruments. A PXI mainframe populated with Model 4472B Dynamic Signal Acquisition (DSA) Modules. Each DSA module has 8 input channels with 24-bit analog to digital converters. The DSA modules also provided the excitation voltage to the accelerometers, which were interfaced to the modules using RG58U (50 Ohm) coaxial cables. All measurement data were sampled at 1000 Hz which provided a usable frequency range (500 Hz) that was significantly larger than the frequency range of interest for the bridges that were tested.

The dynamic excitation devices used for the controlled vibration tests of each bridge included a modally tuned impact hammer and a portable long-stroke linear shaker. The specific impact hammer used for the testing was a Model 086D50 instrumented sledge from PCB

Piezotronics, Inc. (Figure 3.12). The impulse hammer has a dynamic load cell integrated into the tip to record the force versus time for each hammer strike. The load cell has a nominal sensitivity of 1 mV/lbf and a measurement range of +/- 5000 lbf. The impact hammer produces a broadband impulse excitation and the frequency range of the input is controlled by the stiffness of the rubber tip used on the hammer. Using a harder tip provides a shorter contact time and leads to a broader frequency range while a softer tip leads to a longer contact time and shorter frequency band for the excitation. A tip with medium hardness (red tip) was found to provide the best combination of input force and frequency band for the two bridges tested. The impact testing data was collected using a commercially available software package designed specifically for this type of dynamic testing. This software package, Smart Office Dynamic Signal Analyzer from M+P International, controlled the operation of the PXI data acquisition hardware for the impact test.

Controlled vibration testing of each bridge was also performed using a portable, long-stroke electro dynamic shaker (Model 113) from APS Dynamics. The shaker (Figure 3.13) was operated in reaction mass mode in which heavy steel plates were attached to the shaker's armature to provide dynamic excitation with the accelerations of the armature. This shaker can produce a maximum excitation force of 42 lbf with the appropriate amplifier, and can produce both harmonic (sinusoidal) and random excitation signals. The excitation signals used for the bridge testing were generated using an Agilent 33220A Waveform Generator. The analog signals were sent to an APS Model 145 amplifier before being sent to the shaker. The waveform generator and the shaker amplifier were mounted together in an equipment rack as shown in Figure 3.14.

Figure 3.7 PCB Model 393B05 Accelerometer (www.pcb.com).

Figure 3.8 PDC Model 393C Accelerometer (www.pcb.com).

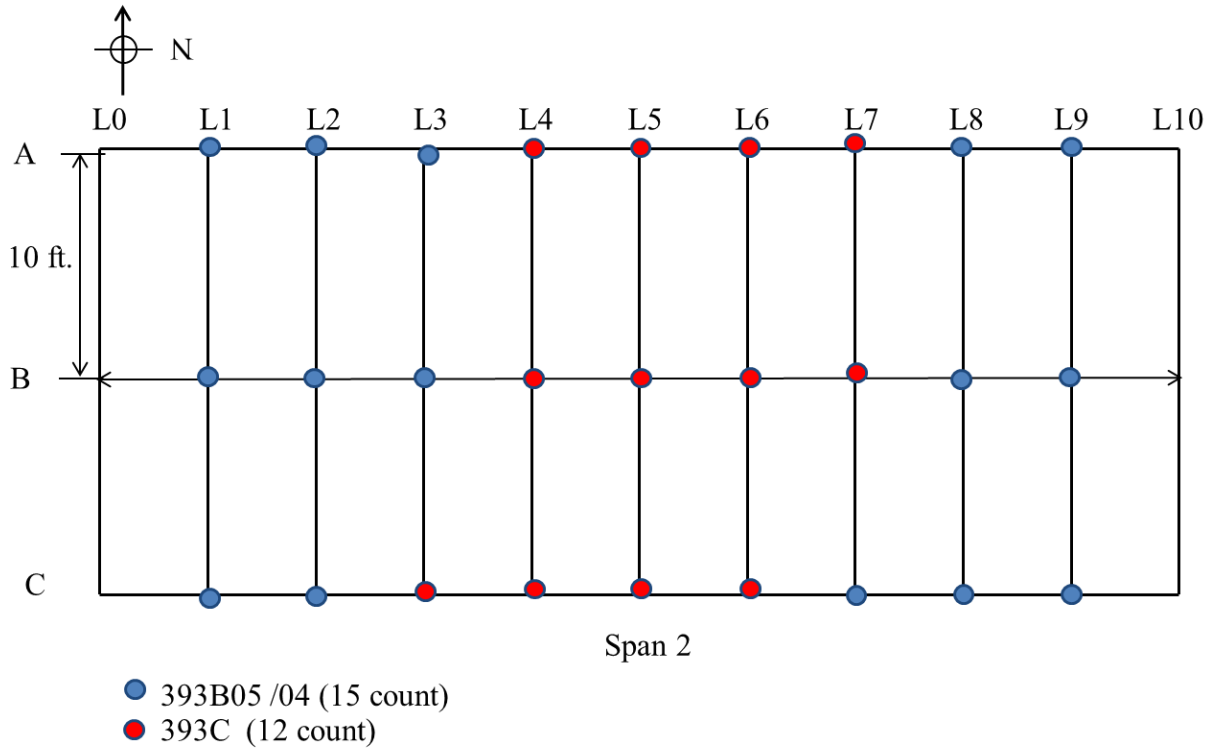

Figure 3.9 Instrumentation Layout for the Baptist Ford Bridge.

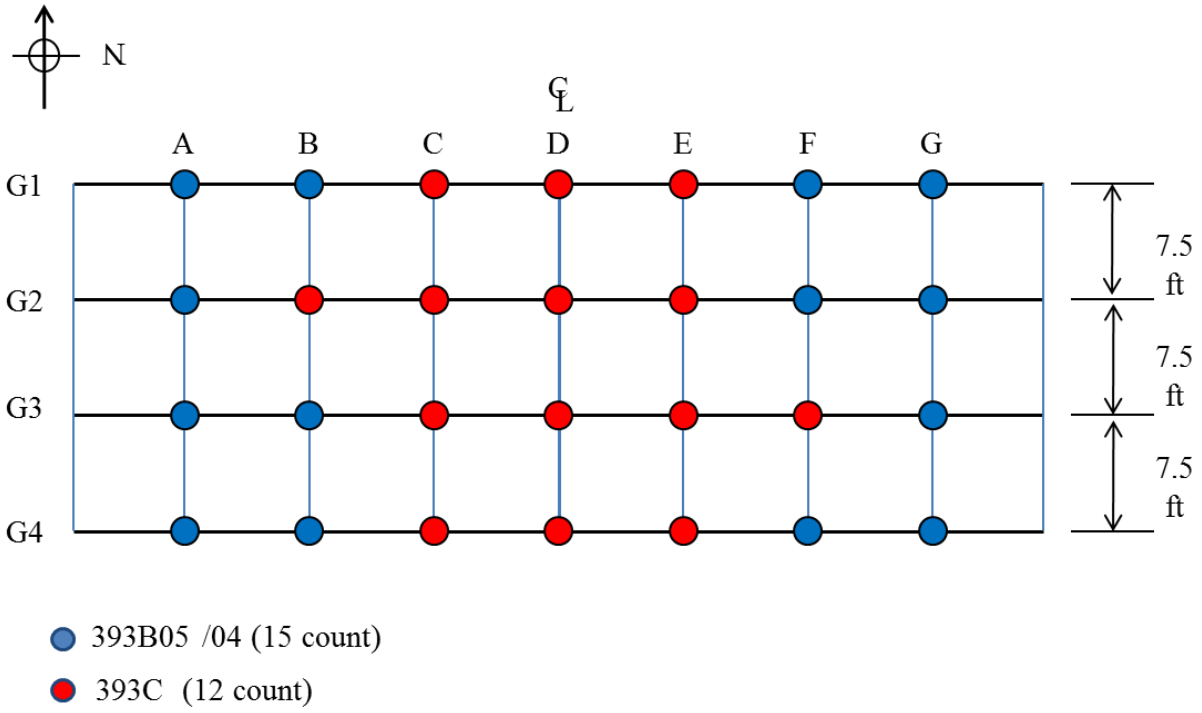

Figure 3. 10 Instrumentation Layout for the Hartbarger Bridge.

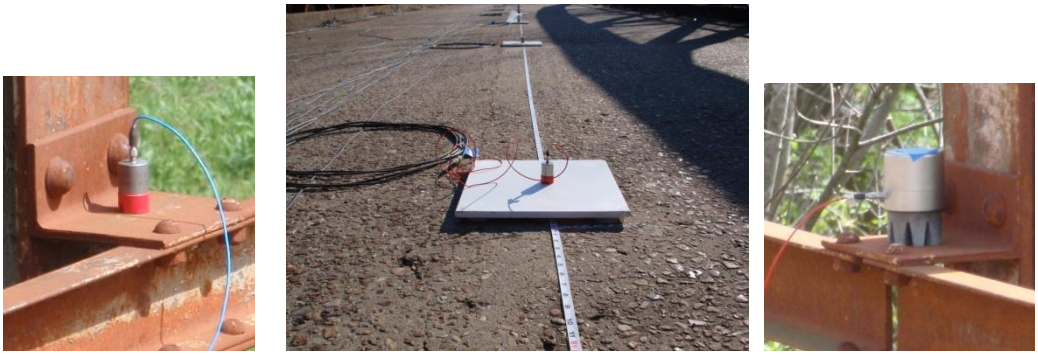

Figure 3.11 Sensor Installation Details (Torres Goitia, AR, 2012).

Figure 3.12 Large Sledge Impact Hammer (with different rubber tips) (www.pcb.com).

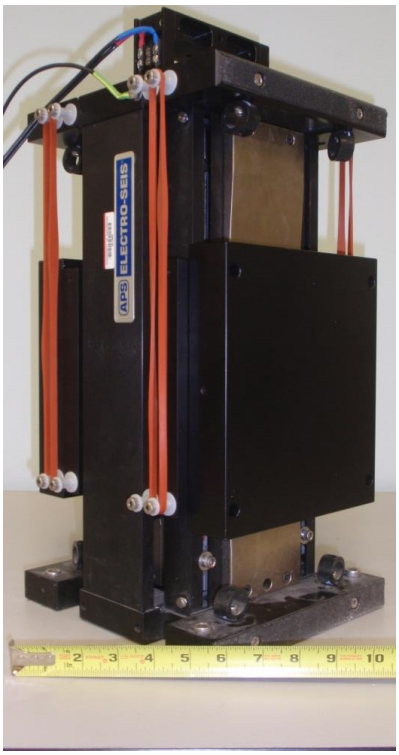

Figure 3.13 Electro-dynamic Shaker with Reaction Masses (Torres Goitia, AR, 2012).

Figure 3.14 Waveform Generator and Shaker Amplifier (Torres Goitia, AR, 2012).

3.3.2 Ambient Vibration Testing

A total of four hours of data were collected from each bridge during the ambient vibration testing. During the ambient vibration tests, the vibration responses of the bridge resulting from ambient excitation sources (wind, waves, micro-tremors, etc) and operating traffic were measured. The traffic on both bridges was minimal, so the majority of the dynamic excitation was provided by ambient natural excitation sources.

3.3.3 Impact Hammer Testing

Multiple reference impact testing (MRIT) was performed on each bridge using the instrumented sledge hammer. A total of five impacts were produced at each measurement degree of freedom (28 locations for the girder bridge, 27 locations for the truss bridge). The five input-output records measured at each sensor location were subsequently averaged together to

minimize the effects of noise and other experimental variations. This testing approach is fundamentally different from ambient vibration testing in that both the excitation and the vibration response of the structure are recorded during each hammer strike. The data from each hammer impact was recorded for 16 seconds which was more than adequate to allow the vibration response of the structure to return to zero. The impact tests are considered a single input-multiple output (SIMO) since the response at all accelerometer locations is recorded for each impact point. Frequency response functions (FRFs), which represent the measured output divided by the measured input were generated from each impact location. Each impact location produces one column of the FRF matrix, and each impact locations produces a column of the FRF matrix. Impact locations that correspond to one of the accelerometer locations are considered driving point measurements and these measurements can be used to scale the resulting modal vectors.

3.3.4 Shaker Testing

Shaker testing was performed on both bridges using a SIMO test. As was the case for the impact tests, the shaker excitation signals were applied to each measurement degree of freedom. In other words, driving point data was measured from each sensor location. The dynamic force provided by the shaker was computed using Newton's second law from acceleration measurements of the shaker's reaction mass. The reaction masses weighed a total of 22.75 lb and were physically attached to the moving armature of the shaker. Four medium thickness rubber bands (provided by the shaker manufacturer) were also connected between the armature and the shaker body to maximize the force of the excitation. Again, the input-output data was used in the data processing stage to formulate an FRF matrix for each excitation signal type used for the testing.

An automatic rising edge trigger was defined in the waveform generator in order to automatically trigger simultaneous recording of the input and output measurements (accelerometers) when the excitation signal was started in a given test run. Two different types of excitation signals were fed to the shaker for testing on each bridge. The first type was a burst random signal and a total of five sets of data using this signal were recorded at each measurement degree of freedom and subsequently averaged together. The second excitation signal used was a swept sine signal that was repeated a total of three times and averaged for each measurement degree of freedom. Traditionally, swept sine testing involves sweeping a sine wave over a range of frequencies in either a linear or logarithmic fashion. The sweep is executed over a defined frequency band, which if large, will require a significant amount of time to execute. This is because the rate of change in the frequency of the excitation signal must be slow enough to allow the transient response to die out and for the steady state response to occur at each frequency. For this research, it was decided to employ a targeted sine sweep in which the sinusoidal excitation would only be swept over frequency bands that were known to contain modes of each bridge. This would permit the time required for each swept sine testing run to be reduced significantly because the excitation would not be sweeping over frequencies where no modes are located. This approach can be implemented if the natural frequencies of the structure are determined (to a reasonable degree of confidence) from finite element analysis or from prior experimental results such as from ambient vibration testing. The specific details of the shaker excitation signals used for testing each bridge are discussed in the following section. Figure 3.15 shows the experimental equipment that was used for the shaker testing of the two bridges.

Figure 3.15 PXI Mainframe, APS Shaker Amplifier and APS Shaker (left to right) (Torres Goitia, AR, 2012).

3.3.4.1 Design of the Shaker Excitation Signals

The first excitation signal designed for testing of both bridges was a burst random signal that was 64 seconds in length. The signal was zero padded for five seconds before the start of the excitation and for ten seconds after the end of the excitation, so the actual duration of the excitation was 49 seconds. The burst random signal was used since it is periodic over the sampling duration. This minimizes the potential for leakage when the signal is transformed into the frequency domain. The signal was generated using the Agilent IntuiLink Wave Form Editor program. A low pass filter of 80 Hz was also applied to the excitation signal since the frequency band of interest for both bridges was identified as between 1 Hz and 60 Hz. The signal was played five times at each location for averaging purposes and to increase signal to noise (S/N) ratios of the measurements. Figure 3.16 shows the time domain representation of the burst

random signal used for the bridge tests. The frequency domain representation of this input signal, as generated by Fast Fourier Transform (FFT), is shown in Figure 3.17. The FFT of the signal was computed for a sampling rate of 1000 Hz (samples/sec) and by concatenating five repetitions of the burst random input signal. This made the block size (NFFT) for the FFT equal to 320000 points.

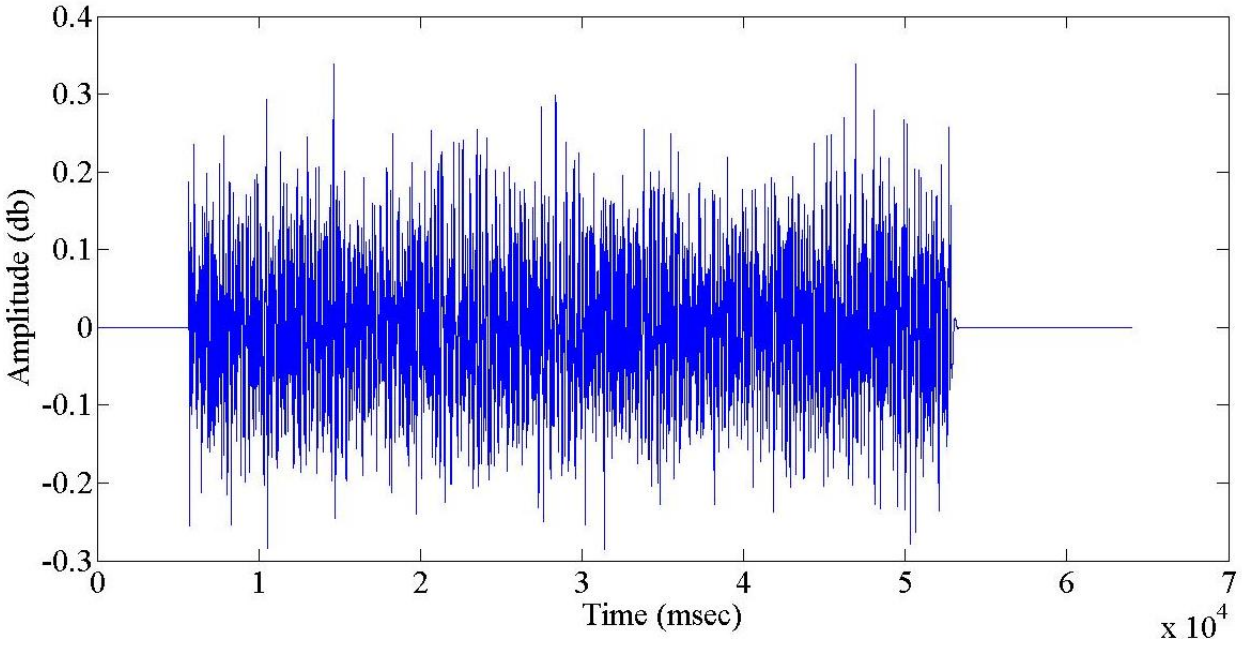

Figure 3. 16 Time Domain Representation of the Burst Random Excitation Signal.

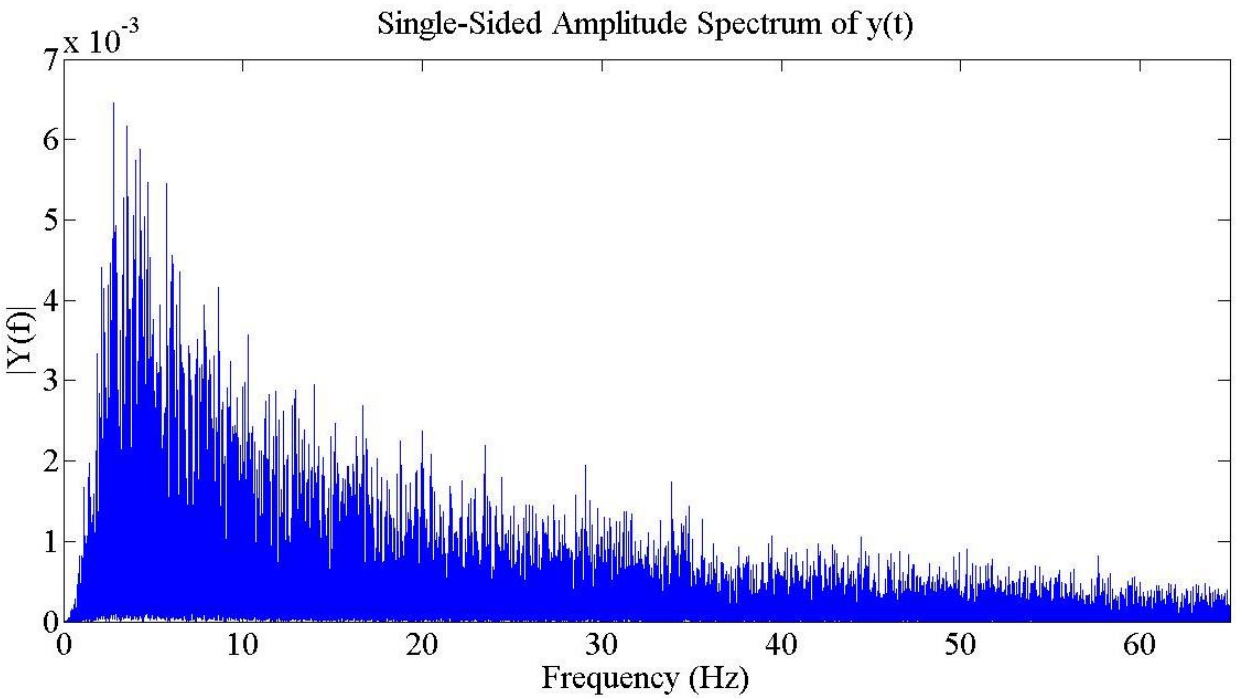

Figure 3. 17 Frequency Domain Representation of the Burst Random Excitation Signal.

The sine sweep signal used for the testing was designed in stages and evaluated in the laboratory and preliminary field tests before being implemented for the two bridges. The sine sweep signal was first created using MATLAB as follows. A linear sine sweep covering the frequencies in the range of interest for the bridges was generated. The start frequency for the sweep was 1 Hz and the end frequency was 55 Hz. The sine sweep signal was sampled at a rate of 1,000 Hz. Figure 3.18 shows the time domain representation of the sweep from 1 Hz to 55 Hz. The buildup of this signal function is linear over a total duration of 100 seconds. The FFT of the generated sine sweep signal is shown in Figure 3.19. Ideally, the frequency spectrum for the input signal should be flat over the frequency band of interest.

The FFT of the sine sweep shown in Figure 3.19 appeared noisy and due to the nature of the Fourier transform, the amplitude of the signal's amplitude increases at the beginning and end of

the sweep. The input signal should ideally be flat in the frequency domain. To minimize this effect, a Tukey window was applied to the sine sweep signal. Windowing of the signal involves multiplying the signal with a window vector in the time domain to modify the shape of the original signal. This is done to improve the characteristics of the signal in the frequency domain. The Tukey window vector was created using the "tukeywin" function available in the signal processing toolbox of MATLAB (MATLAB, 2010). A Tukey window is a rectangular window vector of length L with the first and last r/2 percent of the signal equal to parts of a cosine. If the r parameter is assigned a value less than or equal to zero, a rectangular window vector is produced. If the r parameter is assigned a value greater than or equal to one, a Hanning window vector is produced. The windowed sine sweep signal was examined in the frequency domain for various values of the r parameter. An r parameter value of 0.7 produced the cleanest FFT for the sine sweep signal. Figure 3.20 shows the time domain representation of the sine sweep signal after multiplication with the Tukey window. The resulting signal in the frequency domain is shown in Figure 3.21.

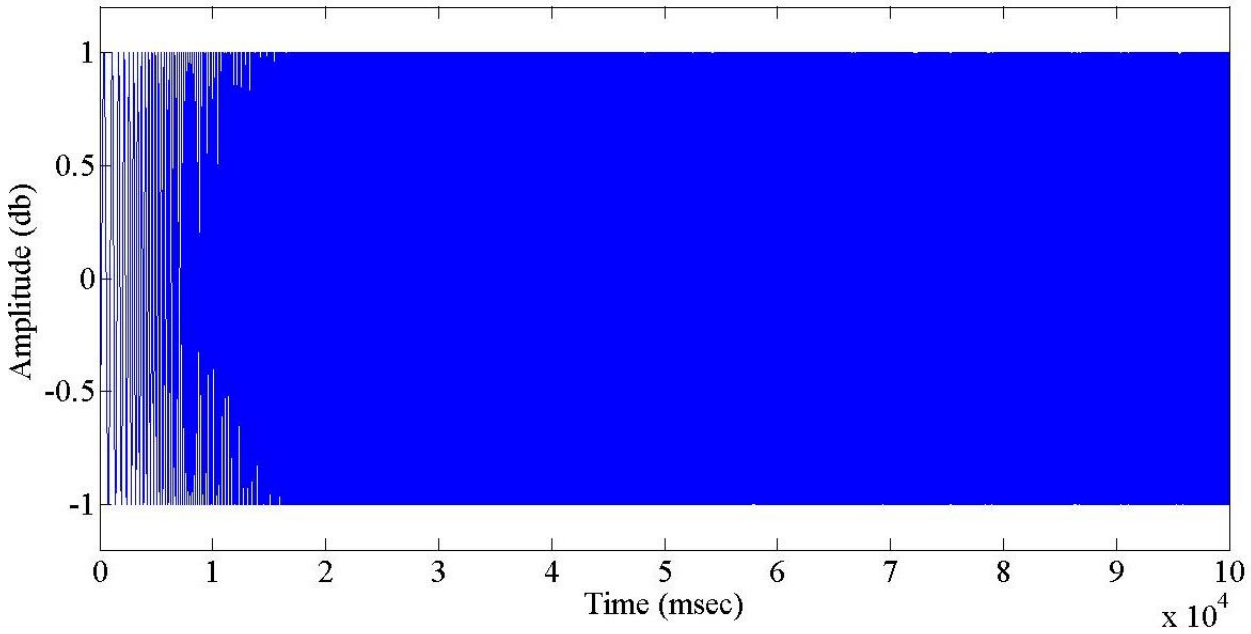

Figure 3.18 Time Domain Representation of the linear sine sweep signal (100 sec, 1-55 Hz).

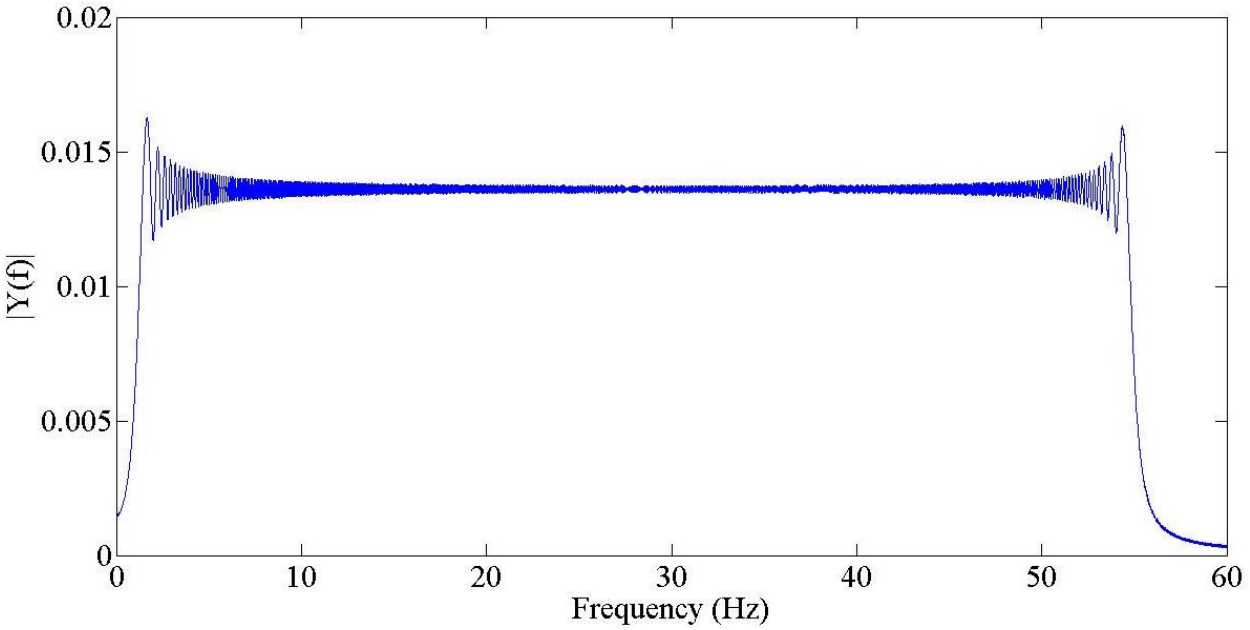

Figure 3.19 Frequency Domain Representation (FFT) of the Sine Sweep Signal (Single sided absolute value amplitude spectrum of Y(t), 1Hz – 55 Hz).

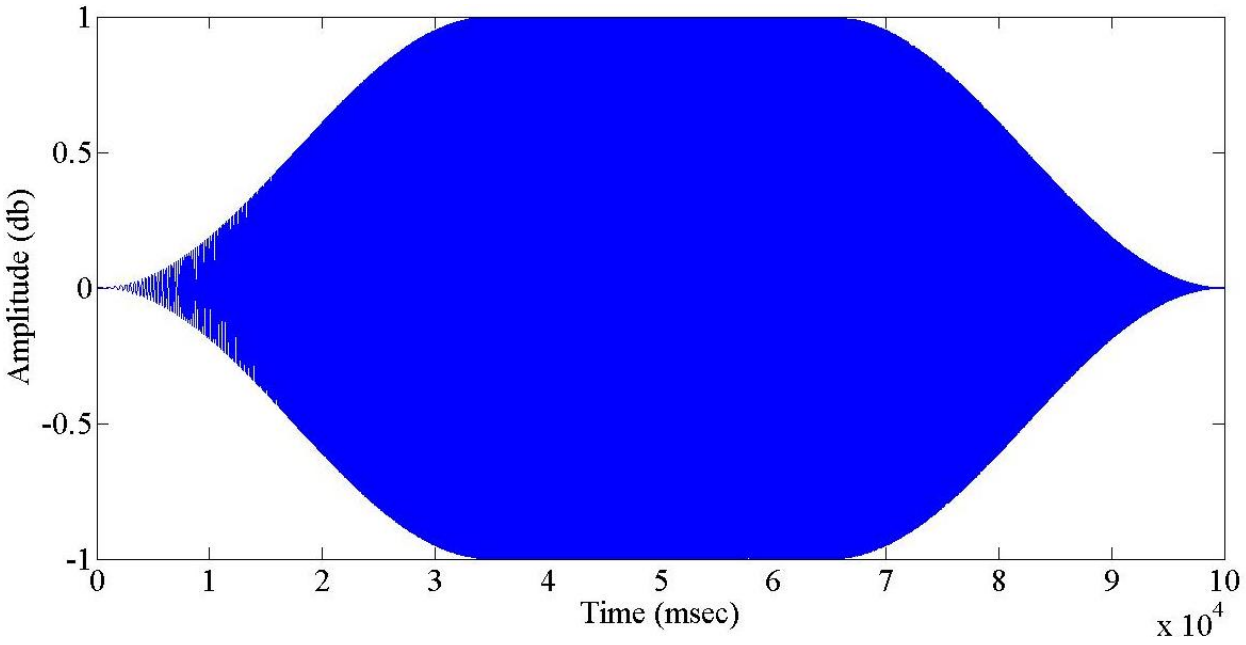

Figure 3. 20 Time Domain Representation of the Tukey Windowed Sine Sweep (100 sec, 1-55 Hz).

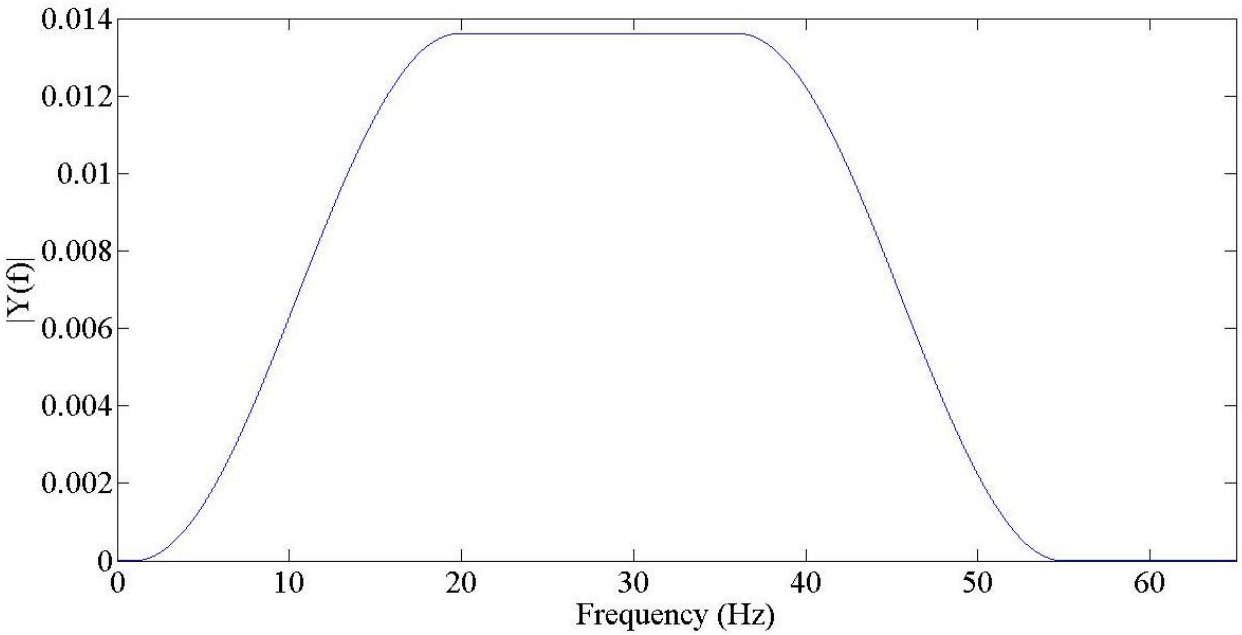

Figure 3.21 Frequency Domain Representation (FFT) of the Single Sided Amplitude Spectrum of the Tukey Windowed Sine Sweep signal (1 Hz – 55 Hz).

After the creation of the sine sweep signal and its windowing parameters were established, a targeted sine sweep excitation signal was created. The target sine sweep was created to provide input to frequency bands where the natural frequencies of the bridge were known to be located. As mentioned previously, this was done to minimize the test time by not having to sweep the input over frequency bands that contained no modes for the bridges. Based on ambient vibration testing results, the natural frequencies of the truss bridge were known to be located within the following frequency bands: 4 Hz to 7 Hz, 9 Hz to 21 Hz, 23 Hz to 28 Hz, 31 Hz to 40 Hz, 43 Hz to 45 Hz and 53 Hz to 55 Hz. Thus, the sine sweep signal was tailored to include only those frequency bands of interest. Figure 3.22 shows a time domain representation of the targeted sine sweep signal that contained six windowed sine sweeps over the frequency bands of interest. The

FFT of this signal is shown in Figure 3.23. The sine sweep signal for the Hartbarger Bridge was created similarly by taking advantage of its known frequencies from ambient vibration testing.

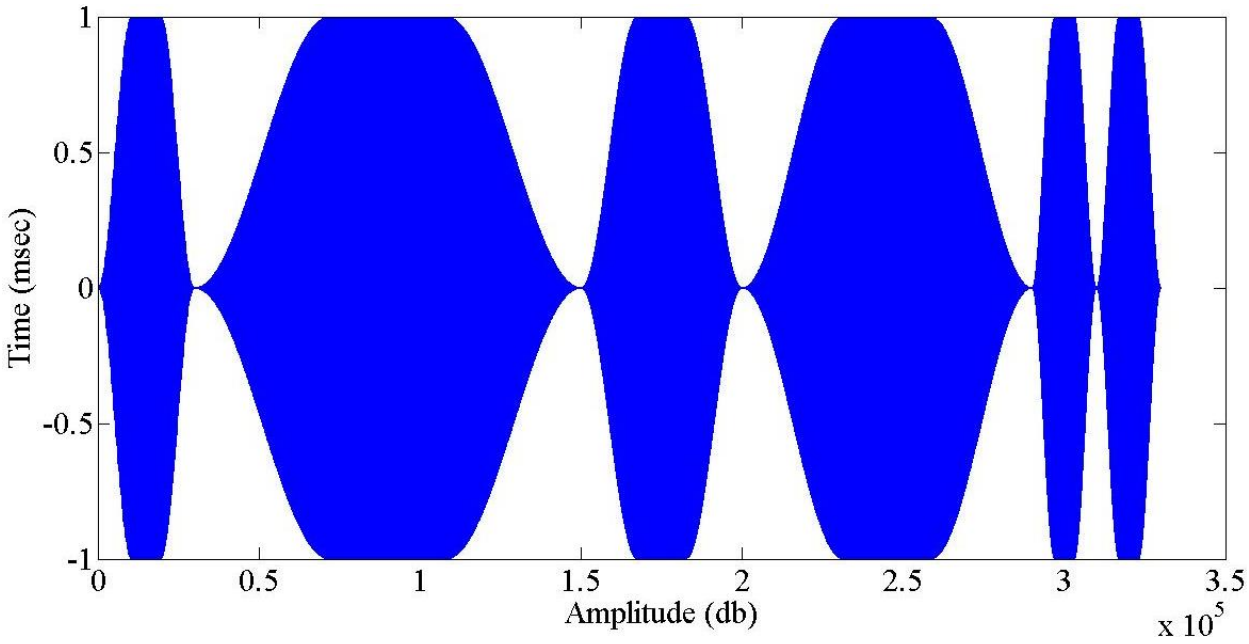

Figure 3.22 Time Domain of Tukey Windowed Targeted Sine Sweep Signal.

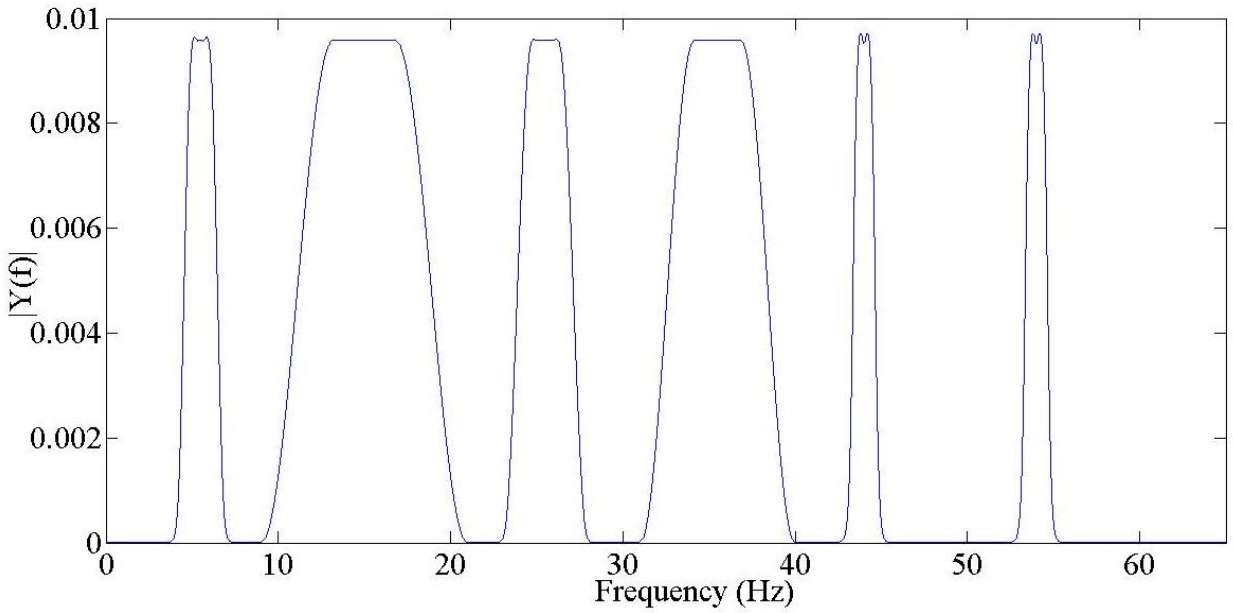

Figure 3.23 Frequency Domain Representation (FFT) of the Single Sided Amplitude Spectrum of the Tukey Windowed Targeted Sine Sweep signal (1 Hz – 55 Hz).

A preliminary evaluation of the sine sweep and targeted sine sweep signals was performed on the Baptist Ford bridge using a limited number of accelerometers to assess which signal best excited the structure. A total of five accelerometers were used in this trial field test, and all of them were placed along the downstream truss line of the bridge to be able to capture both bending and torsion modes. Figure 3.24 shows the sensor layout used for this trial field test. Six different excitation signals were compared: a burst random signal (BR), three linear sine sweeps (SS) from 3 Hz to 60 Hz with signal durations of 60, 120 and 180 seconds, a Tukey windowed sine sweep signal (TWSS) (3 Hz to 60 Hz) and a Tukey windowed targeted sine sweep signal (TWTSS). Table 3.1 summarizes the characteristics of each excitation signal evaluated during the preliminary field test. For the preliminary testing, the shaker was placed between locations

A1 and A2 (Figure 3.25) to avoid exciting the bridge at one of the nodal locations (point of zero motion) for the second bending mode or the second torsion mode.

The acceleration data collected from each of the input signals used were subsequently processed in MATLAB. FFTs were computed and plotted for each sensor location. Since the different sine sweep signals had different lengths, the shorter signals were zero padded to match the length of the longest signal (TWTSS). This allowed the same block size to be used in computing the FFTs for each signal case and provided the same frequency resolution for all of the measurements. The FFTs computed for the accelerometer at location A3 for each input signal are shown in Figure 3.26. The figure clearly shows peaks which occur at the natural frequencies of the structure and also agree with the peaks found by ambient vibration testing. The figure also shows that the TWTSS excitation signal provided the most power at the natural frequencies. This indicates that the TWTSS signal will provide better signal to noise ratio in the measurements, and this sine sweep excitation signal was selected for the full-scale vibration tests of the two bridges.

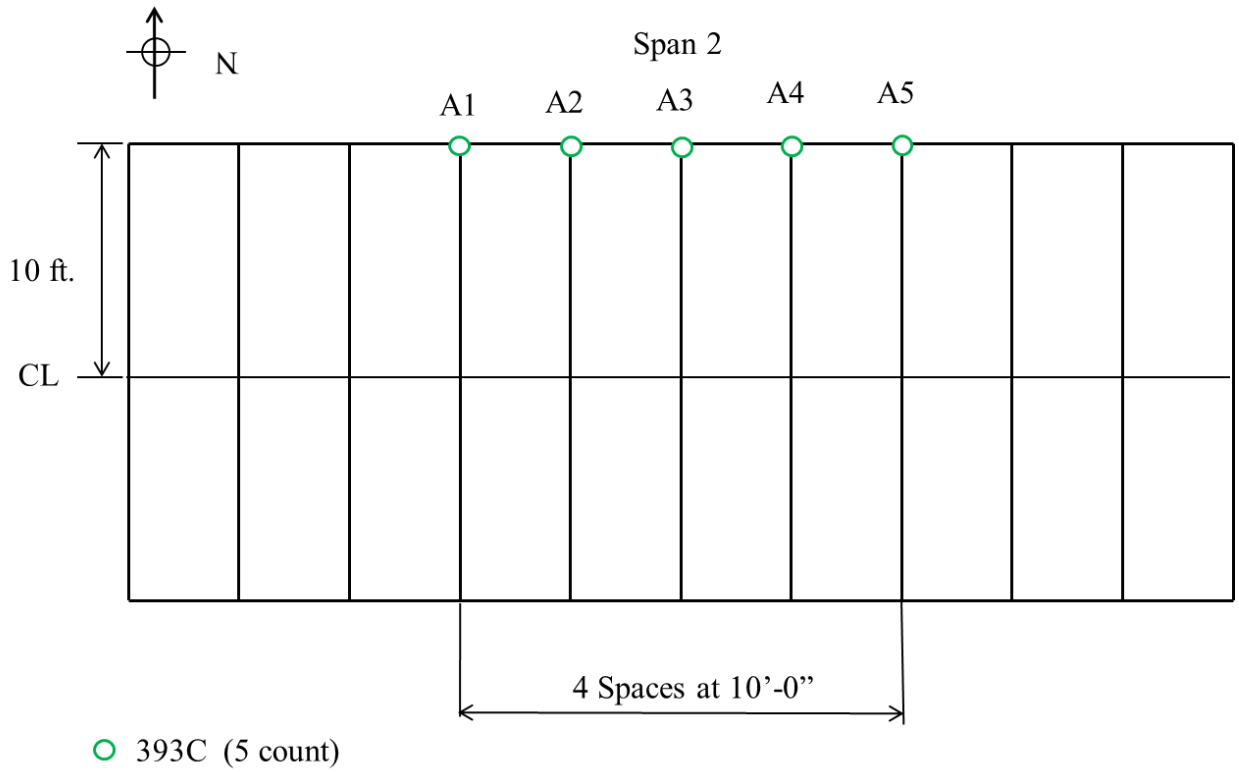

Figure 3.24 Accelerometer Layout for Preliminary Testing of the Baptist Ford Bridge.

Table 3.1 Shaker Excitation Signals Evaluated in Preliminary Field Test.

	Duration	# of Averages	Sample Rate	Δ freq.	Freq Band	Decimation	Window shaping
TWTSS	320 s	3	1000 Hz	0.244 Hz	Targeted	None	Tukey
TWSS	100 s	4	1000 Hz	0.244 Hz	Filtered (3-60 Hz)	None	Tukey
SS(60)	60 s	10	1000 Hz	0.244 Hz	Filtered (3-60 Hz)	None	None
SS(120)	120 s	5	1000 Hz	0.244 Hz	Filtered (3-60 Hz)	None	None
SS(180)	180 s	3	1000 Hz	0.244 Hz	Filtered (3-60 Hz)	None	None
BR	64 s	10	1000 Hz	0.244 Hz	Filtered (3-80 Hz)	None	None

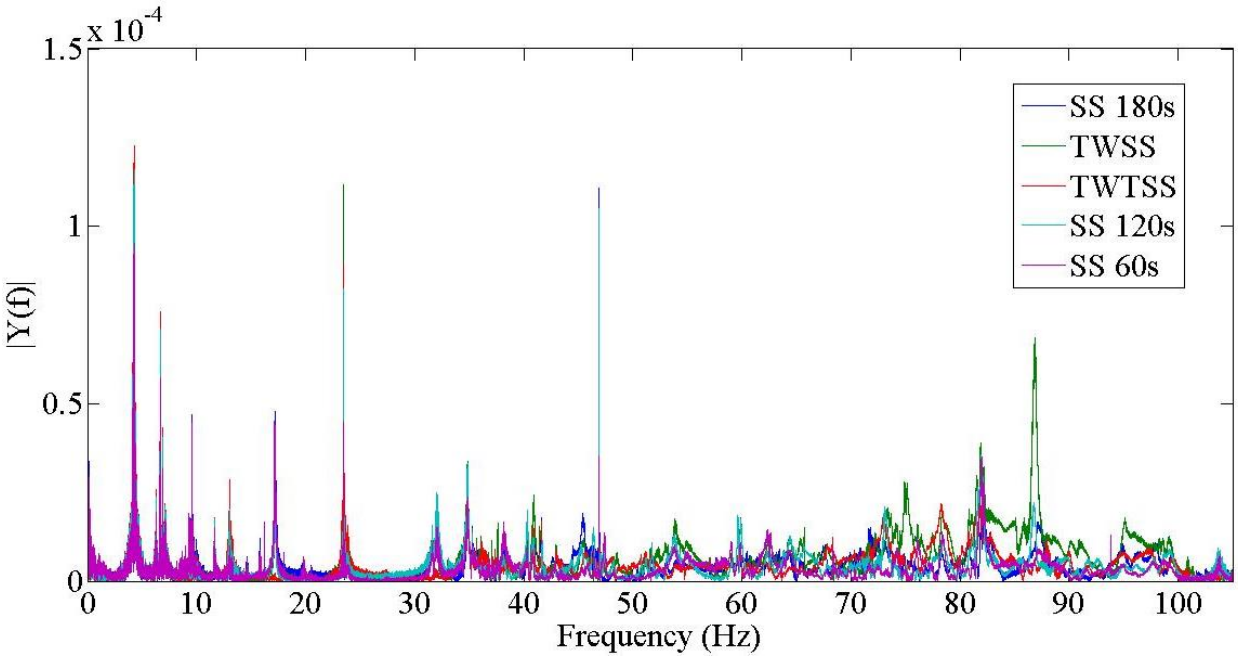

Figure 3.25 Frequency Domain Response Single Sided Amplitude Spectrum of Y(f) of Sensor A3 for Each Excitation Signal.

3.4 Data Analysis Methods

Each bridge was evaluated by ambient vibration testing and forced vibration testing. A separate data analysis approach was employed for the ambient vibration measurements and the forced vibration measurements. The ambient vibration measurements are output only measurements and these can only be used to identify natural frequencies, operating deflection shapes (which approximate mode shapes) and damping ratios. The forced vibration tests yield input-output measurements, and these can be used to identify natural frequencies, scaled mode shapes and damping ratios. In addition, the modal flexibility matrix for each bridge can be computed from the input-output measurement data. In order to avoid inconsistencies in the results due to different data analysis approaches, only one approach was used to analyze the data from the ambient vibration tests on each bridge, and only one approach was used to analyze the forced vibration tests on each bridge. The details of the data analysis methods for the ambient and forced vibration tests are presented in the following sections.

3.4.1 Ambient Vibration Data Analysis

In the case of ambient vibration testing, the excitation forces are random and not measureable. This requires that these measurements be analyzed using an output-only modal analysis algorithm. A technique developed by James et al. (1995) called the Natural Excitation Technique (NeXT), was selected for the modal parameter estimation of the ambient vibration data. The ability to process output-only vibration data using the NeXT approach makes structural dynamic testing of large operational structures more feasible. Bridges in particular, are subject to highly uncertain operating environments that cannot be easily measured or quantified. Conventional modal analysis utilizes frequency response functions (FRFs) or impulse response functions, which require measurements of both the input force and the resulting response;

however, un-measurable environmental excitations due to sources such as wind, waves and traffic, do not lend themselves to FRF calculations (James et al., 1995).

NeXT is a four step data processing technique in the time domain, however only the first two stages of the process were used in this thesis. Naturally, the first step is to acquire raw time domain response data from the operating structure. In this research, these time domain responses were in the form of measured accelerations. Long time histories of continuous data are desired, provided the operating conditions are relatively stationary. The second step is to calculate auto and cross-correlation functions from these time histories using standard techniques (Akins 1990). Correlation functions are commonly used to analyze randomly excited systems (Bendat & Piersol, 1980). Correlation functions can be expressed as summations of decaying sinusoids. Each decaying sinusoid has a damped natural frequency and damping ratio that is identical to that of a corresponding structural mode (James et al., 1993). The cross-correlation of each output channel was calculated with respect to a subset of the output channels which function as references. Then, the pseudo Impulse Response Function (pIRF) was extracted from the second half of the correlation functions, since these functions are two-sided symmetric functions. By taking the FFT of the pIRF and assuming the input to be unity at all frequency lines to simulate white noise, the pseudo Frequency Response Functions (pFRF) were estimated for each output pair.

At this point, all the parameters needed to implement the Complex Mode Indicator Function (CMIF) algorithm were obtained. The CMIF is further explained in the next section on forced vibration data analysis. Damping estimates were obtained using the same procedures described in Section 3.4.2. However, it should be noted that it will not be possible to calculate the mass-scaling for the mode shapes. This prevents modal flexibility from being calculated directly from

the output-only measurements. This is one of the most significant limitations of ambient vibration testing.

3.4.2 Forced Vibration Data Analysis

The complex mode indicator function (CMIF) algorithm was used for modal parameter estimation with the forced vibration measurements since it has a long and well-documented application history for vibration tests of bridges. The CMIF algorithm is often combined with another algorithm, the Enhanced Frequency Response Function (eFRF), to accurately scale the mode shape vectors. This is a critical step for obtaining an accurate estimate of modal flexibility. These two algorithms were combined and coded in MATLAB, and implemented with additional data processing procedures to identify the dynamic characteristics and modal flexibility of both bridges. Figure 3.27 shows a flowchart of the processing steps required to obtain the modal parameters, which are then used to compute modal flexibility. The details of these data processing steps are further described below.

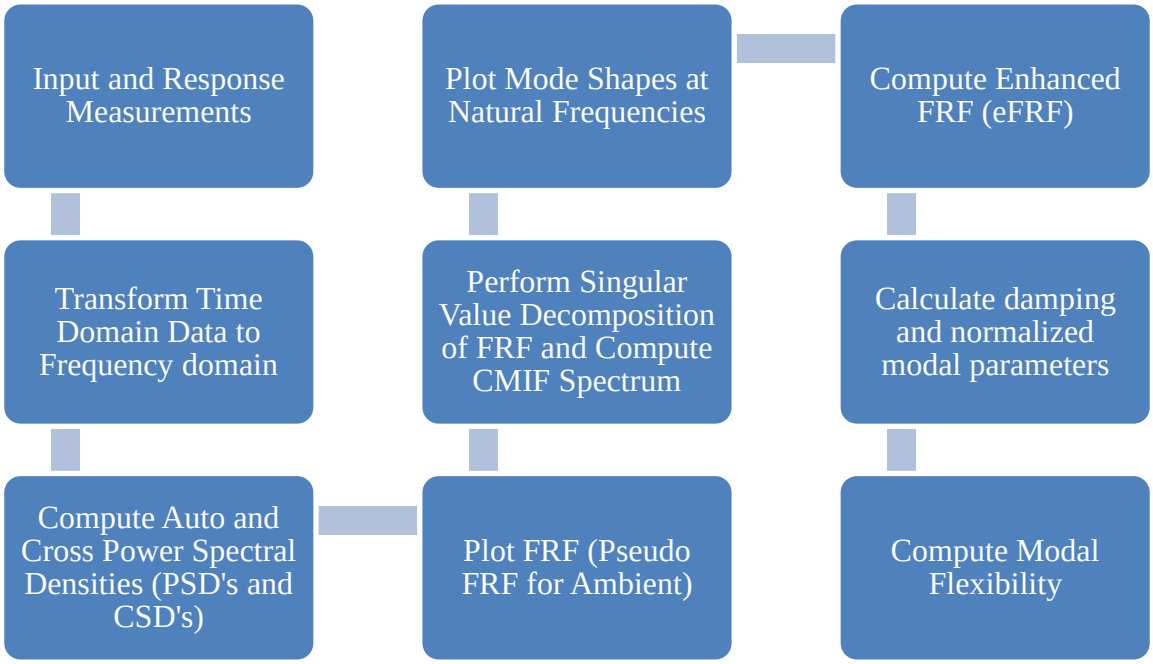

Figure 3. 26 Data Processing Flow Chart.

For the control input type tests, it is important to accurately capture the initial equilibrium state of the structure before the excitation is applied to the structure. This was accomplished by setting the data acquisition system to acquire data 30 time steps before the trigger was initiated. The measured response data were detrended to remove any DC offset in the signals. The measured input and output signals were transformed to the frequency domain employing the Fast Fourier Transform function in MATLAB. The data sets were then used to compute auto and cross power spectrums for the inputs and outputs. The expressions used to compute the cross power spectrums of the inputs and outputs are shown in equation (3.1) and (3.2) and those for computing the auto power spectrums for the output and input signals are given in equation (3.3) and equation (3.4), respectively.

$$GFX_{qp} = \sum_{1}^{N_{avg}} F_q X_p^* \tag{3.1}$$

$$GXF_{pq} = \sum_{1}^{N_{avg}} X_p F_q^* \tag{3.2}$$

$$GXX_{pp} = \sum_{1}^{N_{avg}} X_p X_p^* \tag{3.3}$$

$$GFF_{qq} = \sum_{1}^{N_{avg}} F_q F_q^* \tag{3.1}$$

Where

F = input force spectrum (in frequency domain).

X = response spectrum (in frequency domain).

p = output DOF.

q = input DOF

N_{avg} = number of averages used in the data set.

* denotes the complex conjugate of the spectrum.

The term G refers to a one sided spectrum.

Two different methods were explored to compute frequency response functions (FRFs) from the measured data: the H1 algorithm and the H2 algorithm. The H1 algorithm (Eq. (3.5)) is the most common formulation of the FRF, and tends to minimize the noise on the output measurements. On the other hand, a less commonly used algorithm, the H2 (Eq. (3.6)), tends to minimize the noise on the input measurement. The FRFs estimated using both algorithms were compared to identify any extraneous noise present in either the response or the input

measurements. Taking advantage of the higher fidelity of the H1 algorithm, this algorithm will be used for the singular value decomposition (SVD) and CMIF algorithm.

$$H1_{pq} = \frac{GXF_{pq}}{GFF_{qq}} \tag{3.5}$$

$$H2_{pq} = \frac{GXX_{pp}}{GFX_{qp}} \tag{3.6}$$

Where GXF and GFX are the cross power spectrums of the inputs and outputs and GFF and GXX are the auto-power spectrums for the input and outputs, respectively. Since the measured data was acceleration ("inertance" FRF, A/F → Acceleration spectrum divided by force spectrum), each spectral line was divided by $j\omega^2$ to convert the acceleration data into displacement data ("receptance" FRF, X/F → Displacement spectrum divided by force spectrum).

When the FRF matrix (H(ω)) is computed using the H1 algorithm, the input locations represent columns in the matrix and the output locations represent the rows in the matrix. The third dimension of the matrix contains frequency lines. To obtain the CMIF spectrum, the FRF matrix is decomposed at each frequency line. Allemang et al., (2006) suggest that the most efficient approach for decomposing the FRF at each spectral line is singular value decomposition (SVD). The CMIF method requires a good estimate of the number of modes in a given frequency interval. This can be accomplished by plotting the singular values, S(ω), of the FRF matrix at each spectral line (Catbas et al., 2004). The formulation of SVD at each spectral line, ω, can be described by Eq. (3.7).

$$\left[imag(H(\omega))\right]_{N_o x N_i} = \left[U(\omega)\right]_{N_o x N_i} \left[S(\omega)\right]_{N_i x N_i} \left[V(\omega)\right]^H_{N_i x N_i} \tag{3.7}$$

Where

'*imag'* refers to the imaginary portion of the matrix

$U(\omega)$ = left singular vectors.

$V(\omega)$ = right singular vectors.

N_o = number of outputs.

N_i = number of inputs.

$[\ ]^H$ denotes the Hermitian transpose.

Employing SVD on the imaginary part of the FRF plot produces real-valued singular vectors, which are easier to interpret and use for identifying modal frequencies. The singular values can then be plotted over the entire frequency band of interest. A separate singular value spectrum is produced for each input location utilized in the CMIF formulation. The peaks in the CMIF spectra represent possible modes of the system. It should be noted that experimental error and other factors lead to spurious peaks in the CMIF spectra that are not natural modes of the structure. An automated peak-picking algorithm was implemented for the CMIF spectra and was inspected to avoid including spurious peaks in latter processing stages.

The first stage for estimating modal parameters using the CMIF method is the estimation of spatial information, or modal vectors (Phillips and Allemang, 1998). Besides producing a clear plot of the possible locations of modes in the structure, SVD provides approximate mode shape vectors at every frequency line, which are found in the left singular vectors, $U(\omega)$. By taking the $U(\omega)$ at the same spectral line corresponding to a peak in the CMIF spectra, those vectors can be plotted to obtain a visual representation of the mode shapes. Since the mode shapes that contribute to each peak do not change much in the vicinity of each peak, any given number of

spectral lines around the peak of interest may give the same shape (Allemang and Brown, 2006). These mode shapes are useful for verifying the resonant vibration modes of the structure, but in this form have arbitrary scaling and will not produce an accurate estimate of modal flexibility. Therefore, scaling of the mode shapes is important, and is found in the second stage of the CMIF method.

This second stage estimates the temporal information, i.e. modal frequencies and modal scaling. These parameters can be estimated through the formulation of an enhanced FRF (eFRF), which effectively decouples a multiple degree of freedom (MDOF) system into a series of single degree of freedom (SDOF) systems. In this stage, the eFRF utilizes U(ω) as a modal filter to represent the overall FRF as a SDOF system for each mode. In order to obtain correct scaling for the eFRF, a scaling vector obtained from the left and right singular vectors is used. The H(ω) matrix is then pre- and post-multiplied by the corresponding filter and scaling vectors at each frequency line to obtain the eFRF, as seen in the expression below (Eq, 3.8) (Phillips and Allemang, 1998; Catbas, Brown, and Aktan, 2004).

$$
\begin{aligned}
u &= U(\omega_r) \\
v_{sc} &= pinv(V(\omega_r)) * u(dpt) * V(\omega_r) \\
eFRF(\omega) &= u^T * H(\omega) * v_{sc}
\end{aligned}
\qquad (3.8)
$$

Where

r = mode of interest

u = modal filter vector (a column from U(ω) corresponding to the chosen singular value)

v_{sc} = modal scaling vector

pinv denotes the pseudo inverse of a matrix

dpt = driving points

^{T} denotes the transpose of a matrix

Once the eFRF is obtained, a least squares curve fitting algorithm was used to fit a curve to the peak in each eFRF. The least squares estimation produces a complex modal frequency, containing frequency and damping, for each mode (Allemang et al, 1998).

$$\begin{bmatrix} eFRF(\omega_p) - eFRF(\omega_1) \\ eFRF(\omega_p) - eFRF(\omega_2) \\ eFRF(\omega_p) - eFRF(\omega_p) \\ \vdots \\ eFRF(\omega_p) - eFRF(\omega_s) \end{bmatrix} \lambda_r = \begin{bmatrix} j\omega_p * eFRF(\omega_p) - j\omega_1 * eFRF(\omega_1) \\ j\omega_p * eFRF(\omega_p) - j\omega_2 * eFRF(\omega_2) \\ j\omega_p * eFRF(\omega_p) - j\omega_p * eFRF(\omega_p) \\ \vdots \\ j\omega_p * eFRF(\omega_p) - j\omega_s * eFRF(\omega_s) \end{bmatrix} \quad (3.9)$$

where

ω_p = frequency at the peak of interest

$\omega_1 - \omega_s$ = frequencies above and below the peak of interest.

λ_r = complex modal frequency for each mode *r*.

The above set of over-determined linear equations is then solved using a pseudo-inverse approach to determine the complex modal frequency. The scaling factor (Modal A) is found in a similar manner. This factor allows the modal vectors to be mass unit normalized without assuming a mass matrix, thus providing the proper scaling of the modal flexibility matrix (Catbas, Brown, and Aktan, 2004).

$$M_{A_r} = s_1 * s_2 * B * pinv(A) \quad (3.10)$$

where

M_{A_r} = Modal A for each mode r.

$s_1 = \phi_r^T * \phi_r$

$s_2 = \phi_r (dpt)^T * v_{sc}$

$$A = \begin{bmatrix} eFRF(\omega_1) \\ eFRF(\omega_2) \\ eFRF(\omega_p) \\ \vdots \\ eFRF(\omega_s) \end{bmatrix}$$

$$B = \begin{bmatrix} 1/(j\omega_1 - \lambda_r) \\ 1/(j\omega_2 - \lambda_r) \\ 1/(j\omega_p - \lambda_r) \\ \vdots \\ 1/(j\omega_s - \lambda_r) \end{bmatrix}$$

ϕ_r = mode shape vector for each mode *r*.

3.4.3 Modal Flexibility

After having obtained the modal parameters of each structure in the previous steps, a modal flexibility matrix was formulated for each bridge.. This step culminates the data processing stage and, as mentioned in previous chapters, is the end goal of the data analysis stage being the final result with which the different characterization approaches will be compared. Catbas et al. (2006) define modal flexibility (MF) as shown in Eq (3.11):

$$MF = \sum_{r=1}^{\#MODES} \frac{\phi_r \cdot \phi_r^T}{M_{A_r}(-\lambda_r)} + conj\left(\frac{\phi_r \cdot \phi_r^T}{M_{A_r}(-\lambda_r)}\right) \qquad (3.11)$$

where

ϕ_r = mode shape vector for mode r.

M_{A_r} = Modal A for each mode r

λ_r = complex modal frequency for mode r.

'*conj'* denotes the complex conjugate of the value.

It was already noted in Chapter 2 that MF is only an approximation of real flexibility. Uncertainties in the measured data can introduce error into this approximation. Since modal flexibility contains a summation over the number of modes observed, it would be necessary to perform the summation over an infinite number of modes to compute the exact flexibility for a given structure from its measured modal parameters,. Thus, using only a subset of these modes will never provide an exact estimate of the actual structural flexibility. That being said, if enough modes are used in the summation, a very close approximation of the flexibility of the structure can be obtained. Furthermore, the dynamic response of most structures is largely determined by its first few fundamental modes. The error in the modal flexibility identified from a finite number of modes in dynamic testing is likely to be less than the uncertainty levels associated with the in-situ mechanical characteristics of constructed systems.

4 Results

4.1 Introduction

This chapter presents the results obtained from the field vibration tests of the two bridges evaluated for this study. These results include the natural frequencies, mode shapes and damping ratios identified for each bridge from each type of vibration test. Also, modal scaling and the modal flexibility matrices computed from the controlled input vibration tests of each bridge will also be presented and discussed. The dynamic characterization results are also compared across the two very different bridge types evaluated for this study. Because of the observed quality and consistency of the results obtained from the multiple reference impact tests (MRIT), these results are used as the baseline for comparing the dynamic characterization results from the other vibration testing methods that were implemented.

4.2 Natural Frequencies and Damping Ratios

4.2.1 Hartbarger Bridge

The following section presents the natural frequencies and damping ratios identified from the three different dynamic tests performed on the Hartbarger Bridge. Figure 4.1 shows the CMIF plot after singular value decomposition was performed on the impact test data sets to illustrate how the natural frequencies were identified from the vibration measurements. Circles filled with asterisks are located at peaks in the trace of the largest singular values versus frequency. These peaks represent the probable locations of the damped natural frequencies of the structure (assuming no harmonic forces were acting on the structure and that numerical and experimental errors are minimal). Singular value decomposition of the frequency response function matrix at each frequency line yields a diagonal matrix of singular values, $S(\omega)$, which are ordered from

largest to smallest along the diagonal and defined at each frequency line. The number of traces shown in the CMIF plot is equal to the number of singular values that exist at each frequency line, and is equal to the number of reference locations. Most of the modal frequencies were located on the upper leftmost location of the diagonal of the S(ω) matrix, however some modal frequencies were found on lower energy locations in the singular value matrix (e.g. the S(2,2), S(3,3) and even the S(4,4) locations). Figure 4.1 only shows the first 5 modal frequencies for illustration purposes. The natural frequencies from the shaker testing measurements were found in a similar manner.

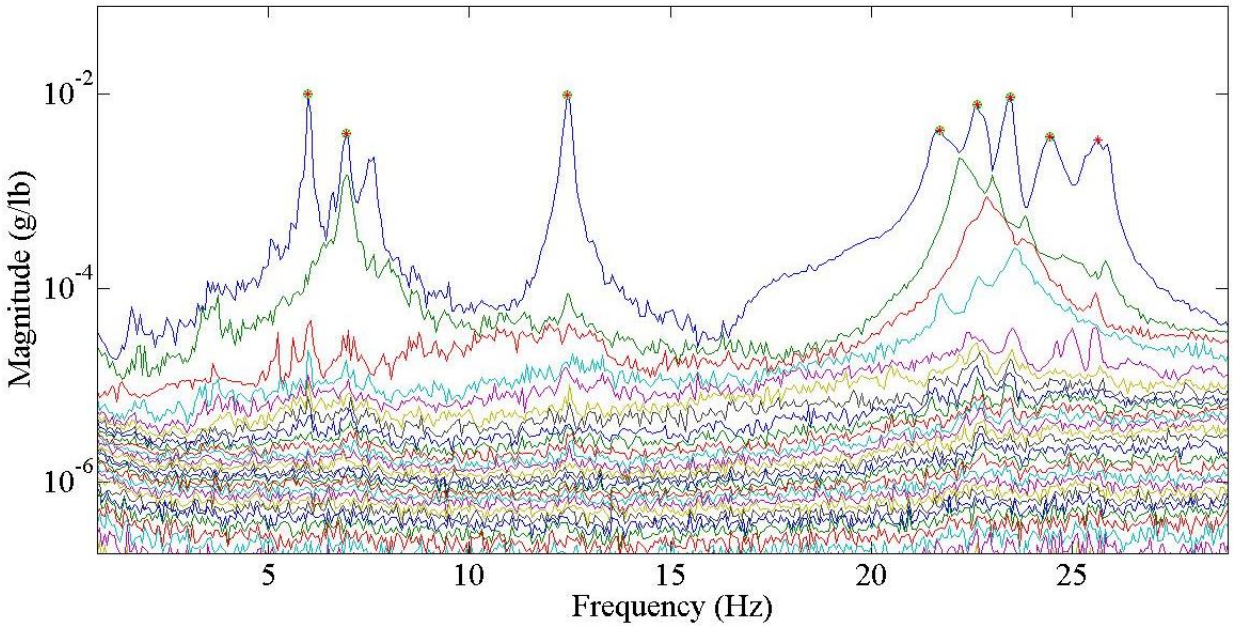

Figure 4.1 CMIF plot, Impact Test.

As mentioned in Chapter 3, the ambient vibration test data was analyzed using the NeXT approach. First, the auto and cross-correlation functions from the vibration measurements (outputs only) were estimated. Then, pseudo impulse response functions (pIRFs) were extracted from the correlation functions and then plotted to verify the quality of the results. Each plot should resemble a free vibration decay response as shown in Figure 4.2. Once the quality of the plots was verified, pseudo frequency response functions (pFRFs) were estimated by taking the fft of the pIRFs assuming the unmeasured input was white noise. The pFRFs were also plotted in Figure 4.3 to verify the results in the frequency domain. Then, the pFRF matrix was reshaped in the proper format for applying the CMIF algorithm. At this point, the data analysis methods used for the ambient vibration test data and the controlled input vibration test data are almost identical. However, for the controlled input tests, the FRFs were converted from the inertance form (A/F) to the receptance form (X/F) by dividing the FRF by $(j\ \omega)^2$ at each frequency line. Also, since the input data had units of g and lbf, it was converted from g to ft/s^2 which converted the units of the FRF to ft/lb.

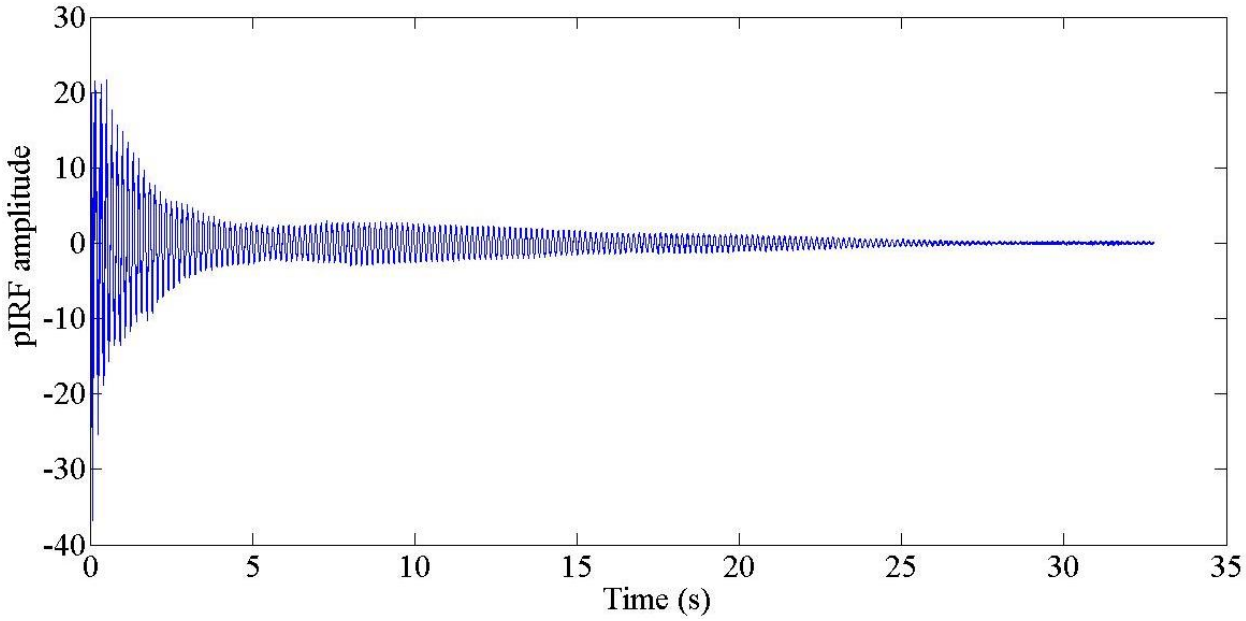

Figure 4.2 Pseudo impulse response function plot from ambient vibration data (Hartbarger Bridge).

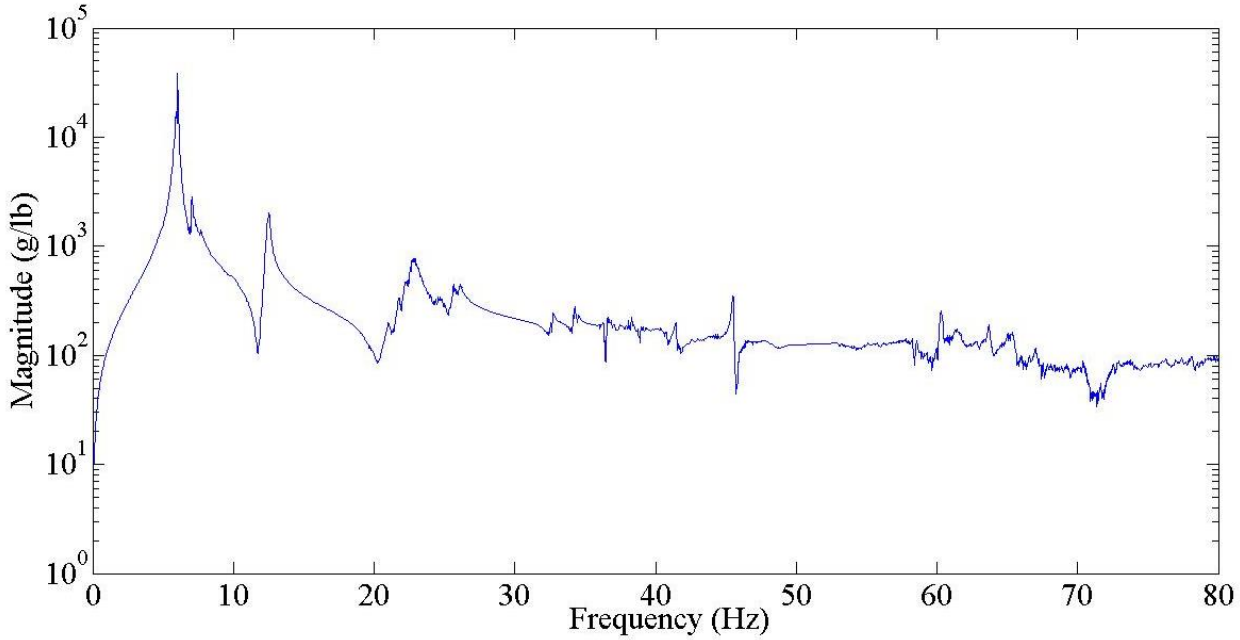

Figure 4.3 Pseudo frequency response function plot from ambient vibration data (Hartbarger Bridge).

In order to estimate modal damping and modal scaling, enhanced frequency response functions (eFRFs) were generated by modal filtering the FRF data. This is accomplished using by pre and post multiplying the FRF with the estimated mode shape vector for each mode. Due to the orthogonality of the modes, this serves to filter out the contributions of other modes at each peak leading to a SDOF model for each peak in the FRF. The singular vectors that are associated with the singular values selected previously were estimates of the mode shapes at the corresponding frequency lines. Each mode shape was used as a modal filter to enhance the contribution of a single mode while diminishing the effects of other neighboring modes. With the use of multi-vector scaling, which uses only the left singular vectors, more than one modal

vector was used as a filter which further reduced the impact of other close by modes to the eFRFs. This improved the accuracy of the parameter estimation by making the eFRFs a closer estimate of a SDOF system. It is the assumption of an SDOF system that allowed the modal parameters to be estimated from each peak. It should be noted that at a peak, the first column of each singular vector contains an estimate of the dominant mode shape and that the left and right vectors are essentially equal in magnitude; the right vectors are dominantly real and the left vectors are dominantly complex. This means that the left and right vectors are only different by a complex scalar, which allows the use of the left vectors only. In the use of multi-vector scaling, the number of modes used to produce the eFRF must be less than the number of input locations so that the pseudo-inverse can be computed (Allemang and Brown, 2006). Thus, a group of peaks was selected for use, which was less than the total number of modes. The filtering process works better when the filter peaks are not spatially related to the peak being magnified. Thus, Modal Assurance Criterion (MAC) values were check to select the modes that were the least related to the current mode (Fernstrom, 2012). This metric is discussed further in relation to the mode shapes later in this chapter.

Once the eFRFs were known, the poles (lambda) of the system were found. The poles contain the damped natural frequency and modal damping information. Lambda was found by fitting a solution, based on the Least Squares Local SDOF method (Allemang, 1998), to the shape of the eFRF curves in the vicinity of the peaks. A total of five points ahead of and five points after each peak were used for estimating for a total of eleven frequency lines. Some peaks of the eFRF were not perfectly aligned with the CMIF peaks and the parameter estimation was considered flawed if the eFRF peak was not within the eleven frequency lines considered. Thus,

the index number of the eFRF peaks was selected and used as the center point of the eFRF segment used for parameter estimation. This method also provides the residue which is proportional to the modal scaling. For the controlled input vibration tests, the eFRFs were plotted for each mode along with the SDOF FRF synthesized from the identified modal parameters. An example of this eFRF and the synthesized FRF is shown in Figure 4.4 for the first mode of impact test data. For the ambient test data, only the eFRFs were plotted without the synthesized eFRF overlay as can be seen in Figure 4.5. However, the process for obtaining lambda was the same than for the impact test data. Plots of the synthesized FRFs were reviewed in order to check the fit of the modal parameters as a whole to the actual FRF data. This was done by adding the eFRFs together, which is equivalent to recombining the SDOF systems into an MDOF system. The actual FRF data is also shown so the fit of the synthesized FRF can be seen in Figures 4.6 for the eFRF of the same output / input location and Figure 4.7 for the eFRF of the different output / input locations. As can be seen in these figures, the phase of the response is also plotted and shows the expected in-phase and out-of-phase variations aligning with the eFRF peaks.

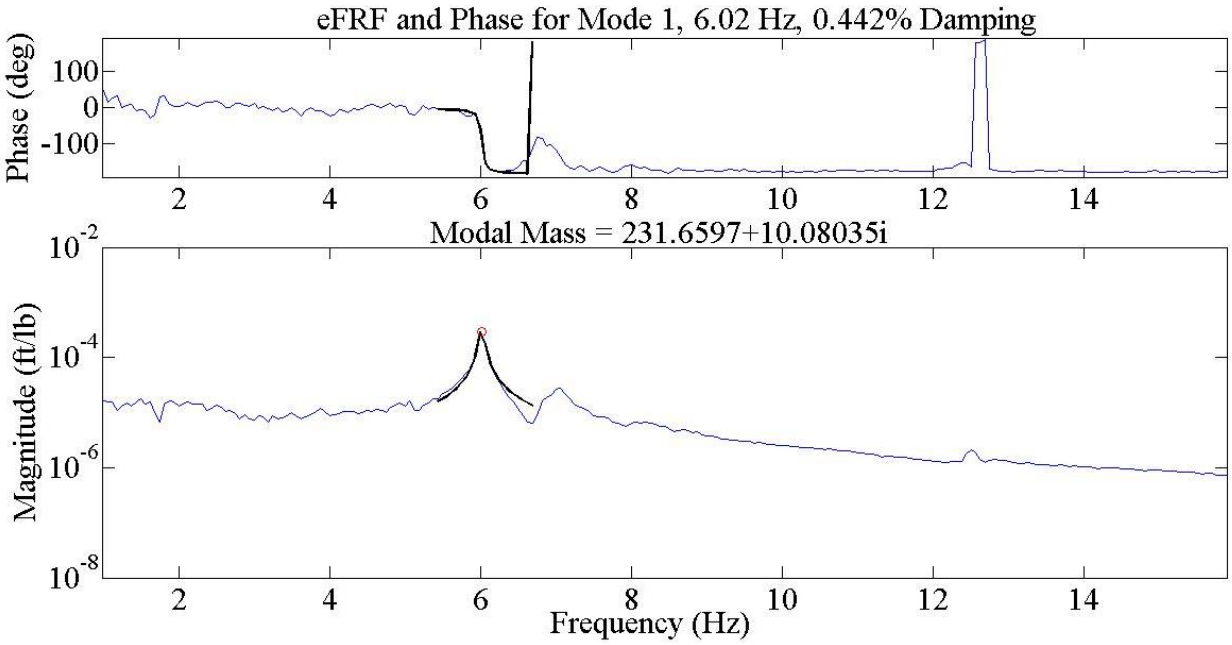

Figure 4.4 eFRF plot for mode 1, impact test, (Hartbarger Bridge).

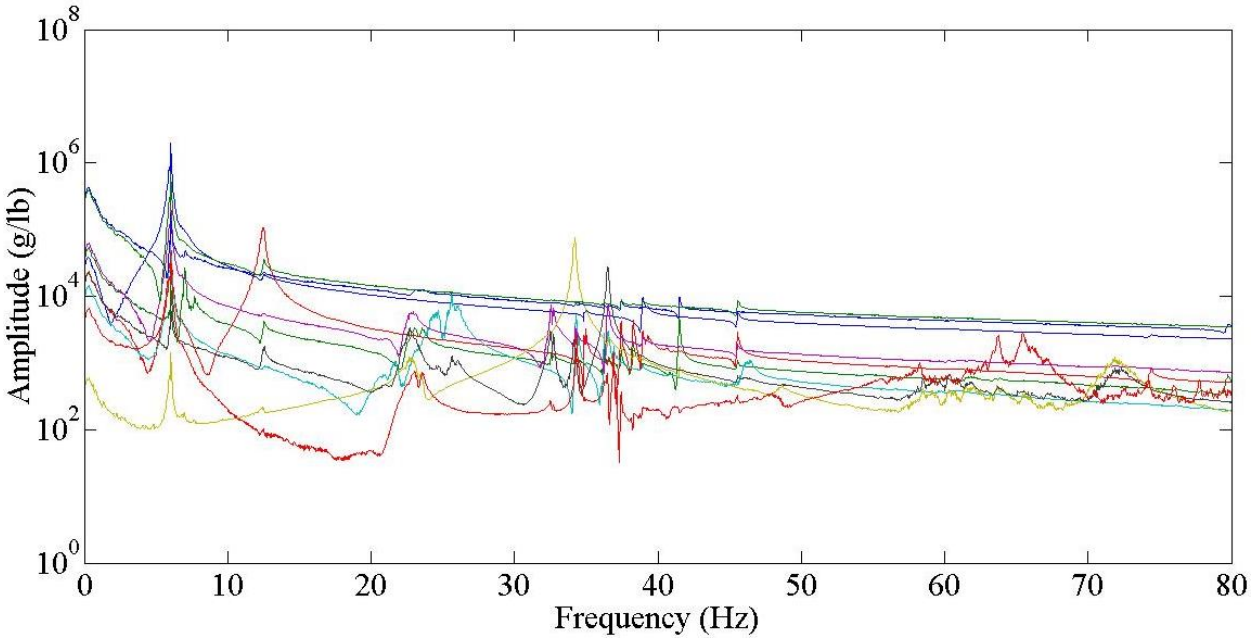

Figure 4.5 eFRFs for all modes from ambient vibration test (Hartbarger Bridge).

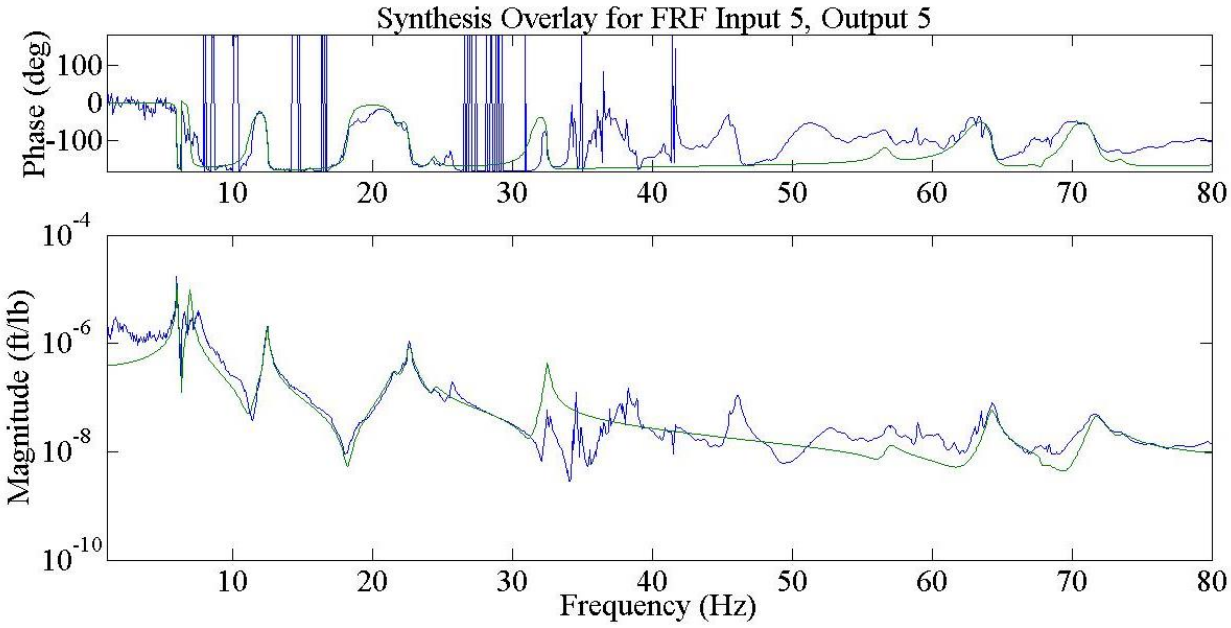

Figure 4. 6 Synthesized eFRF for same output/input location (Hartbarger Bridge).

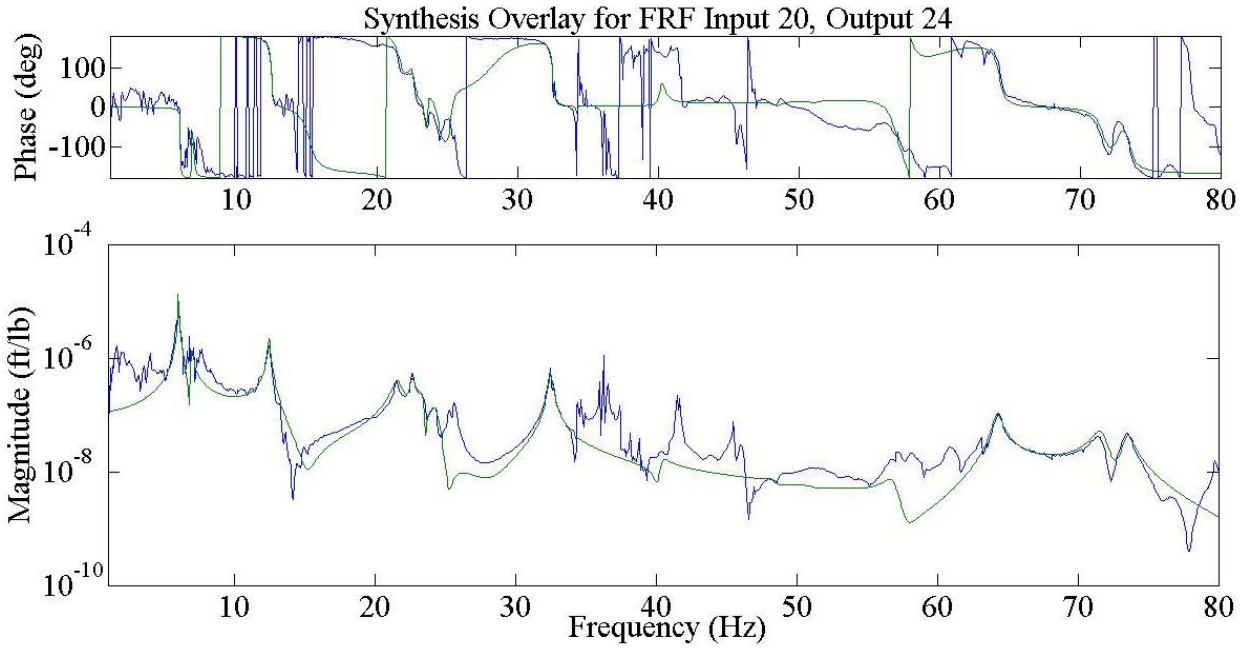

Figure 4. 7 Synthesized eFRF for different output/input locations (Hartbarger Bridge).

At this point it is necessary to discuss the data obtained from the shaker test on this bridge. The shaker testing was performed overnight to take advantage of the reduced traffic traveling during that time. Due to time, equipment and personnel limitations, both of the shakers tests (Burst Random and Swept Sine) were only implemented on half of the span. Figure 4.8 shows the input locations that were able to be completed before higher morning commute traffic on the bridge made it impossible to find a lapse of time long enough to allow either of the two signals to be played without interruption. Also, an issue was found with three of the sensors and thus the shaker test had only 25 output DOFs instead of the 28 available for ambient and impact testing. Despite these setbacks, most of the higher order modal frequencies were found and mode shape estimates were plotted for these frequencies, although their quality was far from that of the full

grid impact or ambient tests. Moreover, these issues affected the quality of the modal parameters in such a way that damping ratio estimates found were extremely inaccurate and unrealistic and are thus not included in Table 4.1, neither was the modal flexibility formulated from this test.

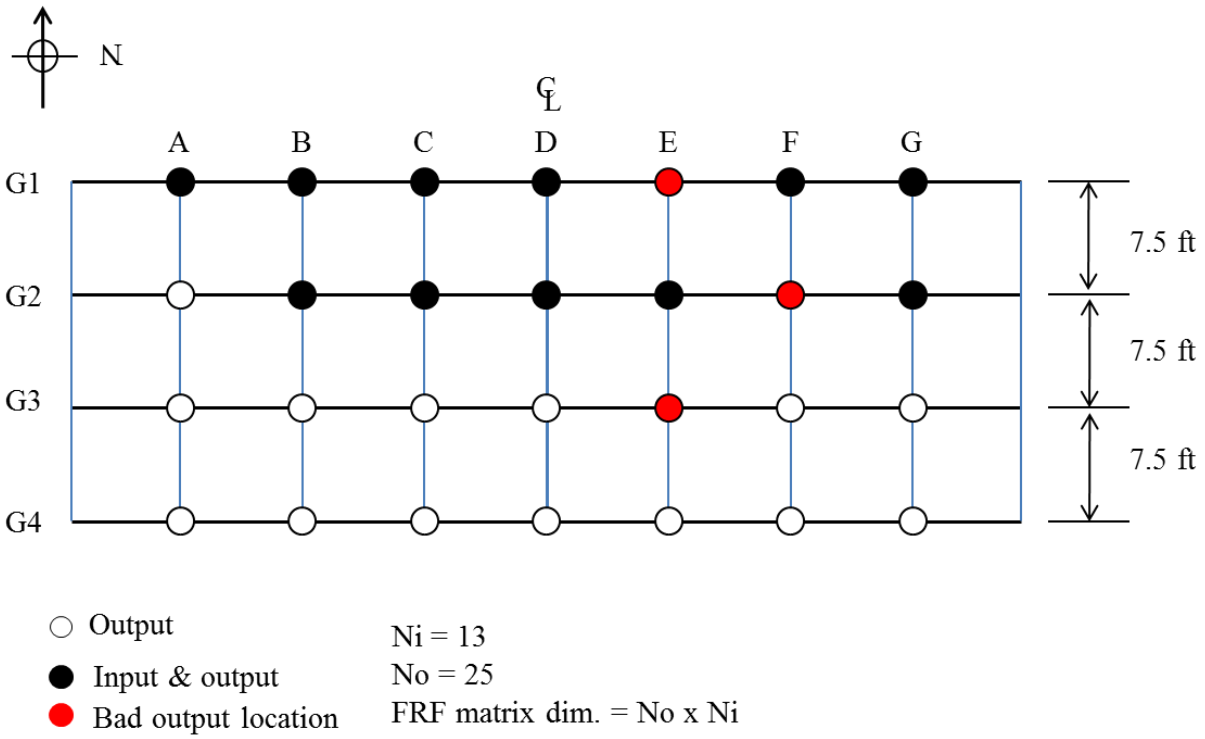

Figure 4.8 Actual shaker field test execution, Hartbarger Bridge.

The natural frequencies for the two types of tests are tabulated in Table 4.1. The values from the ambient and shaker test were compared against the values from impact tests, however as mentioned above, only the comparison between ambient vibration test and shaker test are presented. A total of 11 modal frequencies were found within the frequency range of interest,

which was set from 0 to 80 Hz. Each identified natural frequency was within 5% of the frequency identified from the other vibration testing methods for a given mode. It can be seen that some closely spaced modal frequencies, such as mode four, were not found in the ambient data. This can be attributed to a couple of reasons. First, the nature and magnitude of the excitation in the ambient field test might not have excited this mode, which is the second global bending mode as will be shown in the mode shape section latter on this chapter. Second, the processing techniques used between controlled input tests and ambient tests are different, which might cause the peak of this frequency to be hidden behind higher energy neighboring modal frequency peaks, as is the case with mode five shadowing mode four. Some mode shapes were found to repeat at higher frequencies, in which cases the higher energy lower modal frequency was chosen to be included in the Table 4.1. This happened for mode six, repeating at 64.3 Hz, for mode eight, repeating at 71.7 Hz and for mode ten, repeating at 73.6 Hz. As is shown later in the discussion of the mode shapes, these represent the first, second and third bending modes of the second and third steel girders supporting the bridge deck. Modes nine through eleven were not found from the ambient vibration test data, which can be attributed to the reasons listed above for mode four and also due to the lower energy of these higher frequency modes which were not excited by the ambient excitation sources at the bridge.

Damping estimates were found to vary greatly from test to test. Since the method used to determine damping estimates relied on fitting a curve to the shape of the eFRF curves at the natural frequency peaks, the sharpness of the peaks directly influenced the estimates, which in turn are influenced by the type and magnitude of excitation acting on the structure. The signal to noise ratio in the impact test is far better than in the ambient test, which can be a reason why the

damping estimates vary so much between these tests. The impact on the bridge excites the structure in such a way that the elastic response sees much greater amplitude, which makes the mechanisms of energy dissipation in vibration, i.e. damping, more observable. In the case of the ambient excitation, the low magnitude broad band nature of the excitation of the structure caused much smaller response amplitude, making the measurement of the energy dissipation extremely hard to measure and quantify. This also has an effect in the curve fitting process of the eFRF plots, having a larger amplitude peak makes the curve fitting process more immune to noise near the peak, a smaller amplitude peak will be more likely to deviate from a representative curve fit if noise is present close by the peak.

Table 4.1 Summary of Natural Frequencies & Damping Estimates for Hartbarger Bridge.

	Impact Vibration		Ambient Vibration			
	Frequency	Damping	Frequency		Damping	
			Value	Difference	Value	Difference
Mode 1	6.02 Hz	0.442 %	6.04 Hz	0.39 %	0.749 %	69.45 %
Mode 2	6.94 Hz	0.974 %	7.02 Hz	1.14 %	1.024 %	5.17 %
Mode 3	12.50 Hz	0.693 %	12.42 Hz	-0.64 %	1.062 %	53.28 %
Mode 4	21.6 Hz	1.800 %	NA	NA	NA	NA
Mode 5	22.6 Hz	0.894 %	22.71 Hz	0.49 %	1.764 %	97.26 %
Mode 6	23.4 Hz	0.520 %	23.59 Hz	0.81 %	1.928 %	270.77 %
Mode 7	24.4 Hz	1.160 %	25.5737	4.81 %	0.745 %	-35.77 %
Mode 8	34.2 Hz	0.114 %	34.21 Hz	0.03 %	0.191 %	67.97 %
Mode 9	40.3 Hz	0.733 %	NA	NA	NA	NA
Mode 10	48.5 Hz	0.667 %	NA	NA	NA	NA
Mode 11	56.9 Hz	0.882 %	NA	NA	NA	NA

4.2.2 Baptist Ford Bridge

This section presents the natural frequencies and damping ratio estimates found from the three types of vibration tests performed on the Baptist Ford Bridge. The presentation and comparison between different values will be done in a similar way as the previous section on the Hartbarger Bridge. However, the in-depth explanation of how these modal parameters were found will be omitted to avoid repetition. Because of the minimal traffic using this bridge, the ease of instrumenting the bridge deck and the easier accessibility to the instruments during the tests, the bridge was tested for the full input locations for both impact and shaker tests. This also permitted a dense sensor grid layout to be employed for this structure. Overall, the results found on this bridge were more consistent and reliable than those found from the Hartbarger Bridge, which can in part be attributed to the overall ease of performing the field tests on this bridge. Also, this bridge showed a more flexible response than the stiffer Hartbarger Bridge which resulted in a larger number of modes being identified within the frequency range of interest.

As explained in the previous section, the CMIF algorithm was applied to the controlled input tests data. Figure 4.9 shows the selected peaks from the CMIF plot of the first five natural frequencies found from the impact vibration test. For the ambient test data, the pIRFs were plotted after the correlation functions were applied to the time data, Figure 4.10 shows a sample of a typical free vibration decay pIRF plot. From these pIRF, the pFRF were computed and the results were plotted and are shown in Figure 4.11, which shows a sample pFRF plot obtained from the shown pIRF. To calculate damping estimates, the eFRFs from both types of tests were generated and filtered as explained in the previous section and are shown in Figures 4.12 for Mode 3 from the impact vibration data, and Figure 4.13 for all DOFs and all mode shapes found

from the ambient vibration test. In a similar way as for the Hartbarger Bridge the synthesized FRFs were reviewed to check their fit of the modal parameters as a whole to the actual FRF data for same input/output locations, Figure 4.14, and for different output/input, Figure 4.15. The plots show, as was the case above, the relationship between the phase change and the peaks of the eFRF plot.

A total of fifteen natural frequencies were found and are summarized in Table 4.2. Due to the more flexible response nature of this structure, it can be seen that the peaks were more clearly defined and dominant without other overpowering neighboring modes as was the case for the other structure. Another characteristic that can be seen is that the modal frequencies are not as closely spaced as in the Hartbarger bridge.. The data acquired from the shaker test showed the great majority of modes found from the impact test, with the exception of the last couple of natural frequencies from the burst random type of signal. The ambient vibration test data revealed seven of the modal frequencies, most of them being the ones representing the first higher energy modes. This is expected due to the low amplitude and broad band nature of the excitation, which will only excite these higher energy modes. The same situation is seen between damping estimates comparison from impact to ambient test. In the case of the shaker tests, the comparison of damping estimates showed a much greater variance. The reasons behind the poor damping estimate comparison are similar as the ones previously listed for the other structure. Shaker test estimates for damping ratios also showed significant variance as compared to the impact test estimates. The same reasons as those for the ambient tests can be attributed to this type of test. Furthermore, the peaks at the natural frequencies on the CMIF plot were found to be much sharper than the ones for both impact and ambient data. As pointed before, the shape of

these peaks has a direct influence on the curve fitting procedure to estimate damping. Finally, the signal to noise ratio from the shaker test was poor, thus making the measurements of damping estimates very inaccurate as compared with the more realistic values from the impact data.

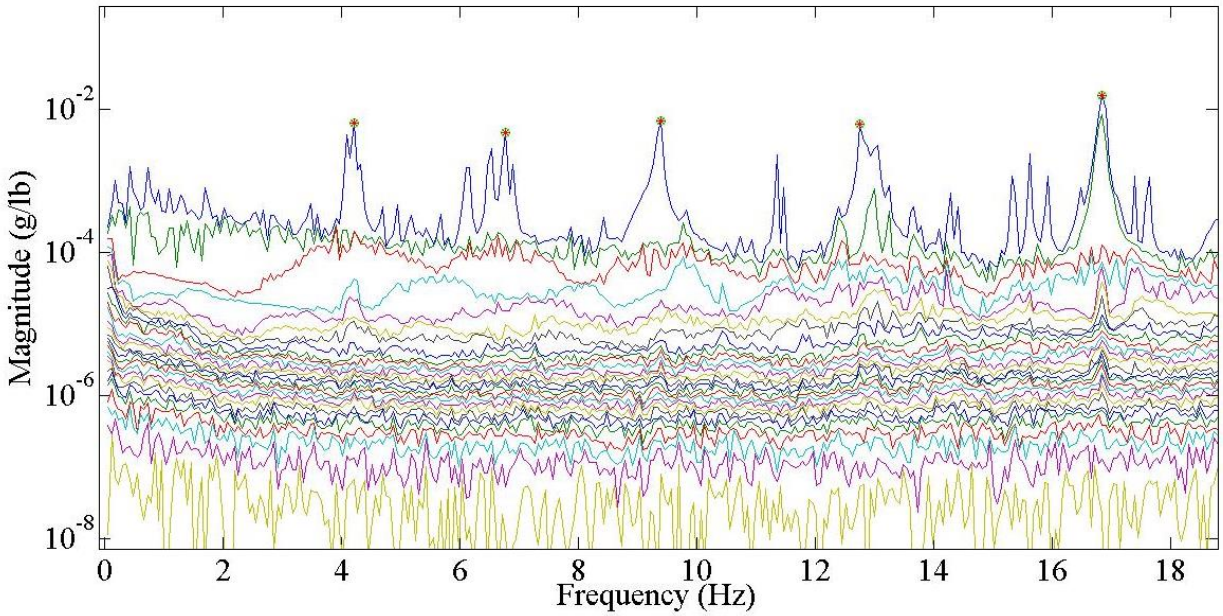

Figure 4.9 CMIF plot, Impact testing.

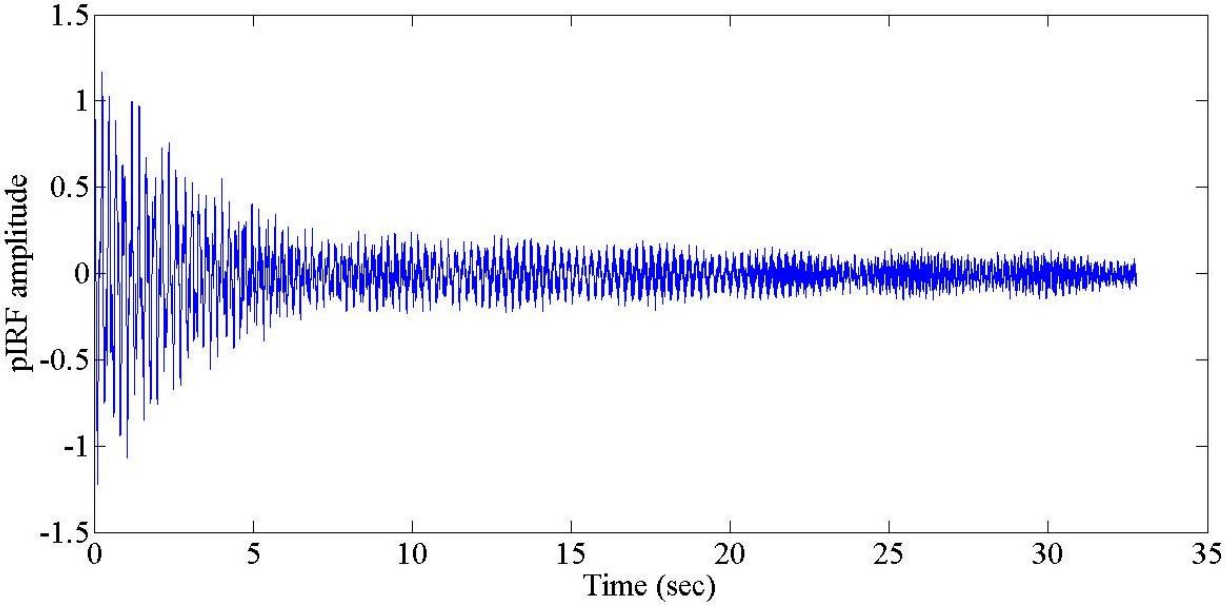

Figure 4.10 pIRF plot, Ambient Data Test.

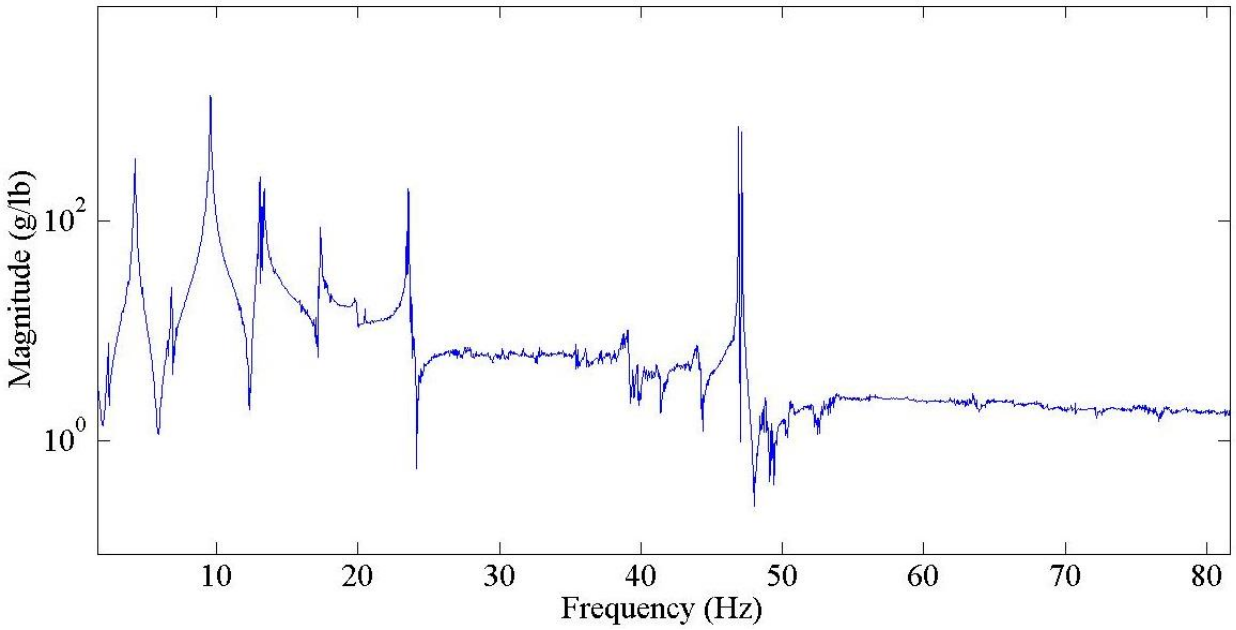

Figure 4.11 pFRF plot, Ambient Data Test.

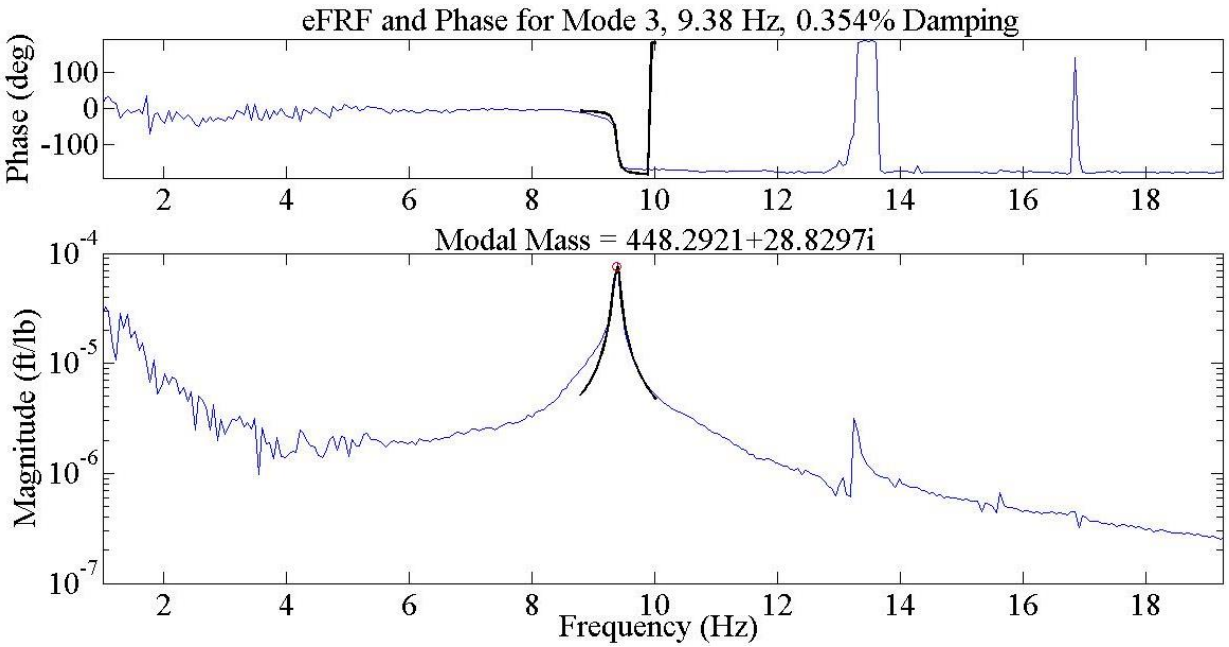

Figure 4.12 eFRF plot, Mode 3, Impact Test Data.

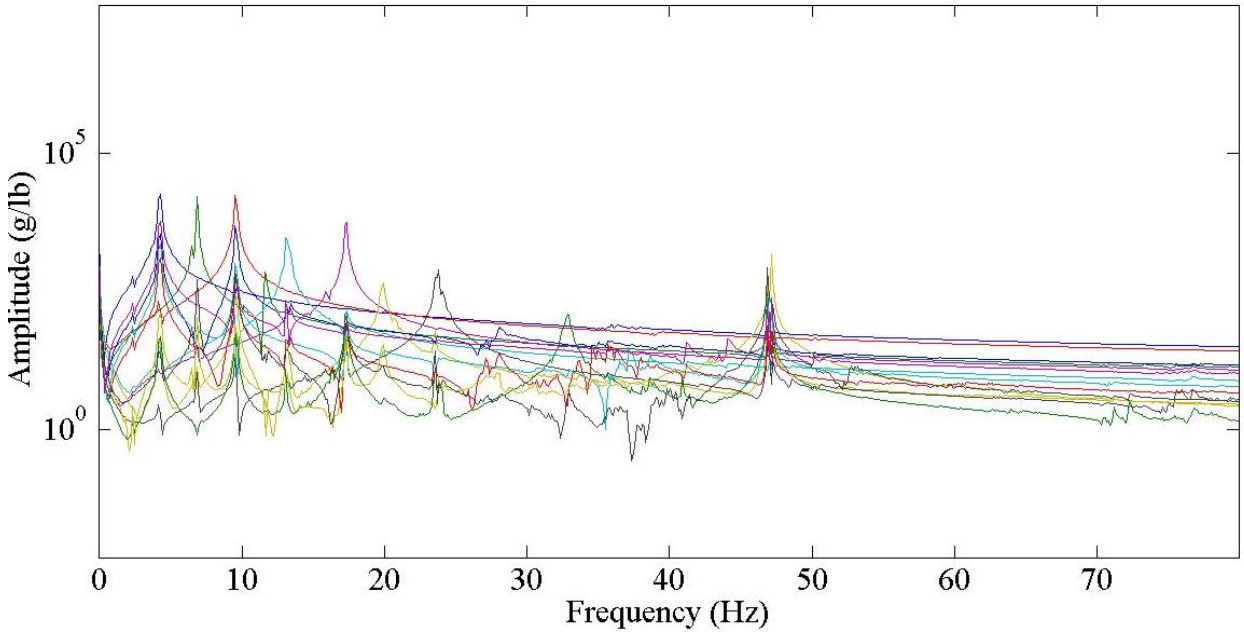

Figure 4.13 eFRF plot, Ambient Test Data.

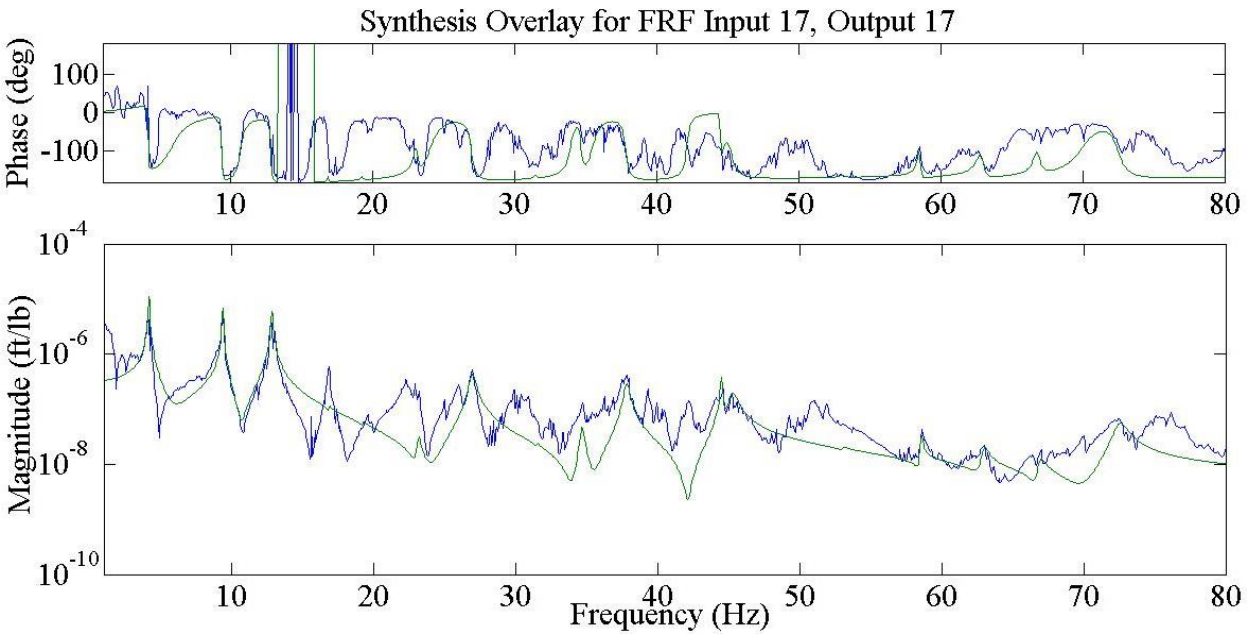

Figure 4.14 Synthesized eFRF same output/input locations, Baptist Ford Bridge.

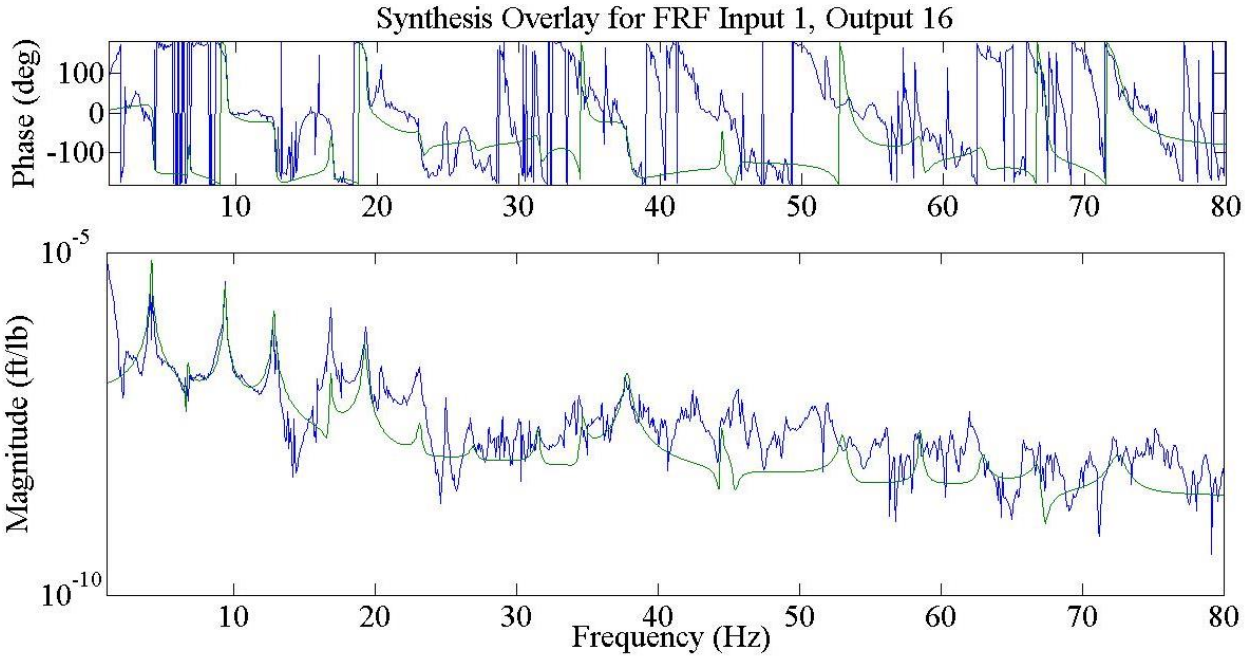

Figure 4.15 Synthesized eFRF different output/input locations, Baptist Ford Bridge.

Table 4.2 Summary of Natural Frequencies & Damping Estimates for Baptist Ford Bridge.

	Impact Field Test		Ambient Field Test		Shaker Field Test			
					Burst Random		Sine Sweep	
	Natural Frequency	Damping Ratios	Natural Frequency	Damping Ratios	Natural Frequency	Damping Ratios	Natural Frequency	Damping Ratios
Mode 1	4.21 Hz	0.777 %	4.21 Hz	0.879 %	5.19 Hz	0.0663 %	4.15 Hz	0.253 %
Mode 2	6.78 Hz	0.699 %	6.84 Hz	0.377 %	6.96 Hz	0.408 %	7.87 Hz	0.0807 %
Mode 3	9.40 Hz	0.455 %	9.52 Hz	0.357 %	9.52 Hz	0.195 %	9.52 Hz	0.0277 %
Mode 4	12.76 Hz	0.495 %	13.06 Hz	0.682 %	13.10 Hz	0.271 %	13.00 Hz	0.516 %
Mode 5	16.85 Hz	0.271 %	NA	NA	17.50 Hz	0.0416 %	17.23 Hz	0.139 %
Mode 6	19.30 Hz	0.475 %	19.28 Hz	0.623 %	19.90 Hz	0.0910 %	19.81 Hz	0.154 %
Mode 7	23.13 Hz	0.533 %	NA	NA	23.44 Hz	0.0064 %	23.30 Hz	0.00363 %
Mode 8	26.98 Hz	0.758 %	24.9 Hz	0.0298 %	27.10 Hz	0.00115 %	27.00 Hz	0.000211 %
Mode 9	31.50 Hz	0.511 %	NA	NA	32.84 Hz	0.0141 %	32.50 Hz	0.0148 %
Mode 10	34.70 Hz	0.537 %	NA	NA	34.80 Hz	0.0462 %	35.20 Hz	0.504 %
Mode 11	37.80 Hz	0.517 %	NA	NA	38.10 Hz	0.1720 %	37.80 Hz	0.0183 %
Mode 12	44.62 Hz	1.81 %	NA	NA	44.70 Hz	0.2980 %	44.00 Hz	0.330 %
Mode 13	53.10 Hz	0.95 %	NA	NA	52.40 Hz	0.7730 %	51.30 Hz	0.0173 %
Mode 14	67.00 Hz	0.522 %	NA	NA	NA	NA	67.40 Hz	0.0210 %
Mode 15	72.50 Hz	0.684 %	NA	NA	NA	NA	70.30 Hz	0.0112 %

4.3 Mode Shapes

4.3.1 Hartbarger Bridge

This section presents the mode shapes of the thirteen natural frequencies identified for this bridge. The figures in this section provide a visual representation of the mode shape vectors at every modal frequency. As mentioned in Chapter 3, these mode shapes are only useful for visual verification of the resonant vibration modes of the structure, but have arbitrary scaling and thus, are not adequate to produce an accurate estimate of modal flexibility. The methods used to obtain the mode shapes were previously described in Chapter 3. This section also discusses the layout of the sensors in the context of spatial or geometric aliasing and nodal locations. The numbering

of the mode shapes shown in the figures below follows the same numbering scheme used in Table 4.1, which was assigned by increasing frequency values and not by sequential mode shapes progression to higher modes, i.e. first bending, second bending, etc.

The mode shapes obtained from the full grid test in the frequency range of interest are shown in Figures 4.16 through 4.19. The mode shapes are grouped into bending and torsional modes and further categorized between global modes and local bridge component modes, such as those for the bridge's girders and the bridge's deck structure. Figure 4.16 shows the first three global bending modes. Figure 4.17 shows the first three identified local bending modes of girders two and three of the structure. The nature of this structure allowed the identification of these local bending modes of the interior girders; their peaks in the CMIF plot had comparable energy amplitudes as to those found for the mode shapes of the global structure. This can be attributed to the stiffness of the W27x94 girder sections, of which cross section characteristics were such that their bending modes were not shadowed by other global modes.

Also, it was found that the three local bending modes had identical mode shapes at higher frequencies; the first bending mode at 23.4 Hz repeated at 64.3 Hz, the second local bending mode at 34.2 Hz repeated at 71.7 Hz and the third local bending mode at 48.5 Hz repeated at 73.6 Hz. One explanation for this could be spatial aliasing of the sensor grid layout which prevented the detection of possibly higher frequency local bending modes. Some of these local bending modes and the second local bending mode in particular, were also dominant in neighboring peaks. The mode shape and modal frequency being presented here were selected by the author's discretion of what seemed a better representation of the mode shape and based on higher MAC values. The MAC metric is further explained below. Figure 4.18 shows the two

global torsion modes found for this structure. As was the case in the global bending modes, no repetition of these modes was found at higher frequencies and their selected peaks were so dominant that other neighboring peaks were completely filtered out. Finally, Figure 4.19 shows the three bending modes found from the 8 in. thick concrete deck. In this case, the mode shapes did not repeat at higher frequencies and their peaks were dominant in their vicinity.

Due to the dense instrumentation grid used in this structure, the location of sensors near nodal points was not a notable problem for characterizing the structure's mode shapes. The span dimensions and overall stiffness characteristics of this bridge resulted in the identification of less global bending and torsional modes as compared to the more flexible truss bridge, as will be shown in the next section. On the other hand, the individual component's mode shapes in this structure were easily found and were represented by high amplitude peaks in the CMIF plot, which was not the case for the truss bridge were component's mode shapes were almost completely shadowed by global mode shapes. This will be explored in more detail in the later section of this chapter.

To compare the level of agreement of the mode shapes vectors, Modal Assurance Criterion (MAC) values were computed using the mode shapes from the impact test and the ambient vibration test (using the full measurement grid). MAC values provide a measure of the degree of linearity between estimates of modal vectors thus providing an additional metric for evaluating the modal vectors obtained from different vibration testing methods (Allemang 2003). Table 4.3 summarizes the MAC values (as a percentage) computed from the mode shape vectors for the various test methods compared to the modal vectors obtained from the impact testing. A MAC value of 100% indicates perfect correlation between two mode shape vectors, while a MAC

value of 0% indicates no correlation exists. As can be seen from Table 4.3, the MAC values are very high for the first four mode shapes and still relatively high for the higher frequency modes.

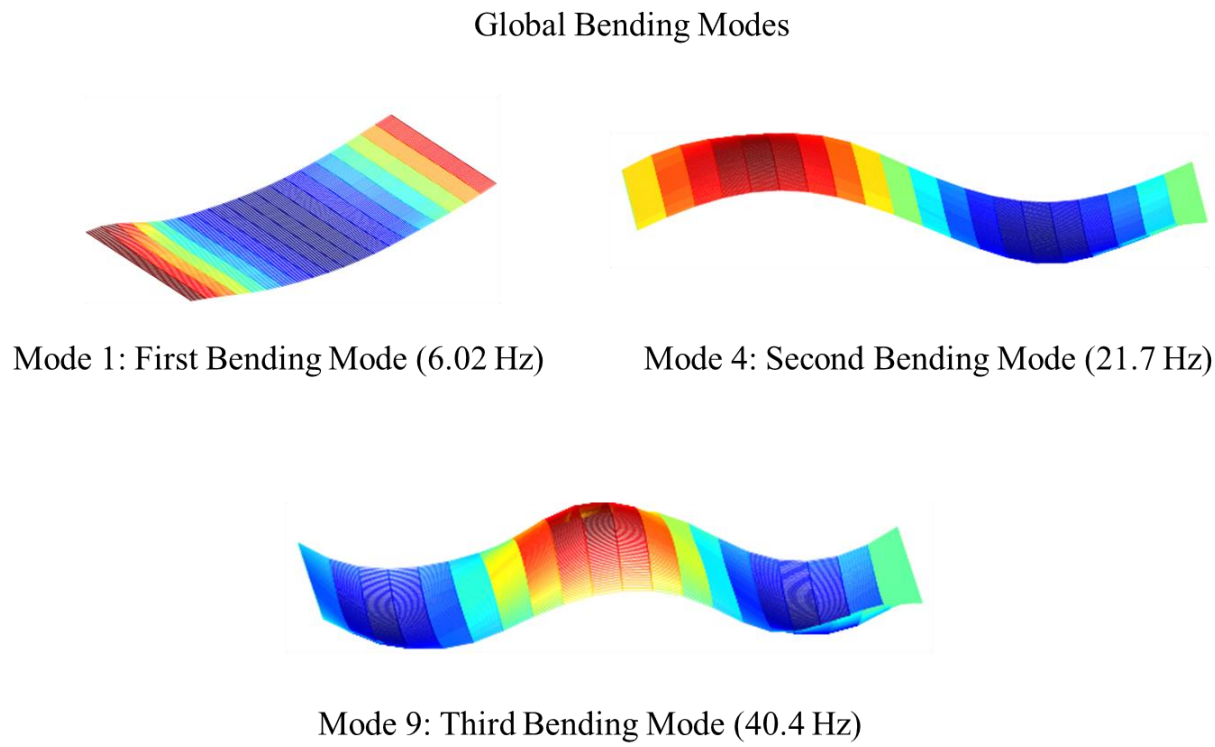

Figure 4.16 Global Bending Mode Shapes, Hartbarger Bridge.

Girder Bending Modes

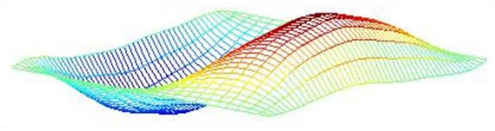

Mode 6: Girder First Bending Mode
(23.4 Hz)

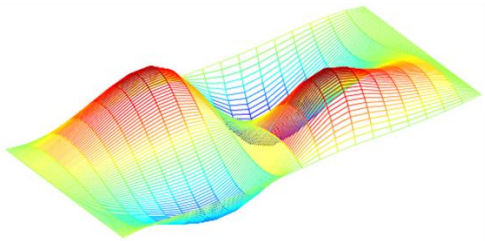

Mode 8: Girder Second Bending Mode
(34.2 Hz)

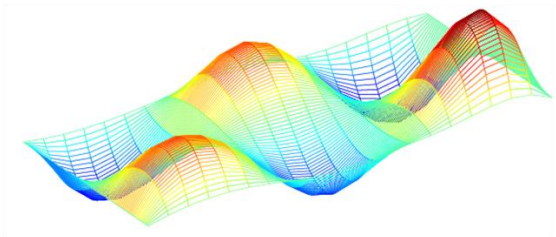

Mode 10: Girder Third Bending Mode
(48.5 Hz)

Figure 4.17 Localized Bending Mode Shapes, Hartbarger Bridge.

Global Torsion Modes

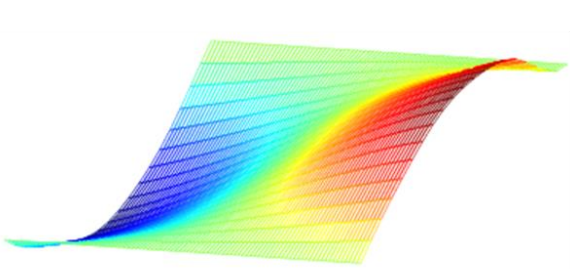

Mode 2: First Torsion Mode
(6.94 Hz)

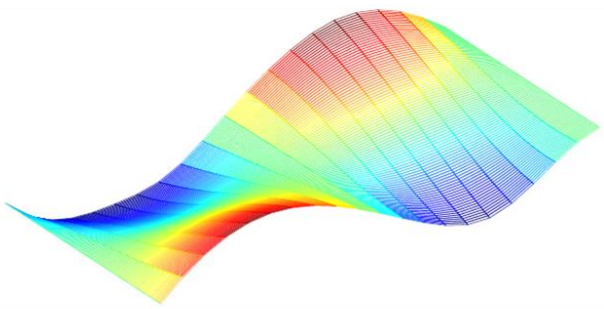

Mode 5: Second Torsion Mode
(22.6 Hz)

Figure 4.18 Global Torsion Mode Shapes, Hartbarger Bridge.

Deck Bending Modes

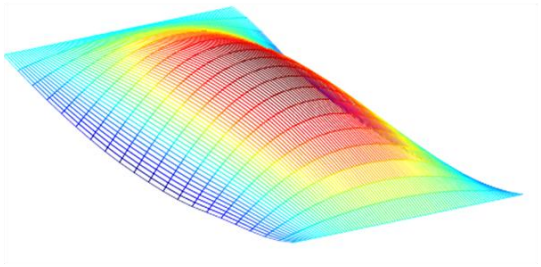

Mode 3: Deck First Bending Mode
(12.4 Hz)

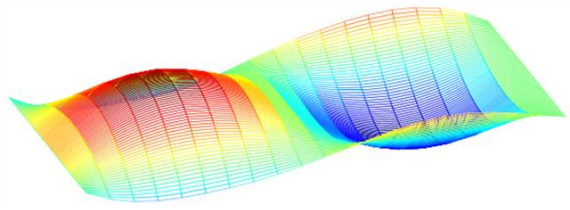

Mode 7: Deck Second Bending Mode
(24.4 Hz)

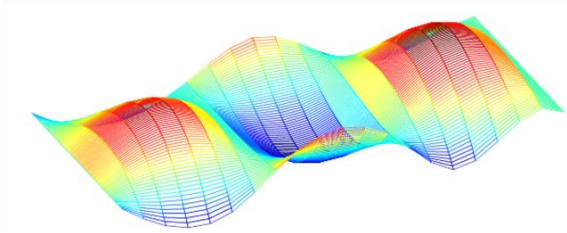

Mode 11: Deck Third Bending Mode
(56.9 Hz)

Figure 4.19 Bride Deck's Bending Modes, Hartbarger Bridge.

Table 4.3 MAC values (%) between mode shapes identified from impact testing and ambient vibration testing.

Impact to Ambient	
Mode #	MAC
1	100%
2	96%
3	99%
4	NA
5	88%
6	94%
7	88%
8	82%
9	NA
10	NA
11	NA

4.3.2 Baptist Ford Bridge

The mode shapes associated with the identified modal frequencies identified for this bridge are presented in Figures 4.20 through 4.22. The numbering of the mode shapes was assigned as explained in the previous section. As briefly mentioned before, the global geometric and structural characteristics of this bridge were such that a larger number of both bending and torsional global modes could be identified than for the Hartbarger Bridge. Local mode shapes for various bridge elements were not identified for this structure, with the exception of several bending mode shapes of the bridge's deck as seen in Figure 4.22. Repetition of mode shapes mainly occurred in the vicinity of a only a few modal frequencies, as was the case of the ninth bending mode shape which repeated at 45.2 Hz and the deck's third bending mode shape repeating at 58.5 Hz. The deck's fourth mode shape at 72.5 Hz also repeated, but in this case it

happened at a lower frequency of 63.0 Hz with a much weaker peak and with a less representative mode shape.

Figure 4.20 shows all the identified bending modes for this structure. It can be seen that some bending modes are missing in the expected progression for these mode shapes. The fourth, sixth and eight bending mode shapes are examples. This can be attributed to either geometric or spatial aliasing or the global signature response characteristic of the structure. This figure also highlights a case were spatial aliasing prevented the detection of a mode shape. The mode shape at 67 Hz shown towards the bottom of the figure appears to be the sixth bending mode repeating at this higher frequency, but could also represent the tenth or higher bending mode affected by the spatial distribution of the sensor grid or due to sensors being placed near nodal locations for this mode. Table 4.4 presents the MAC values computed by comparing the mode shapes estimated from the impact testing with other three tests: (1) burst random (B.R.), (2) swept sine (S.S.) shakers testing and, (3) ambient vibration testing. As was expected, the first mode shapes compared very well with high MAC values, but as the comparison progressed to higher order modes, the MAC results were lower. Many of the higher frequency mode shapes still showed good agreement with those from the impact testing, and this was particularly the case for the mode shapes identified from both of the shaker tests.

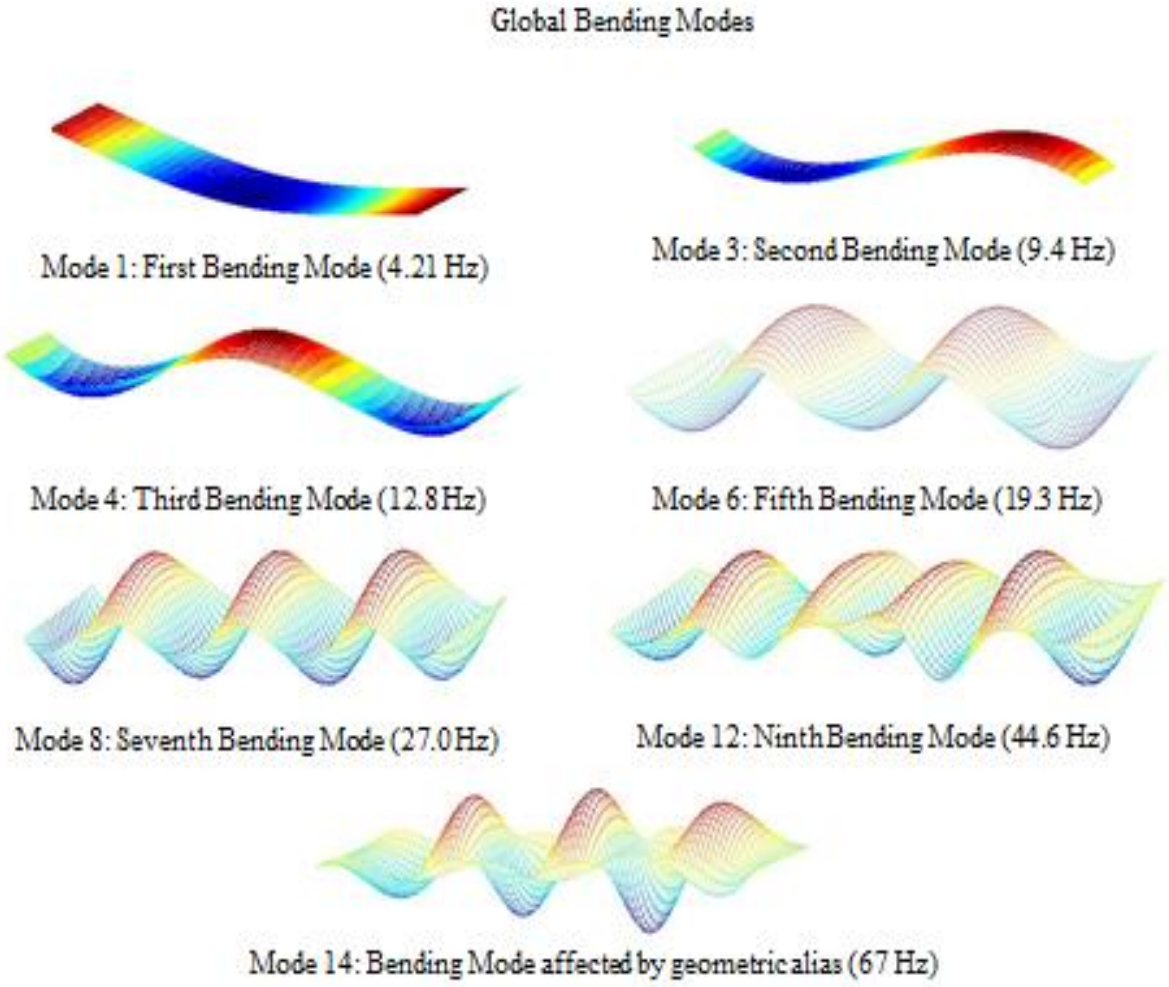

Figure 4.20 Global bending mode shapes (Baptist Ford Bridge).

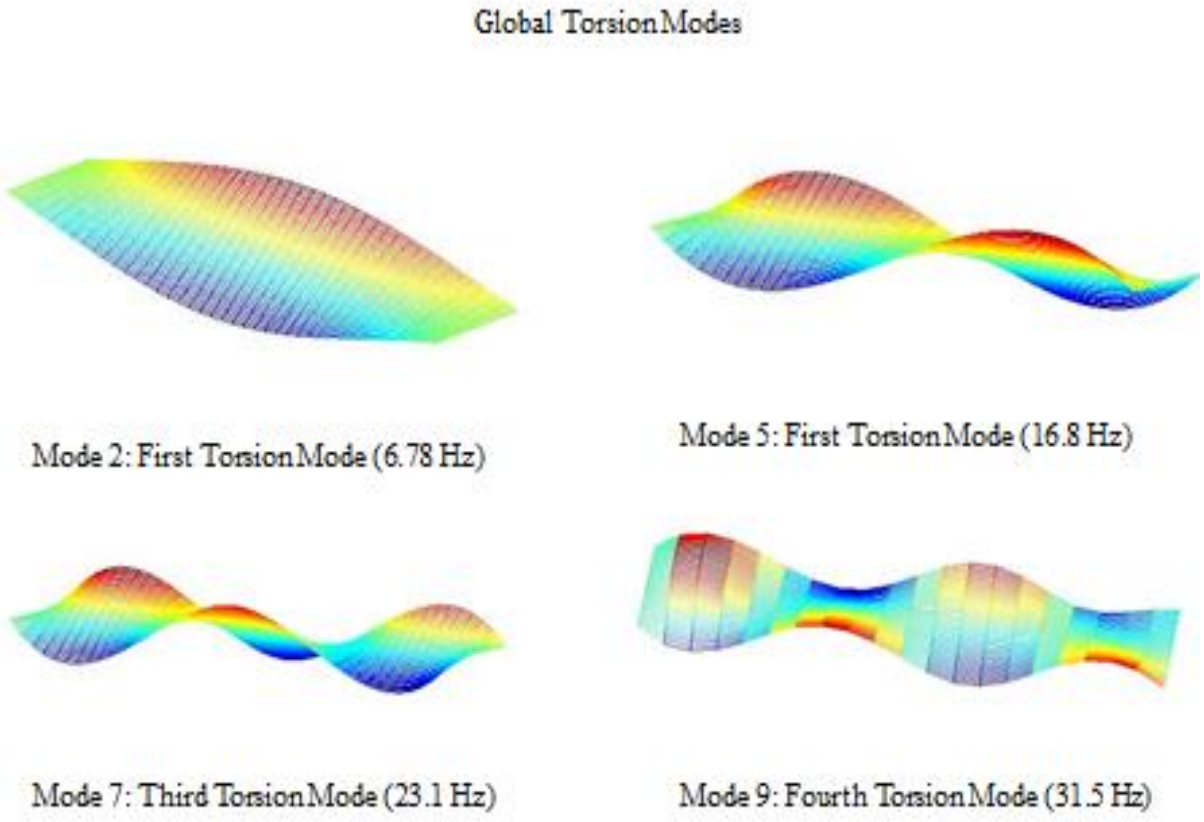

Figure 4.21 Global torsional mode shapes (Baptist Ford Bridge).

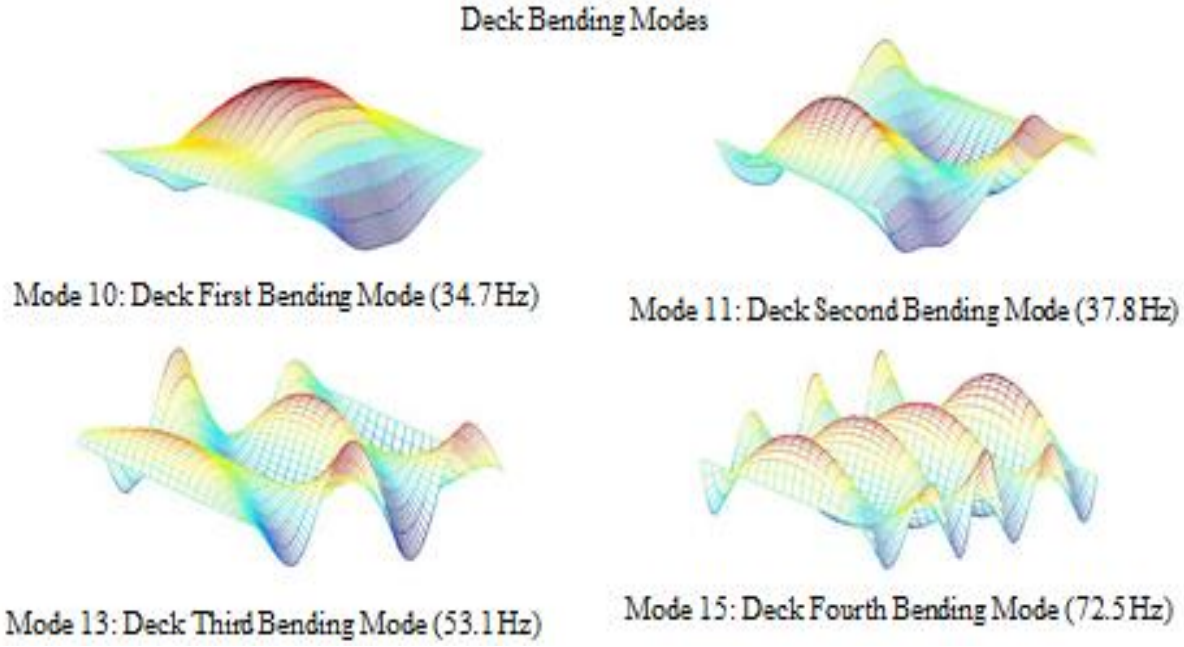

Figure 4.22 Local bridge deck modes (Baptist Ford Bridge).

Table 4.4 MAC values (%) for different vibration test methods in relation to impact testing results.

Impact to Ambient		Impact to B. R.		Impact to S.S.	
Mode #	MAC	Mode #	MAC	Mode #	MAC
1	100%	1	100%	1	100%
2	98%	2	100%	2	100%
3	100%	3	92%	3	99%
4	93%	4	99%	4	100%
5	NA	5	66%	5	98%
6	94%	6	98%	6	98%
7	NA	7	85%	7	100%
8	96%	8	90%	8	92%
9	NA	9	97%	9	92%
10	NA	10	90%	10	84%
11	NA	11	91%	11	91%
12	NA	12	27%	12	84%
13	NA	13	1%	13	9%
14	NA	14	NA	14	22%
15	NA	15	NA	15	43%

4.4 Modal Flexibility Matrix

4.4.1 Hartbarger Bridge

The modal flexibility matrix estimated from the impact testing is presented in this section. Since the input for the ambient vibration test was not measurable, modal scaling cannot be estimated for this test. The modal flexibility matrix for the bridge was only computed from the vibration testing results that employed a controlled/measured excitation input. Modal flexibility was calculated using the modal vectors, poles and scaling factors (Modal A). As mentioned in Chapter 3, the Modal A parameter allows the modal vectors to be mass unit normalized without

assuming a mass matrix, thus providing the proper scaling of the modal flexibility matrix. Table 4.5 lists the scaling factors for all the modes found from impact testing of the Hartbarger Bridge. As can be expected, the values on this table are dominantly imaginary with all of the imaginary values being positive. The convergence of the modal flexibility matrix was evaluated with the increasing numbers of modes being included in the formulation as shown in Figure 4.23. The convergence was evaluated by examining the mean value of the displacements produced at all DOFs from the modal flexibility matrix when a unit load was applied to each DOF (Figure 4.24). As shown in the figure, convergence of 0.977 was reached within the first mode and the result was normalized to the deflected shape with the first bending mode included in the modal flexibility matrix. The deflection profile obtained by applying unit loads to all of the measurement DOFs with the modal flexibility matrix was not compared to analytical predictions for this bridge as this was beyond the scope of this research.

Table 4.5 Modal A Values for Impact Test (Hartbarger Bridge).

Mode	Modal Scaling Factors
1	1650.96 + 16019.87i
2	11021.38 + 13409.96i
3	-1772.38 + 32470.53i
4	22387.35 + 47395.79i
5	-8333.11 + 53468.67i
6	58945.41 + 87199.75i
7	54906.33 + 85918.26i
8	714003.78 + 1271524.07i
9	-61794.74 + 648060.10i
10	222720.02 + 320882.80i
11	-6751.43 + 214305.56i

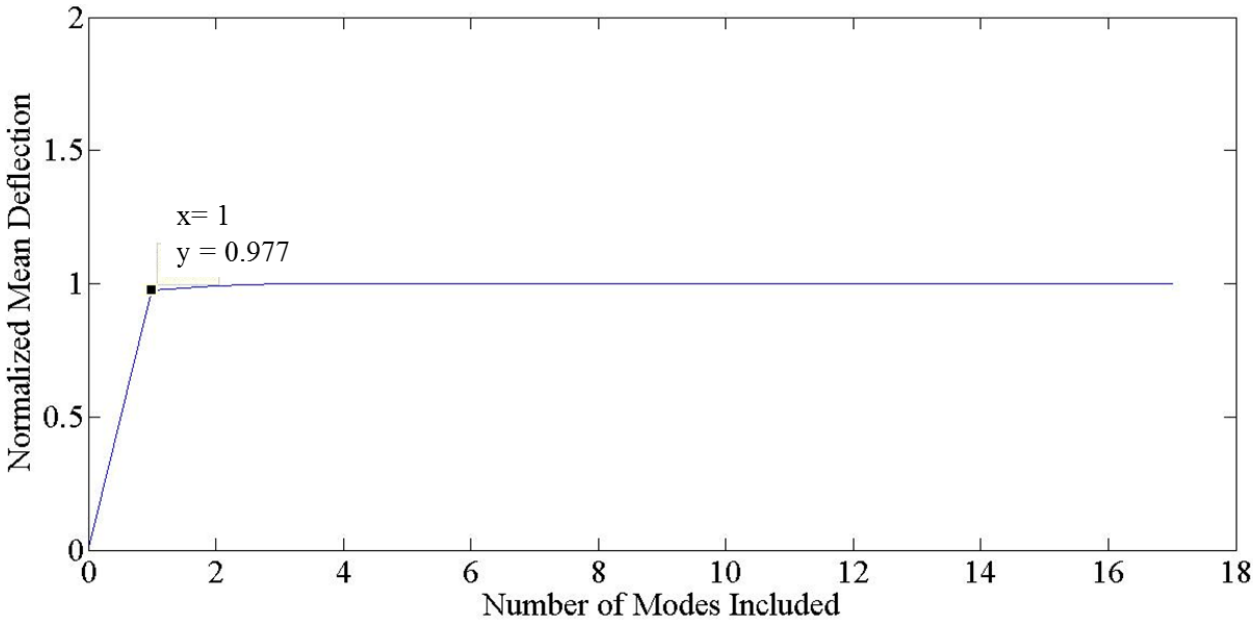

Figure 4. 23 Modal flexibility matrix convergence (Mean Displacements Under Uniform Load Vector) (Hartbarger Bridge).

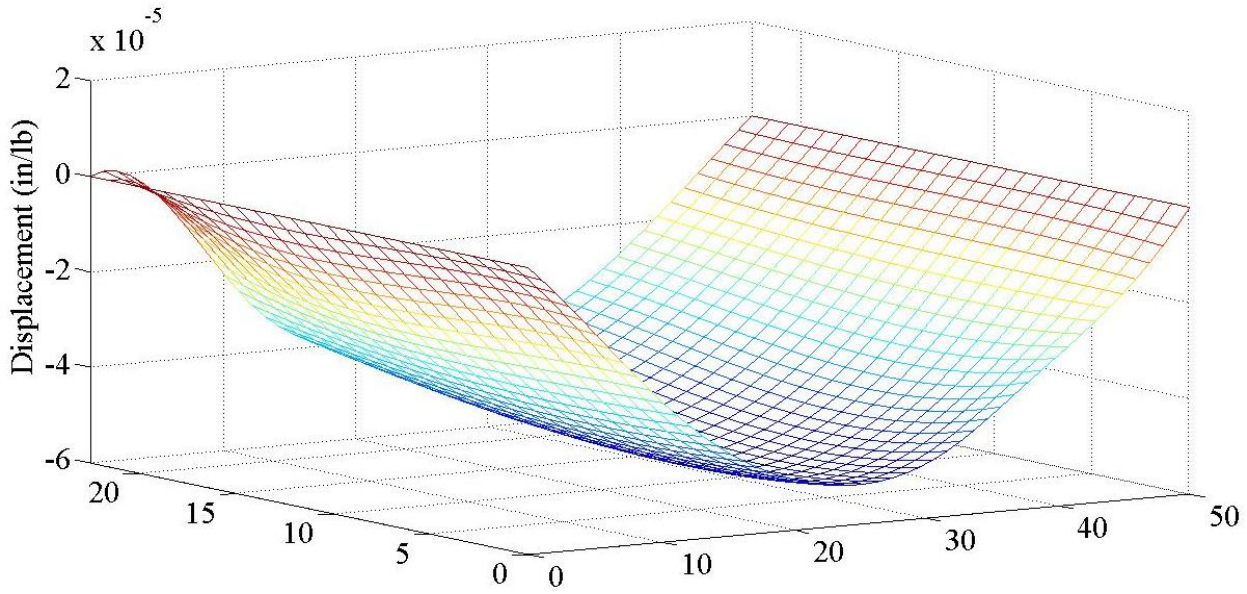

Figure 4.24 Displacement profile obtained by loading modal flexibility matrix from impact testing results with uniform load (1 lb/DOF) (Hartbarger Bridge).

4.4.2 Baptist Ford Bridge

The modal flexibility results from the controlled input dynamic tests done on the Baptist ford bridge are presented in this section. First, the results obtained from the impact dynamic testing are presented. As was the case in the other bridge, the modal scaling factors were found for each mode and it was found that all of them were dominantly imaginary with a positive sign. Similar to the other bridge, the mean deflection under uniform load converged to a value of 0.9913 when just the first mode was included in the modal flexibility matrix formulation (Figure 4.25). The normalized displacement of the bridge from the modal flexibility matrix (based on inclusion of only the first mode) is shown in Figure 4.26.

The results found from both of the shaker tests were not as consistent as for the impact vibration test. As can be seen from Tables 4.6 and 4.7, some of the modal scaling factors had a negative imaginary part which would imply a negative modal mass, which is physically impossible. Also, the imaginary part in these scaling factors was not the dominant part in the complex conjugate values. Convergence was found to be very low (0.444) by only including Mode 1 from the shaker testing that used burst random inputs. The convergence value only reached a value of 1.0 after the first five modes were included in the modal flexibility formulation. Using the shaker testing data with the swept sine input, a convergence value of 1.0 was reached when just the first mode was included in modal flexibility formulation. This result is not consistent with the unrealistic modal scaling factors.

Table 4.6 Modal A values from impact testing (Baptist Ford Bridge).

Mode Number	Modal Scaling Factor
1	2988.29 + 9416.67i
2	10378.83 + 24969.34i
3	-3265.14 + 46567.96i
4	-6076.73 + 42084.39i
5	-2205.70 + 64104.63i
6	42038.60 + 173948.30i
7	-1294.90 + 85624.32i
8	-35007.16 + 270055.80i
9	-72661.94 + 251774.19i
10	3508.78 + 27221.55i
11	23169.71 + 245305.74i
12	18129.09 + 58144.04i
13	12228.42 + 87861.09i
14	25095.74 + 143382.69i
15	705158.60 + 804967.92i

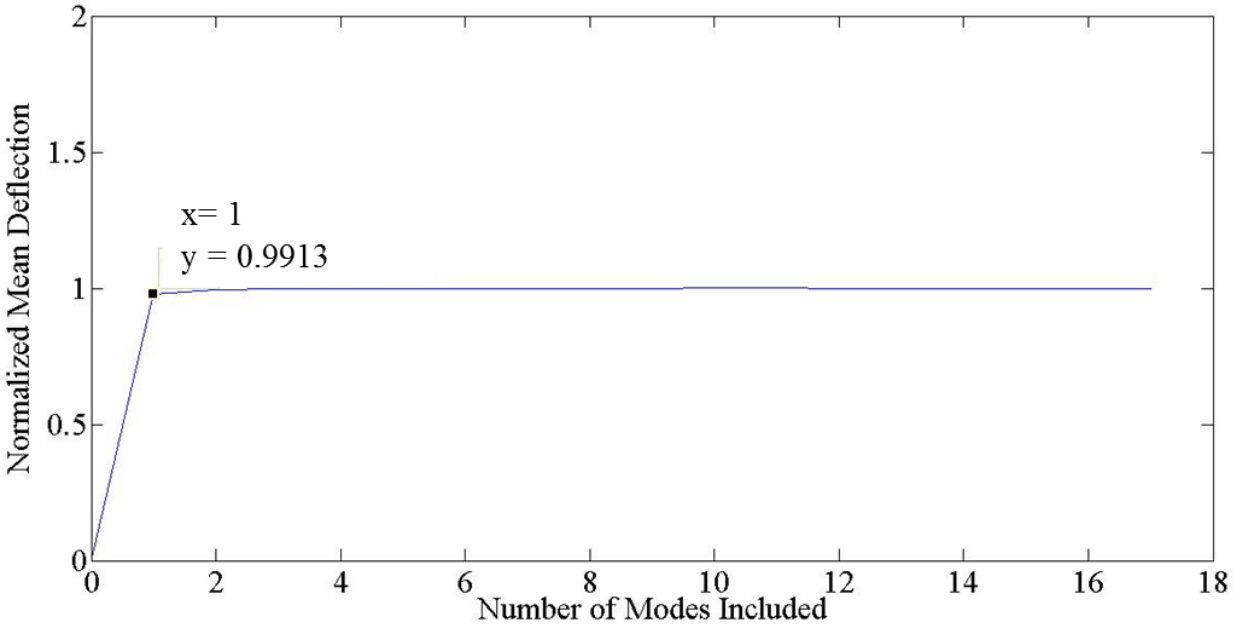

Figure 4. 25. Convergence of Modal Flexibility for impact test (Mean Displacements Under Uniform Load Vector) (Baptist Ford Bridge).

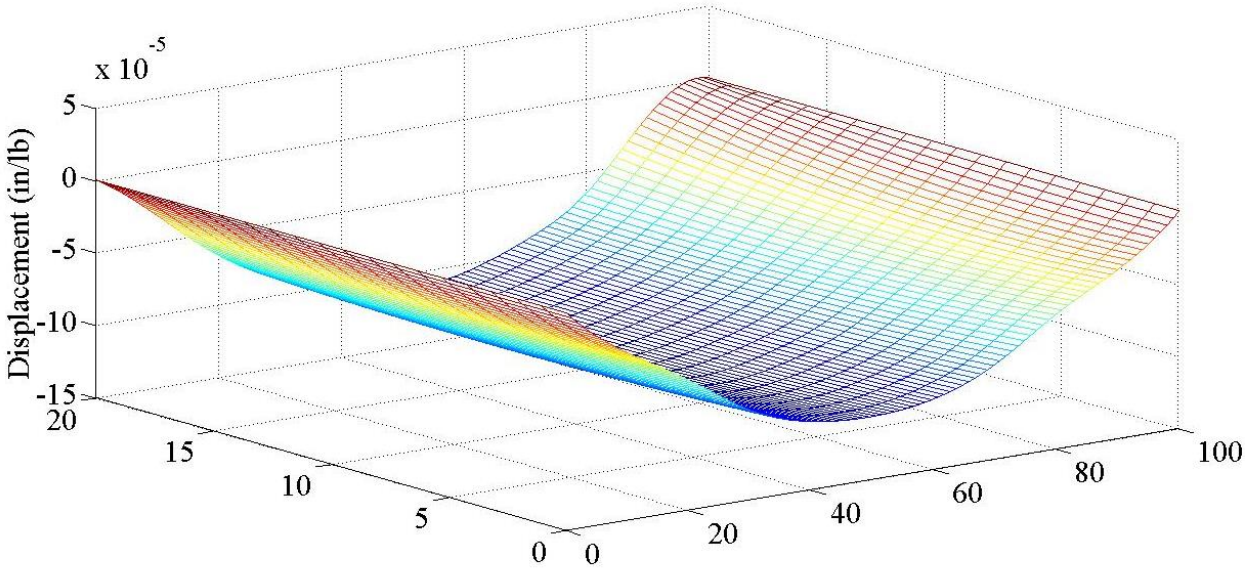

Figure 4.26 Displacement profile obtained by loading modal flexibility matrix from impact testing results with uniform load (1 lb/DOF) (Baptist Ford Bridge).

Table 4.7 Modal A values from shaker testing with burst random input (Baptist Ford).

Mode	Modal Scaling Factor
1	75.23 + 14.08i
2	529.04 - 449.95i
3	1039.56 - 1417.11i
4	51.25 - 27.43i
5	-34.80 - 45.24i
6	1552.98 + 697.20i
7	862.61 + 1359.93i
8	1101.94 + 990.56i
9	5943.62 - 8692.71i
10	14779.16 + 6401.23i
11	-532.86 - 31.98i
12	-8959.55 - 13536.54i
13	-547.64 - 558.07i
14	-3009.92 + 347.29i
15	1765.05 - 8611.30i

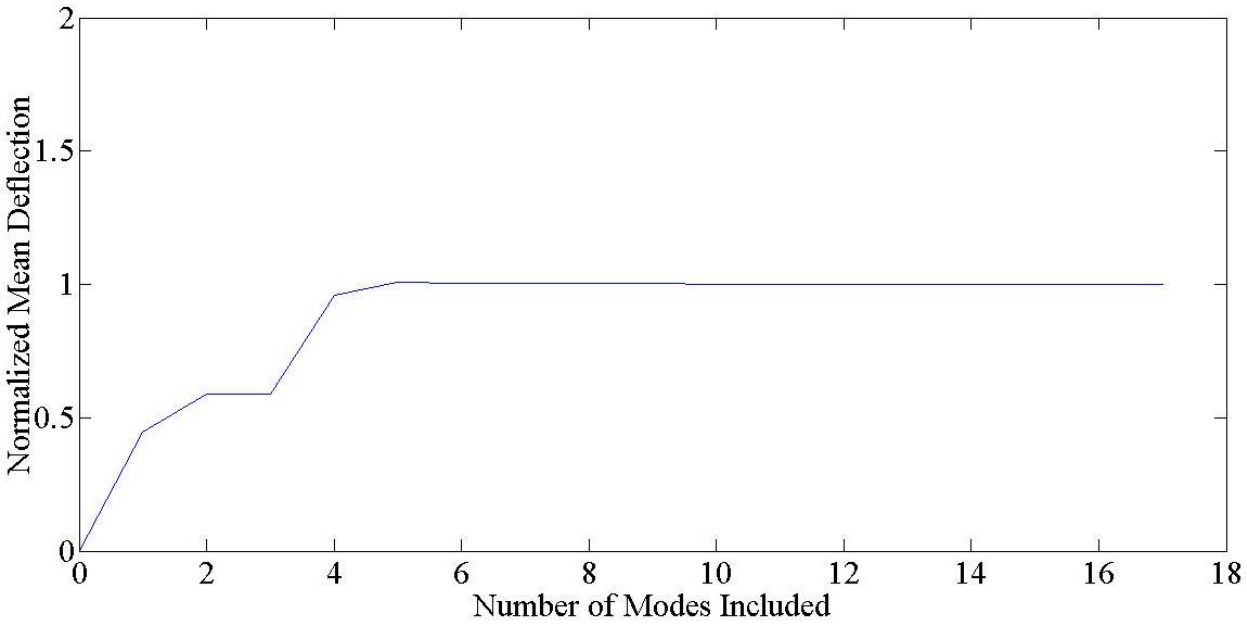

Figure 4.27 Convergence test for modal flexibility using shaker testing data with burst random input (Mean displacements under uniform Load Vector) (Baptist Ford Bridge).

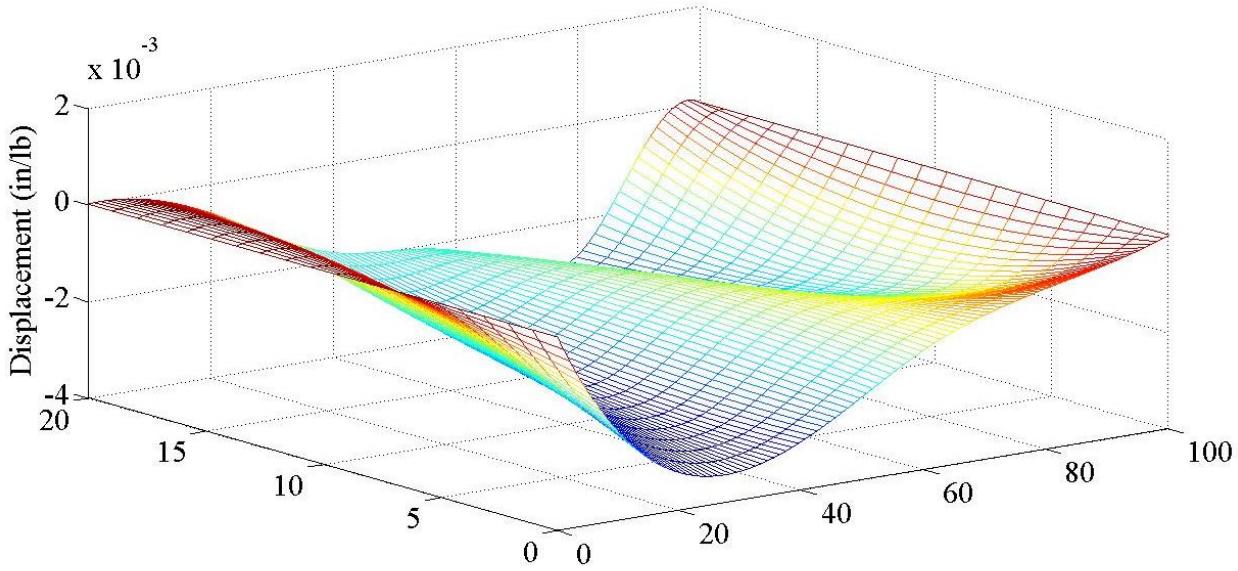

Figure 4.28 Displacement profile obtained by loading modal flexibility matrix from burst random signal shaker testing results with uniform load (1 lb/DOF) (Baptist Ford Bridge).

Table 4.8 Modal A values from shaker testing with swept sine input (Baptist Ford Bridge).

Mode	Modal Scaling Factor
1	132.61 + 122.70i
2	175.30 - 330.20i
3	10.15 - 216.43i
4	720.60 + 22.65i
5	3909.84 + 1329.22i
6	-85.24 + 4794.71i
7	-578.10 - 418.24i
8	27484.42 - 25733.03i
9	12201.28 + 54270.27i
10	-4548.725 + 8732.51i
11	187194.75 - 165806.48i
12	1163.70 + 208.11i
13	1226.24 + 2135.63i
14	-1411.90 - 2583.00i
15	8182.22 + 816.06i

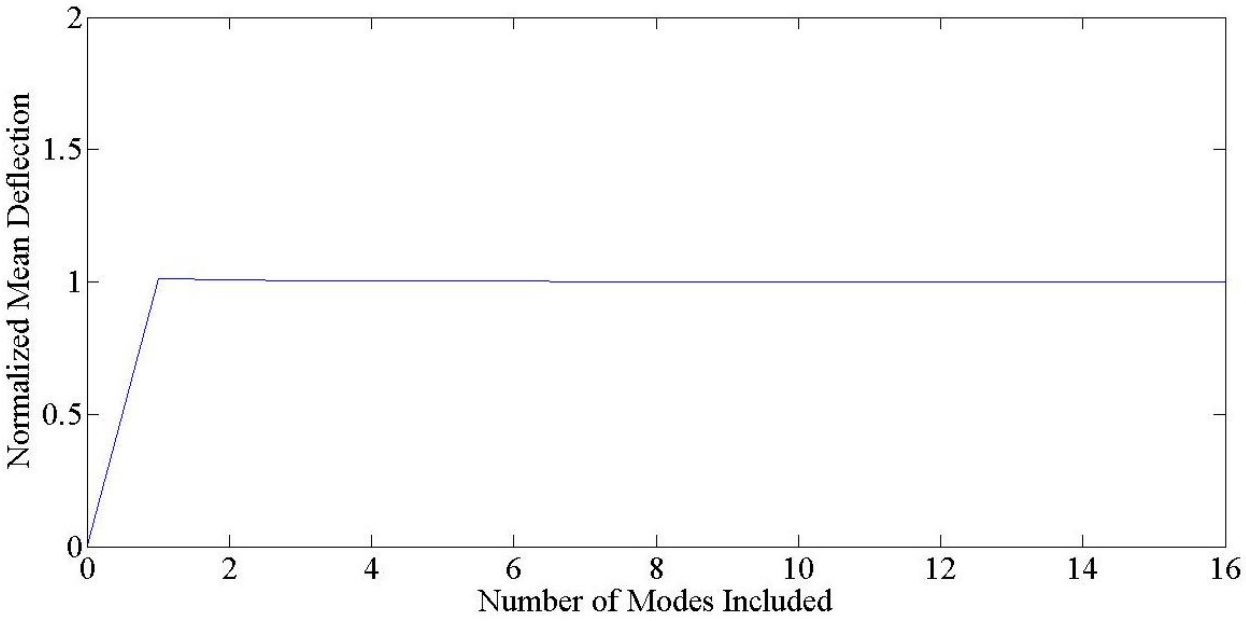

Figure 4.29 Convergence test for modal flexibility using shaker testing data with swept sine input (Mean displacements under uniform Load Vector) (Baptist Ford Bridge).

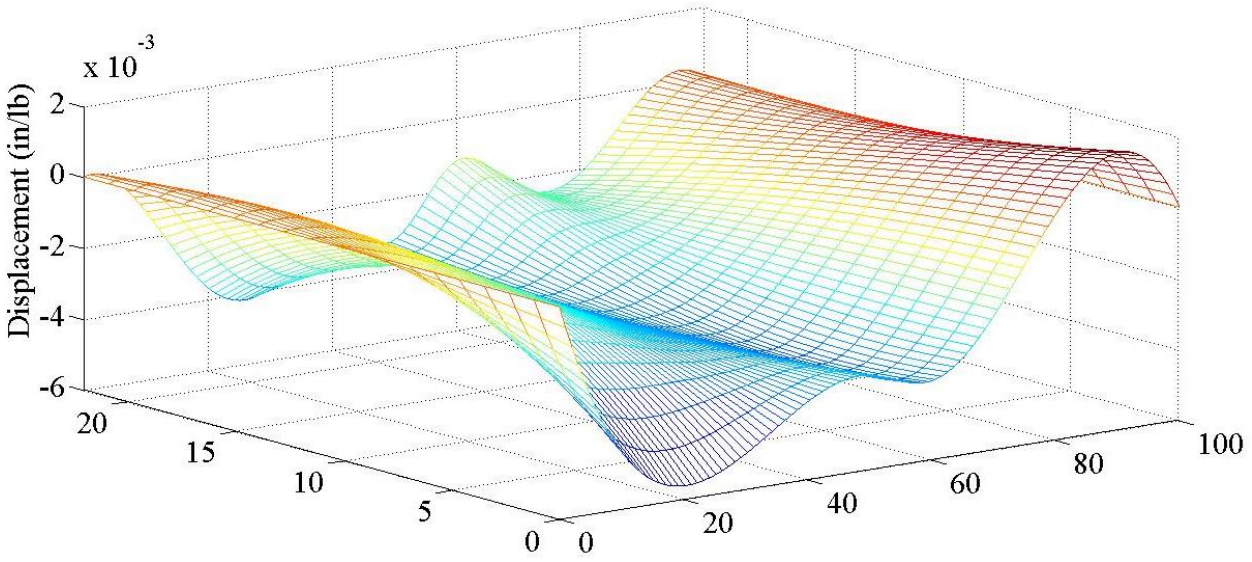

Figure 4.30 Displacement profile obtained by loading modal flexibility matrix from swept sine shaker testing with uniform load (Baptist Ford Bridge).

4.5 Summary

A summary of the results from the field tests is presented in this section. The most relevant findings will be presented in bullet lists format. Some of these conclusions will also be mentioned in the final chapter as part of the overall conclusions of this research study.

- The effort to create the targeted swept sine signal used for the shaker testing is not justified based on the poor results obtained from both field tests. The amplitude of this input signal was not large enough to adequately excite such large structures to obtain representative modal parameters from the bridge's response. Also, the windowing used in the signal

reduced the absolute amplitude of the excitation signal played by the shaker. The simultaneous use of more shakers can better excite the structure.

- The burst random signal was also found to have too small of an amplitude for these large structures. As was the case for the swept sine signal, the simultaneous use of more shakers would enhance the excitation to the structure.
- Overall, the efforts needed to perform the shaker tests as done in this study are not justified based on the poor results obtained from the field tests. The only representative modal parameters obtained from the shaker tests could have also been obtained from the much simpler ambient vibration testing scheme.
- The stiffer structure (the Hartbarger Bridge) allowed for the determination of modal parameters of local structural elements such as girders along with the global dynamic response. On both structures, the response parameters of the bridge's decks were able to be recorded. The more flexible structure's (the Baptist Ford Bridge) global response, shadowed the response of all local structural elements besides the bridge's deck.
- The type of data processing method did not have any observable differences on the type of structure. The NeXT approach allowed retrieving quality modal parameters from both bridges from the ambient vibration field tests. The same can be said about the CMIF algorithm used to process the impact data of both structures.
- Ambient vibration testing can provide a baseline of the basic modal parameters of a structure, but its major limitation is the inability of to provide the necessary parameters to compute the modal flexibility matrix of the structures, which are essential to perform load ratings from dynamic field tests.

- The most complete and reliable results were obtained from the impact vibration testing. This type of testing is far less complex than the shaker testing and provides a type of excitation with adequate amplitude for such large structures. SIMO type of field tests can be performed with impact testing without compromising the quality of results. For structures similar as those used in this research, this testing method is recommended.

5 Conclusions and Future Work

This chapter highlights the most relevant conclusions that could be drawn from the results of the tests performed on both bridge structures. After the conclusions have been listed and explained, the chapter concludes with recommendations for future work to follow up on and complement this research presented in this thesis.

5.1 Conclusions

This section will present the conclusions that can be made based on analysis of the field testing results in a framework that encompasses the overarching objective of this research thesis, which is to compare and evaluate different dynamic characterization approaches for bridges. Each conclusion or discussion point is listed as a bullet point together with a thorough discussion of each topic. These conclusions aim to cover the entire scope of this research to provide a comparison of various aspects for the different dynamic characterization methods used in this study.

- Full scale dynamic field testing is an alternative to current SHM methods:

As was highlighted in Chapter 1 and in various other locations in this thesis, the current methods for evaluating the structural sufficiency of bridge structures after the occurrence of hazard events are largely subjective due to human interpretation, in the case of visual inspections, and unsafe, in the case of nondestructive load testing. Dynamic testing offers a possibly safer and more reliable alternative for rapidly quantifying changes in the behavior of structure by comparing its modal characteristics identified under normal operational conditions to the ones obtained after the occurrence of a hazard event.

- Overall testing effort for performing each type of dynamic characterization field test:

Of the three different types of dynamic testing that were performed and evaluated in this study, shaker testing was by far the most cumbersome and time consuming to implement in the field. This testing generally required more than one run of the input signal at each DOF location. With input signal lengths of 64 seconds for the burst random test and 300 seconds for the swept sine tests, collecting multiple averages from each input location quickly adds to the overall time duration for the field testing program. Clearly, a testing program that requires a significant amount of time to implement for each bridge that is to be evaluated will not be suitable for the rapid assessment of a single or possibly many structures following a hazard event. This test method also required moving the equipment to each DOF locations which proved to be extremely complicated and time consuming for the Hartbarger Bridge field test. As mentioned in Chapter 4, the shaker testing for this bridge could not be completed due to challenges associated with implementing the testing while the structure remained opened to normal traffic. For example, hanging the shaker by metal chains from the underside of the bridge girders introduced noise and inconsistencies in the experimental measurements due to resonance of the chains at their natural frequencies. It was determined that this was not a good approach for attaching the shaker to the bridge. This testing also requires a minimum of two personnel at the site throughout the testing (under more ideal conditions that would permit the shaker to be positioned on the surface of the bridge deck). In the case of the Hartbarger Bridge testing, however, five people were required to perform the test. Traffic disruption is another issue to consider, as this test

requires no traffic circulating the structure during the duration of the input signal. This may or may not be the case for a bridge after a hazard event has occurred.

Ambient vibration testing took the second largest amount of time to execute of the three dynamic testing methods evaluated. Most of this time requirement was the result of the need to acquire long data sets such that the structural responses due to the unmeasured and uncontrolled input are sufficiently representative of the responses expected for an assumed broad-banded white noise input. It is desirable to capture many realizations of the structural responses in each mode as possible in order to obtain a reliable dynamic characterization of the structure, and this could take a long time especially if the level of the ambient dynamic excitation is not significant and the structure is fairly stiff. However, instrumenting the structure for this type of test requires much less effort than for the shaker testing and only one person is required during the duration of the data acquisition stage, mainly to oversee the equipment and monitor the sensor's output. This type of dynamic test ranks first with respect to the least amount of effort required to perform it. This type of dynamic test is also well-suited for a SHM of a bridge structure in the aftermath of a hazard event, although the time required to obtain reliable modal parameters from this test will not be suited for rapid condition assessment.

Overall, impact dynamic testing was the fastest type of testing to perform. Although this test requires multiple averages for each input DOF location for best results, each impact can be accomplished quickly and the amount of time needed to record the bridge's response is considerably less than that required for the shaker testing. After the bridge has been instrumented, the execution of the tests is quite simple since it only requires moving the instrumented impact hammer from one location to the other, which is much easier than moving a

single shaker and all of its associated test equipment. Impact testing requires a minimum of two test personnel to execute and the amount of time traffic needs to be periodically stopped is minimal. This test is also well suited for a SHM of a structure in the aftermath of a hazard event.

- Data processing requirements:

Two different approaches were used to process the data for the ambient vibration testing and the controlled input dynamic testing. The benefits and shortcomings of each approach are outlined in the following. In both types of testing, the raw time data had to be reviewed to identify and remove any signals or portions of signal that were characteristic of measurement errors, such as drifting signals and spurious peaks due to instrument malfunctions or unintended sources of excitation. The data quality validation stage implemented for the raw measurement data was essential but was also by far the most time consuming aspect of the data analysis process. This stage of the data analysis also required the most manipulation since no automated method could be designed to assess the quality of all of the signals in either the time domain or the frequency domain.

In the case of the ambient vibration testing data processing, the NeXT approach was used to pre-process the raw measurement data using auto and cross correlation functions. The lengthiest step in the NeXT approach was the estimation of the cross correlation functions. The average time MATLAB took to estimate the correlation functions was over two hours for both bridges. Once this step concluded and the pseudo FRFs were calculated, the data was reshaped to the "H" matrix to be used with the CMIF algorithm. From this point on, the data processing steps resembled those needed for analyzing the results of the controlled input dynamic tests. For both

types of tests, manual manipulation was required to examine the peak locations in the CMIF plots to assess if the selected peaks represented realistic mode shapes and not repetitions of mode shapes that were already identified at other frequency lines. The longer time required to process this type of data can also be attributed to the much larger volume of data being processed.

In conclusion, the CMIF algorithm used to process the controlled input test data required considerably less time. The MATLAB code used to process this data included various automated verification methods, such as computing modal assurance criterion (MAC) values at multiple frequency lines and the implementation of multi vector scaling in the formulation of eFRFs among others. These codes, developed by other students in the research group, were significantly more automated than the codes developed by this author to implement the NeXT approach. The steps that required the most manual manipulation and verification were the validation of the data quality and the identification of peaks, and these tasks were also necessary for processing the ambient vibration test data. Considering the significantly smaller amount of data that must be collected from controlled input dynamic tests, it was expected that the time required to process this data was going to be less than the time required for processing the ambient vibration test data.

- Reliability and utility of results on a dynamic characterization framework:

After a thorough review of the results, it was found that natural frequencies and mode shapes were identified from all of the dynamic test types that were implemented. The structure type did not have any significant influence on the ability to identify these two types of modal parameters regardless of the dynamic testing method implemented. It was found that the dynamic test results

from the Hartbarger Bridge, which was the stiffer of the two bridges evaluated for this study, showed much clearer bending modes for its structural components, the steel girders and the concrete deck, in addition to the global bending modes of the structure. This could be beneficial for assessing deviations in the baseline modal parameters in a more localized manner. This would help by pinpointing variations in the response of specific structural elements. In the case of the more flexible truss bridge structure, the Baptist Ford Bridge, only the deck showed the local bending modes mentioned above. The other structural elements' modes were shadowed by the higher energy global modes of this structure.

Significant variability was observed for the damping values identified for both structures. As was discussed in Chapter 4, the methods used to estimate damping greatly depend on the signal to noise ratio of the vibration measurements, which affect the shape and sharpness of the resonant peaks of the eFRF plots and from which curve fitting techniques are used to identify the damping parameter. Thus, it is expected that the impact testing damping estimates were more consistent and reliable than the ones from the other two tests were the input was shadowed by noise. Also, another somewhat unrelated reason affecting the quality of damping estimates is the magnitude of the dynamic excitation. The shaker data input signal had magnitudes that did not excite the bridge enough, as compared to the recorded higher acceleration response recordings from the impact test, in its elastic range to create representative FRF plots to allow the curve fitting process to adequately fit a solution to the peak's shape, which was also the case for the ambient data.

In a dynamic characterization framework, the usefulness of the data obtained from ambient vibration testing is limited to the assessment of variations in natural frequencies, damping,

considering the above mentioned issues related with this modal parameter, and mode shapes. This information can be useful when damage to the structure is significant enough that these modal parameters start to deviate from results obtained from benchmark studies of the bridge under normal operating condition and changes in them due to environmental effects on the structural parameters. However, these modal parameters do not allow the global performance of the structure to be described in a quantitative and meaningful manner that is possible through the analysis of a structure's modal flexibility matrix. Any variation of a structure's condition under normal operating conditions will result in an alteration of its modal flexibility matrix, and the changes in condition and performance of the structure can be meaningfully assessed by changes in the structure's modal flexibility matrix. A damaged structure can be expected to produce higher deflections by applying a uniform load profile to its modal flexibility matrix that what would be produced by loading the same modal flexibility matrix obtained for the undamaged structure. Determining the modal flexibility of a bridge structure is perhaps the most valuable result in monitoring the structural sufficiency of a bridge from a global performance perspective, and provided that a baseline measure of the structure's modal flexibility matrix before a hazard event occurs is available, the changes in displacements of the structure estimated by these flexibility matrices can be used quite confidently to assess significant changes to the global condition of a bridge.

- Final recommendations for optimal implementation of a SHM system:

After considering discussions above, it can be concluded that impact testing is the preferred testing method for a rapid and reliable dynamic characterization program. Not only does impact

testing requires far less time and human effort to be performed, but also the nature of this excitation technique proved to be adequate for both types of structures evaluated. Furthermore, the quality of the modal flexibility obtained from impact testing, which is the most useful parameter obtained through full scale dynamic testing of a bridge, was far superior to the ones obtained from both types of shaker testing. Although the modal parameters obtained from ambient testing compared well with those from impact testing, the usefulness and applicability of the results to fully characterize the condition of a damaged bridge structure is limited. However, this ambient vibration testing is ideal for creating a baseline of the modal parameters of a structure at any point during its service life. The equipment and types of signals used in the shaker tests proved to be inadequate relative to the alternative dynamic testing methods for reliable characterization of the bridge structures evaluated for this study.

5.2 Future Work

In order to build up on the conclusions and recommendations mentioned before, the following studies are recommended.

- A more robust data processing technique for ambient vibration testing that would allow a closer comparison of damping estimates between impact test data and ambient test data would enhance the usefulness of the results obtained from ambient vibration testing. This parameter could better represent the extent of the damages of a bridge structure. Also, the processing of shaker test data with an algorithm that can better filter out the noise during the signal input in order to take advantage of the high custom nature of shaker input signals.

- A comparison of a broader range of bridge structure types will highlight any response characteristics associated with any given structure type under different types of dynamic tests. This study would also allow evaluating the accuracy and efficiency of different data processing techniques for very different structure types.
- Finally, the evaluation for controlled damage of full scale structures would be essential for a comparative evaluation of different approaches for damage scenarios consistent with those produced by hazard events. Such a study could show the appropriate procedures for a field test program to adequately identify both localized and global variations caused by the many different damage scenarios caused by a hazard event.

6 Bibliography

Abdel-Ghaffar, A.M. and Housner, G.W. (1978). " Ambient vibration tests of suspension bridge." J. Eng. Mech., 104(5), 983-999.

Ahlborn,T., Vaghefi, K., Oats, R., Harris, D., Brooks, C., Endsley, K. Roussi, C., Shuchman, R., Burns, J., and Dobson, R. (2012). "Evaluation of Commercially Available Remote Sensors for Highway Bridge Condition Assessment." J. Bridge Eng. 17, SPECIAL ISSUE: Nondestructive Evaluation and Testing for Bridge Inspection and Evaluation, 886-895.

Aktan, A.E., Zhang, Z. (1994). "The damage indices for constructed facilities" Proc., 13th Int. Modal Analysis Conf., 1520-1529.

Aktan, A.E., Catbas, F.N., Turner, A. Zhang, Z.F. (1998) "Structural identification: Analytical aspects" J. Struct. Eng., 124(7), 817-829.

Allemang, R.J., Phillips, A.W., Fladung, W.A. (1998), "The Complex Mode Indicator Function (CMIF) as a Parameter Estimation Method", Proceedings of the 16th IMAC, Santa Barbara (CA), USA.

Allemang, R. J. (2003). "The Modal Assurance Criterion (MAC): Twenty Years of Use and Abuse." Sound and Vibration Magazine, 37(8), 14-23

Allemang, R.J., Brown, D.L. (2006), "A Complete Review of the Complex Mode Indicator Function (CMIF) with Applications", Proceedings of ISMA International Conference on Noise and Vibration Engineering, Katholieke Universiteit Leuven, Belgium.

American Association of State Highway and Transportation Officials. (2008). The Manual For Bridge Evaluation. AASHTO, 444 North Capitol Street, NW Suite 249 Washimgton, DC 20001.

American Association of State Highway and Transportation Officials. (2011). The Manual For Bridge Evaluation. AASHTO, 444 North Capitol Street, NW Suite 249 Washimgton, DC 20001.

Asmussen, J. C., Brinker, R., and Rytter, A. (1998). "Ambient Modal Testing of the Vestvej Bridge Using Random Decrement." 16th International IMAC Conference, Santa Barbara CA, USA.

Baraka, M., and El- Shazly, A. (2005). "Monitoring Bridge Deformations during Static Loading Tests Using GPS." From Pharaohs to Geoinformatics FIG Working Week 2005 and GSDI-8 Cairo, Egypt.

Bernal, D.(2004). "Modal Scaling from Known Mass Perurbations." J. Eng. Mech., 130(9), 1083-1088.

Bowen, C. (2003). "Analysis, Testing, and Load Rating of Historic Steel Truss Bridge Decks". Doctor of Philosophy. The University of Texas at Austin.

Brincker, R., Zhang, L., and Andersen, P. (2000). "Modal identification of output-only systems using frequency domain decomposition." Smart Materials and Structures, Smart Mater. Struct, 10(3), 441.

Cantieni, R., Pietrzko. S. (1993). "Modal testing of a wooden footbridge using random excitation." Proceedings of the 11th International Modal Analysis Conference, Society of Experimental Mechanics, Orlando, USA.

Catbas, F. N. (1997). "Investigation of global condition assessment and structural damage identification of bridges with dynamic testing and modal analysis." Doctor of Philosophy, University of Cincinnati, Cincinnati, OH

Catbas, F. N., Lenett, M., Brown, D. L., Doebling, S., Farrar, C. R. and Turer, A. (1997). "Modal Analysis of Multi-Reference Impact Test Data for Steel Stringer Bridges." Proceedings of the 15th International Modal Analysis Conference, Orlando, FL.

Catbas, N., and Aktan, E. (2002). "Condition and Damage Assessment: Issues and Some Promising Indices." Journal of Structural Engineeering, 128(8), 126.

Catbas,F., Brown, D., and Aktan,A. (2004). "Parameter Estimation for Multiple-Input Multiple-Output Modal Analysis of Large Structures." J. Eng. Mech., 13(8), 921-930.

Catbas, F. N., Brown, D. L. and Aktan, A. E. (2006). "Use of Modal Flexibility for Damage Detection and Condition Assessment: Case Studies and Demonstrations on Large Structures." Journal of Structural Engineering, ASCE, Vol. 132 (11), 1699-1712.

Douglas, B.M., (1976), "Quick Release Pullback Testing and Analytical Seismic Analysis of a Six-Span Composite Girder Bridge," Engineering Report No. 44, Dept. of Civil Engineering, University of Nevada, Reno, Nevada, US.

Farrar, C. R., Baker, T. M., Bell, K. M., Cone, T. W., Darling, T. A., Duffey, A., and Migliori, A. (1994). "Dynamic Characterizaton and Damage Detection in the I-40 Bridge over the Rio Grande." Rep. No. LA-12767-MS, Los Alamos National Laboratory, Los Alamos, NM.

Farrar, C. R., Cornwell, P. J., Doebling, S. W., and Prime, M. B. (2000). "Structural health monitoring studies of the Alamosa Canyon and I-40 bridges." Rep. No. LA-13635-MS, Los Alamos National Laboratory, Los Alamos, NM.

Federal Highway Administration. (2010). "Assessment of FHWA Oversight of the Highway Bridge Program and the National Bridge Inspection Program." Rep. No. MH-2010-039, U.S. Department of Transportation.

Fernstrom, E.V., Wank, T.R., Grimmelsman, K.A. “Evaluation of a Vibroseis Truck for Dynamic Testing of Bridges” Transportation Research Board 91st Annual Meeting Compendium of Papers, 2012

Glaser, S. D., and Tolman, A. (2008). "Sense of Sensing: From Data to Informed Decisions for the Built Environment." Journal of Infrastruct. System, 14(1), 4-14.

Herman, J. K. (2011). "Laboratory Evaluation of Dynamic Characterization Methods for Rapid Condition Assessment of Bridges". Master of Science in Civil Engineering. University of Arkansas.

Ibrahim, S.R., Asmussen, J.C. & Brincker, R. “Modal Parameter Estimation From Responses of General Unknown Random Inputs”. Proc. 14th International Modal Analysis Conference, Dearborn, Michigan, USA, February 1996, Vol 1, pp. 446-452.

James III, G. H., Carrie, T. G., and Lauffer, J. P. (1993). "The Natural Excitation Technique (NExT) for Modal Parameter Extraction From Operating Wind Turbines." Rep. No. SAND92–1666, Sandia National Laboratories, Albuquerque, New Mexico, USA.

Kawasumi H. and Shima E. (1965). “Some Applications of a Correlator to Engineering Problems”. Proc. 3rd World Conf. on Eq. Eng., Vol. 1, p II - 298.

Lenett, M. S., Griessman, A. Helmicki, A. J., and Aktan, A. E. (1999). "Subjective and objective evaluations of bridge damage." Journal of the Transportation Research Board, J. Transp. Res. Board, 1688 76-86.

Mackie, K. R., Wong, J., and Stojadinovic, B. (2009). "Seismic Risk Evaluation for the Baseline PEER Bridge Testbed." Proceedings of the 2009 ASCE Technical Council on Lifeline Earthquake Engineering Conference, ASCE, Oakland, CA, 58-70.

MATLAB R2012a, The MathWorks Inc., Natick, MA, 2000.

Mayes, R. J., and Gomez, A. J. (2006). "Part 4: What's Shakin', Dude? Effective Use of Modal Shakers." Experimental Techniques, 30(4), 44-50.

Muria-Vila,D., Gomez, R., and King, C. (1991).”Dynamic Structural Properties of Cable Stayed Tampico Bridge.” J. Struct. Eng., 117(11), 3396-3416.

Pardoen,G. C., Carr, A.J. and Moss, P.J. (1981). "Bridge Model Identification Problems." Special Publication on Dynamic Response of Structures, Experimentation, Observation, Prediction and Control.

Pernica, G., and Rainer, J. (1979). "Dynamic Testing of a Modern Concrete Bridge." Canadian Journal of Civil Engineering, 6(3), 447-445.

Phares, B., Washer, G., Rolander, D., Graybeal, B., and Moore, M. (2004). “Routine Highway Bridge Inspection Condition Documentation Acuracy and Reliability.” J. Bridge Eng., 9(4). 403-413.

Piombo, B., Giorcelli, E., Garibaldi, L. and Fasana, A. (1993). "Structural Identification using ARMAV models." Proceedings of 11th International Modal Analysis Conference, IMAC, Orlando USA, 588-592.

Ren, W.-X., Zhao, T. and Harik, I. E. (2004). “Experimental and analytical modal analysis of steel arch bridge”. Journal of Structural Engineering, 130(7), 1022-1031.

Sanayei, M., Phelps, J., Sipplt, J., Bell, E., and Brenner, B. (2012). “Instrumentation, Nondestructive Testing, and Finite-Element Model Updating from Bridge Evaluation Using Strain Measurements.” J. Bridge Eng., 17(1), 130-138.

State Transportation Statistics. (2011) RITA, Bureau of Transportation Statistics, Department of Transportation, Washington, DC.

Transportation Engineering Technology Bridge Safety Inspection Program Detail Manual. (2004) National Institute for Certification in Engineering Technologies, NICET.

Torres Goitia, Juan Javier, “Baptist Ford Bridge / Hartbarger Bridge” 2012, .jpg.

Torres Goitia, Juan Javier, “Experimental Equipment” 2012, .jpg.

Wardhana, K. and Hadipriono, F. C. (2003) “Study of recent building failures in the United States” Journal of Performance of Constructed Facilities, 17(3), pp. 151-158.